Universität Zürich[UZH]

Geographisches Institut

Differences in Anatomical Structure and Isotope Composition of Swiss Willow (Salix helvetica) Shrubs Growing on Active and Inactive Rockglaciers in the Turtmann Valley (Switzerland)

GEO 511 Master's Thesis

Author: Kai Frey, 19-734-391

Supervised by: Dr. Holger Gärtner (holger.gaertner@wsl.ch)

Faculty representative: Prof. Dr. Markus Egli

23.04.2026

Abstract

Rockglaciers are important geomorphic features in alpine environments. Monitoring rockglaciers and understanding their internal processes is of high relevance in today's warming climate, as they serve as indicators of permafrost presence. This thesis aims to gain insights into rockglacier dynamics and hydrology by studying Swiss Willow (*Salix helvetica*) shrubs growing on the Gruob rockglacier in the Turtmann valley, Switzerland. Studies have shown that shrubs growing on permafrost exhibit different wood-anatomical properties and stable isotope signatures than those not affected by permafrost. However, shrubs growing on rockglaciers are largely understudied. In this thesis, ring width, vessel lumen area (VLA) and stable isotope ratios of oxygen ($\delta^{18}O$) and carbon ($\delta^{13}C$) of Swiss willow were compared between shrubs growing on rockglacier sites of different activity levels, as well as a reference site not influenced by permafrost. The results show that the shrubs on the active rockglacier have significantly different properties than those at sites that are less or not affected by permafrost. While other sites remain mostly stable over time, large changes of multiple analysed parameters could be recorded for the shrubs at the active rockglacier site. Shrub growth has increased significantly over the last decade, which indicates that growing conditions have improved disproportionally on the Gruob rockglacier compared to neighbouring sites. The carbon isotope signal converges with the other sites, and the oxygen isotope signal on the active rockglacier differs significantly from other sites. These results suggest that growing conditions on an active rockglacier are distinct from permafrost-unaffected sites and are changing at a very high rate. These trends can be explained by melt in the permafrost body of the Gruob rockglacier. Shrub growth likely increases due to higher soil temperatures, caused by an increased active layer thickness. While questions about processes and relationships between shrubs and the rockglacier remain, this study clearly shows the potential of shrubs as an indicator for climatically caused changes in rockglaciers and permafrost degradation.

Acknowledgments

First and foremost, I want to thank my supervisor Dr. Holger Gärtner for his support and guidance during the entire process of creating this thesis. I also want to thank Dr. Isabelle Gärtner-Roer and Prof. Dr. Jussi Grießinger for their valuable advice in the field and sharing their expertise with me. I am thankful for the help of various people in the Dendrosciences group at the Swiss Federal Institute for Forest, Snow and Landscape Research (WSL) on various occasions. I want to extend special thanks to Loïc Schneider for always taking time to explain work steps and equipment in the laboratory to me. Furthermore, I am very grateful to Dr. Matthias Saurer for discussing the results of the stable isotope analysis with me.

I also want to extend my gratitude to Maurin Karzig for his help with the crossdating of my samples and especially for the many delightful, shared work breaks. Very special thanks go to Ciara O'Sullivan and for her massive help with field work, as well as proofreading this thesis. Finally, I want to thank my family and friends for their emotional support in the past months.

Table of Contents

List of Figures

List of Tables

List of Abbreviations

a.s.l	above sea level
c_a	ambient CO_2 concentration
c_i	internal CO_2 concentration
DTM	Digital Terrain Model
g_s	stomatal conductance
iWUE	internal Water Use Efficiency
PDB	Peedee Belemnite
SMOW	Standard Mean Ocean Water
VPD	Vapor Pressure Deficit
VPDB	Vienna Peedee Belemnite
VSMOW	Vienna Standard Mean Ocean Water
VLA	Vessel Lumen Area

1. Introduction

1.1 Research context and Relevance

Global warming caused by the burning of fossil fuel is one of the most impactful challenges of modern times. Global surface temperatures have already increased 1.1°C between 1850-1900 and 2011-2020. Global warming will continue and the extent of current efforts make it difficult to control a temperature increase by 2°C until the year 2100 (Lee & Romero, 2023). Temperature increase due to global warming is not the same everywhere. Temperature over land has risen more than oceans. Additionally warming is especially severe in polar regions. Also, Switzerland is disproportionately affected by climate change with an average temperature increase of 3°C since pre-industrial (Lee & Romero, 2023).

The implications of climate change on nature and humanity are diverse. The cryosphere is highly sensitive to global warming as the presence of glacial and periglacial landforms is directly temperature dependent. Models show that the permafrost areas in high latitude and high altitude regions will decrease strongly in the next decades. Depending on the climate scenario permafrost in high-altitude regions like the Alps could virtually vanish by the end of the 21st century (Guo & Wang, 2016). Active rockglaciers can only exist with the presence of permafrost and are therefore under severe pressure. Permafrost melting can lead to slope instability and mass movement events like rockfalls or landslides. Devastating events like the rockslide in Bondo (Grisons) in 2017 can be directly linked to permafrost degradation, and highlights the importance of permafrost in slope stability in Switzerland (Baillarget & Scaringi, 2025). In arid regions, rockglaciers can serve as important water resources for the local population (Schaffer et al., 2019). These examples highlight that understanding and surveying permafrost and rockglacier processes and distribution is of high importance to cope with the changing climate of the 21st century.

Established methods in rockglacier research include surface velocity measurements with the use of digital terrain models (DTM) from aerial laser scanning systems and boreholes to investigate the internal properties of rockglaciers (Haeberli et al., 2006). Photogrammetric methods based on aerial images are limited by the frequency of flight campaigns (6-7 years) and displacement accuracy. Terrestrial methods like geodetic observations with GPS allow high accuracy measurements but require annual monitoring in late summer, to avoid seasonal variations (Delaloye et al., 2010). The Swiss Permafrost Monitoring Network (PERMOS) currently includes about 20 rockglaciers that are monitored regularly (PERMOS, 2022). These traditional methods require heavy and expensive material on rockglaciers and labour-intensive field work.

Despite the harsh climatic conditions and the active surface, vegetation can be present on rockglaciers. The vegetation is patchy and depends on the altitude, microtopography and extent of ground movement (Cannone & Gerdol, 2003). In places where fine substrate is present also small shrubs like *Salix* species can grow (Burga et al., 2004). This opens the opportunity to apply dendrogeomorphological and wood anatomical methods on rockglaciers. This approach has rarely been used on rockglacier but a study by Gärtner-Roer et al. (2013) shows that vessel sizes vary depending on the activity status of a rockglacier and can potentially give insights into rockglacier kinematics.

Another potential approach includes the analysis of stable isotopes in wood. The oxygen isotope ratio $\delta^{18}O$ can be used for climate reconstructions and to trace the source water of plants (Barbour, 2007). The carbon isotope ration $\delta^{13}C$ offers insights into plant-physiological processes and environmental stresses experienced by trees and shrubs (McCarroll & Loader, 2004). Stable isotope analyses have been conducted in arctic environments and show that the $\delta^{18}O$ signal can be altered on permafrost due to meltwater (Bryukhanova et al., 2015; Churakova-Sidorova et al., 2020; Fan et al., 2023). The same effect was also observed for a tree stand on permafrost in Val Bever, Switzerland, that shows that the climate signal is weakened by the influence of permafrost and rather shows differing water sources (Grießinger et al., 2021). While this poses challenges for the use of $\delta^{18}O$ for climate reconstruction, it allows one to gain insights on hydrological processes at different locations. Hydrological flow paths in rockglaciers are complex and dependent on the internal structure of individual rockglaciers. These relationships as well as meltwater contribution to stream water are poorly understood and subject to current research (Jones et al., 2019).

The use of dendroecological methods in a periglacial environment on rockglaciers offers an additional method for rockglacier research and potential insights into rockglacier dynamics and hydrology. Especially in the context of climate change, wood anatomy and stable isotopes could have the potential to record changes in the local environment. Moreover, the relationships between plants and rockglaciers are understudied and it is important to understand these interconnections.

1.2 Research Questions and Objectives

This thesis aims to gain insights on relationships between rockglaciers and the vegetation growing on them. These interactions have not yet been studied on a large scale and many research gaps remain. Previous research indicates that relationships are likely, and their influences can be found in vessel sizes and isotopic signatures of shrubs. The effects of rockglacier dynamics on shrub properties are investigated on the Gruob rockglacier in the Turtmanntal, Valais. As there is only little earlier research available, this thesis primarily aims to find which wood-anatomical and isotopic properties are affected most by rockglacier presence and activity. The secondary aim is to explain these differences and trends and connect them to geomorphic, environmental and climatic processes. By this approach the results of this thesis will show if shrubs are a suitable indicator for rockglacier activity, and where knowledge gaps exist in understanding the underlying processes. To reach these objectives the following research questions were developed to guide the thesis.

Overarching Research Question:

- *Are there differences in the anatomical properties and isotopic signature within the annual rings of Salix helvetica shrubs growing on active and inactive rockglaciers in the Turtmanntal, Valais?*

Research Questions:

1. *Do Salix helvetica shrubs growing on active and inactive rockglaciers show differences in their vessel sizes and ring widths compared to a reference site not influenced by permafrost?*
   - ➔ Hypothesis: The vessel sizes and ring width of Salix helvetica shrubs on rockglaciers is influenced by the distinctive conditions on a rockglacier.

2. *Do Salix helvetica shrubs growing on active and inactive rockglaciers show differences in their $\delta^{18}O$ and $\delta^{13}C$ signal compared to a reference site not influenced by a permafrost?*

- ➔ Hypothesis: The isotopic signal of Salix helvetica shrubs growing on rockglaciers reflects the different local environmental conditions on a rockglacier.

3. *Can differences and trends in vessel size, ring width and isotopic signature of Salix hevetica shrubs on rockglaciers be explained by temperature / surface activity and different water uptake sources, respectively?*
   - ➔ Hypothesis: Differences and trends in vessel size, ring width and isotopic signature can be explained by differences and changes in temperature, surface activity and water sources caused by climate change

2. Theory

2.1 Permafrost and Rockglaciers

2.1.1 Rockglacier Definition and Composition

There are several definitions of what constitutes a rock glacier. A widely accepted definition was formulated by Barsch (1996, p. 4): “*Active rockglaciers are lobate or tongue-shaped bodies of perennially frozen unconsolidated material supersaturated with interstitial ice and ice lenses that move downslope or downvalley by creep as a consequence of the deformation of ice contained in them and which are, thus, features of cohesive flow*.” Due to the perennially frozen material, rockglacier are geomorphological indicators for the presence of permafrost (Barsch, 1996; Haeberli, 1985; Humlum, 2000).

Rockglaciers can be recognized by their typical morphology. The Action Group on Rock glacier inventories and kinematics (RGIK) has defined the following three characteristics as visual indicators for rockglaciers (RGIK, 2023):

1. **Rock glacier front**: a clearly discernible, steep talus marking the front of a rockglacier perpendicular to the main flow direction of the rock glacier, usually convexly formed

2. **Lateral margins**: a continuation of the rockglacier front on the sides, sometimes not present in the upper parts of the rockglacier

3. **Ridge and furrow topography**: complex and undulating surface topography caused by the flow of the rockglacier

As introduced by the definition, rockglaciers mainly consist of unconsolidated material (debris) and ice (Barsch, 1996). The uppermost layer in a rockglacier is the active layer. In contrast to the other layers of a rockglacier it is not perennially frozen and acts as a regulative layer between permafrost and atmosphere (Cicoira, 2020; Haeberli, 1985). The amplitude of temperature variation is very large due to seasonal changes of the atmospheric air temperature, which is illustrated in Figure 1.

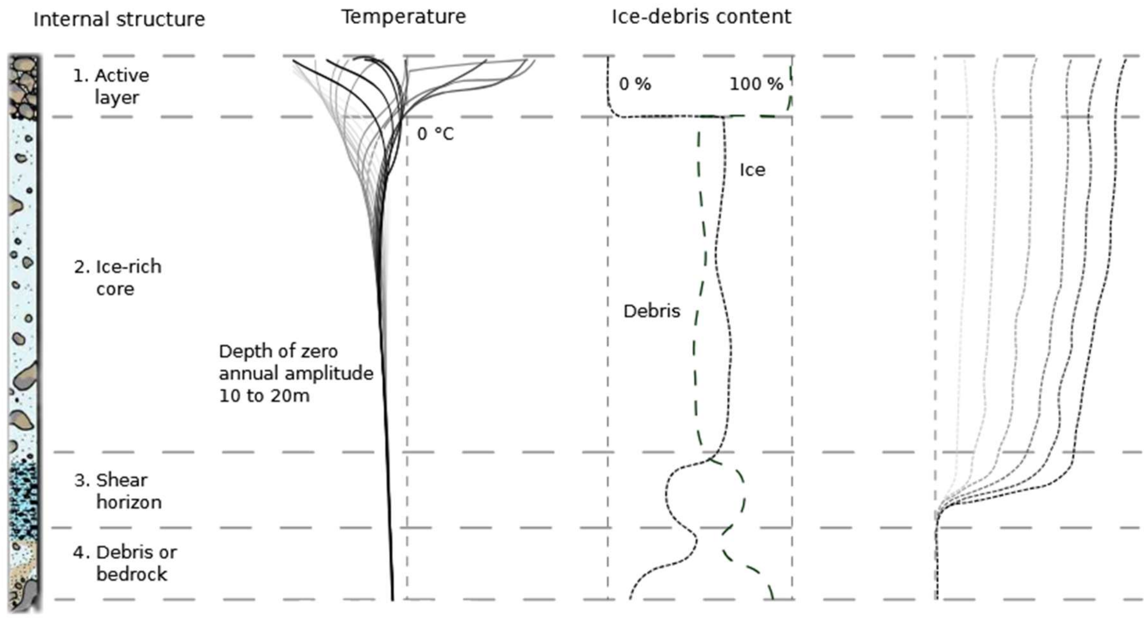

Figure 1: Schematic overview of the internal structure of an active rockglacier. Layers, temperature, ice-debris content and typical displacement profiles are displayed from left to right (Cicoira, 2020, p. 10)

Below the active layer is the ice-rich core, which is also known as permafrost body, where temperatures are more stable and always below 0°C (Haeberli, 1985). The permafrost body consists of a mixture of ice and debris. The share of ice can vary largely and is estimated to usually lie between 40% and 70% in alpine rockglaciers (Arenson et al., 2002; Haeberli et al., 2006; Hausmann et al., 2007). Below the core of the rockglacier lies the shear horizon. While being much thinner than the ice-rich core, it is responsible for a majority of the displacement in the rockglacier, contributing about 60% to 90% of total deformation (Arenson et al., 2002; Cicoira, 2020).

2.1.2 Rockglacier Types

As introduced in Chapter 2.1.1, rockglaciers are composed of large amounts of unconsolidated rock material. Rockglaciers can be classified according to the source of the rock material (Figure 2). Typically, large amounts of loose rock material in alpine environments can be found below rock faces or in moraines. By this distinction, rockglaciers can be classified either as talus rockglaciers (below rock faces) or debris rockglaciers (below moraines) (Barsch, 1996). The Gruob rockglacier on which samples were taken for this thesis is a talus rockglacier, as a majority of the rockglaciers in the Turtmann valley is (Nyenhuis, 2005).

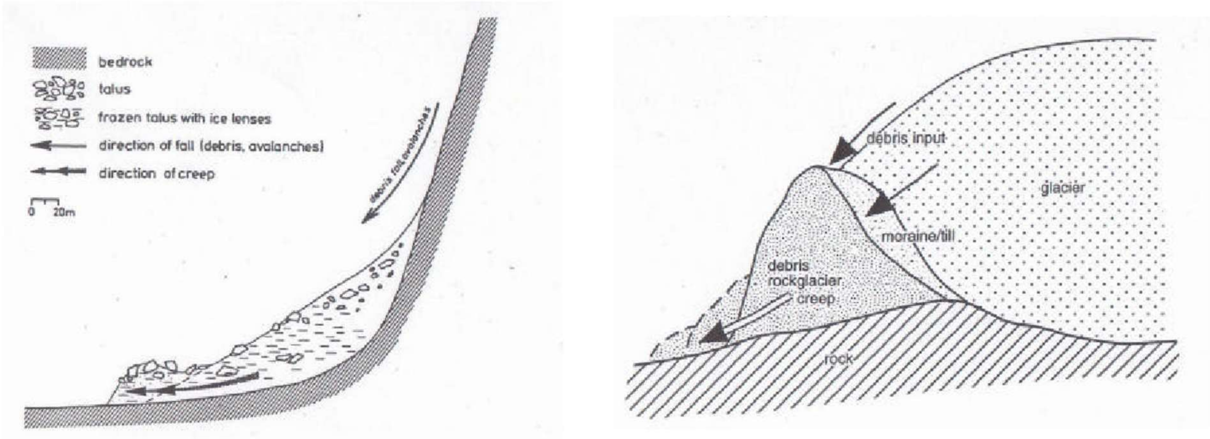

Figure 2:Schematic profiles of a talus rockglacier (left) and a debris rockglacier (right). The illustration indicates different components and movements are indicated by arrows (Barsch, 1996, pp. 186–187)

Rockglaciers are defined as landforms that contain an ice-rich and frozen core and move downslope. Permafrost melt or a decrease of material input can lead to changes in rockglaciers. Due to such changes rockglaciers can lose some of their typical properties but are still recognizable as a geomorphologic landform with some typical features of a rockglacier. So rockglaciers can also be classified due to their flow behaviour and ice content. Active rockglaciers have the classic internal structure summarized in Figure 1. They exhibit creep behaviour, which results in a steep front without vegetation (Barsch, 1996; Haeberli, 1985; Ikeda & Matsuoka, 2002; Roer, 2007). Inactive rockglaciers also contain a permafrost body, but they do not move downslope, which often results in less steep front (Haeberli, 1985). Relict rockglaciers do not contain any ice anymore and do not creep downslope. They are no longer indicators for permafrost but can still be visible in the landscape through their form and are indicators for former permafrost distribution (Roer, 2007). They are characterized by increased vegetation, a shallow front and often a collapsed surface due to internal ice melt (Ikeda & Matsuoka, 2002). Inactivity in rockglaciers can be caused by two factors. Firstly, climatic changes can raise the lower limit of permafrost presence, which leads to a thickening of the active layer and climatic inactivity (Ikeda & Matsuoka, 2002). Dynamically inactive rockglaciers decelerate because of a reduction in debris and ice input, which leads to reduced shear stress (Barsch, 1996). Inactive rockglaciers in discontinuous permafrost regions, like the Gruobtälli are usually climatically inactive (Roer, 2007). Figure 3 shows a schematic overview, how rockglaciers of different activity differ in their structure.

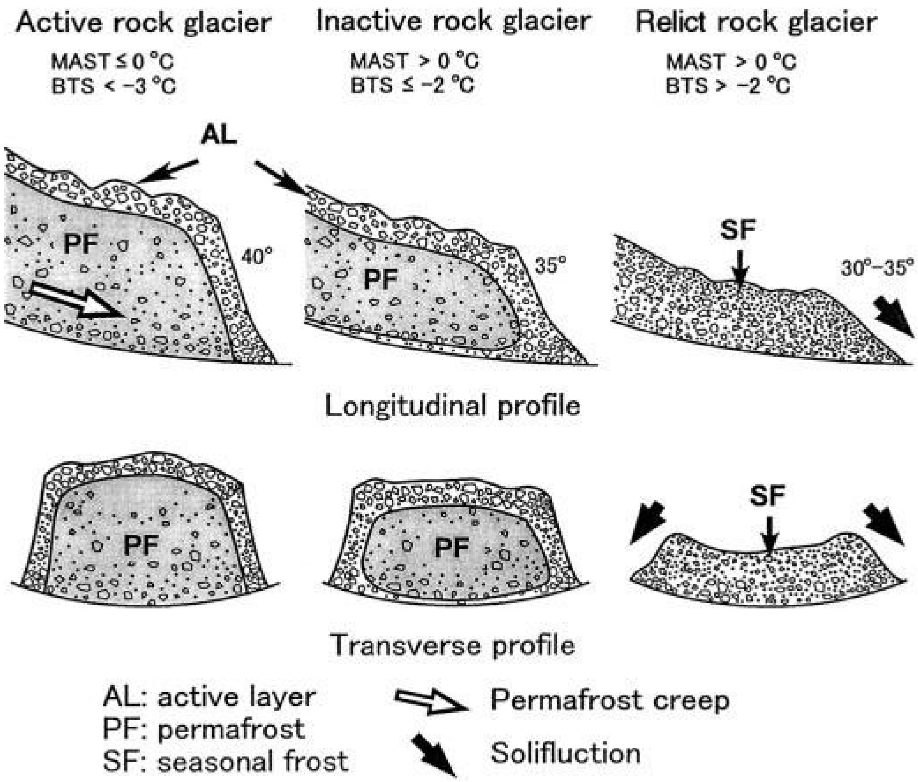

Figure 3: Schematic profiles of active (left), inactive (middle) and relict (right) rockglaciers, including . main components and movement directions. MAST = Mean Annual Surface Temperature, BTS = Bottom Temperature of the Winter Snow Cover (Ikeda & Matsuoka, 2002, p. 158)

2.1.3 Rockglacier Kinematics and Hydrology

One of the defining characteristics of rockglaciers is the downslope creep of permafrost. Typical velocities are in the range of 0.1 to 2 m per year (Barsch, 1996; Delaloye et al., 2010; Haeberli, 1985; Haeberli et al., 2006). As introduced in Chapter 2.1.1, the creep mainly originates from deformation in the shear horizon (Figure 1). In this layer, pore water is present, which has an important impact on deformation by weakening the structure of the ice-debris material and enabling deformation (Buchli et al., 2018; Cicoira, 2020; Ikeda et al., 2008). While the majority of creep takes place in the shear horizon, the ice-rich core can contribute up to 40% to the total rockglacier displacement (Arenson et al., 2002). In this layer, creep is mainly controlled by ice deformation. The mechanic properties of ice are temperature dependent with warmer ice being more ductile than cold ice (Arenson et al., 2007).

Over the past decades, the surface creep velocity of rockglaciers in the Alps has increased. There are variations across years and between rockglaciers, but the overall trend clearly points towards a consistent acceleration (Kellerer-Pirklbauer et al., 2024). Figure 4 visually shows these observed changes in horizontal rockglacier velocity compared to a reference period.

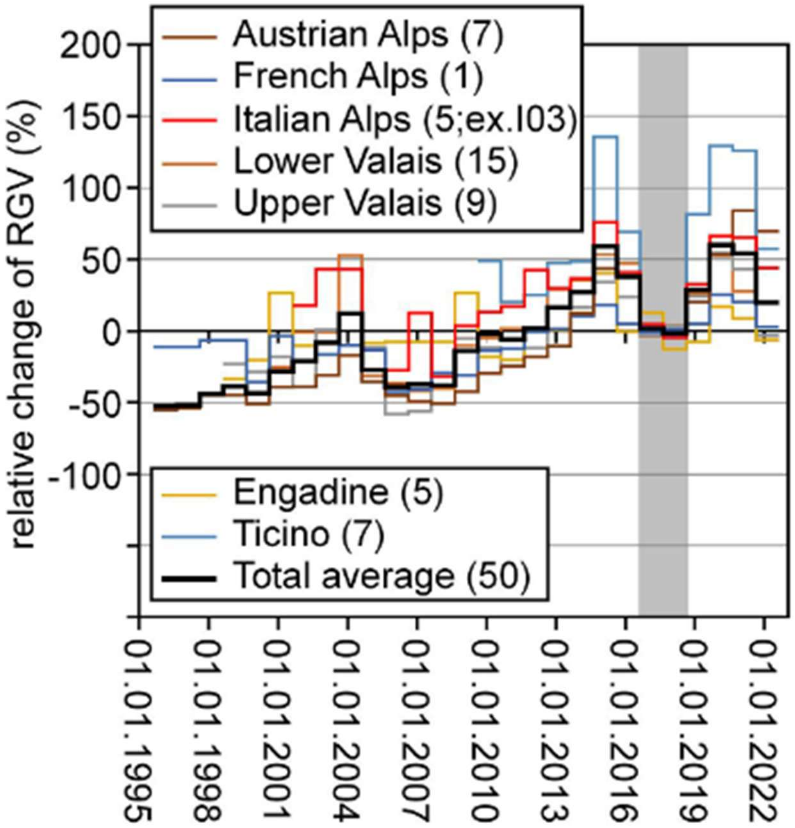

Figure 4: Relative change of rockglacier velocity (RGV) between 1995 and 2022 to the reference period 2016-2018, including values from rockglaciers in seven regions in the alps and a total average (Kellerer-Pirklbauer et al., 2024, p. 14)

This observed acceleration in rockglacier creep can be linked to climatic changes. It is known that higher surface temperatures can lead to increased rockglacier creep velocities (Kääb et al., 2007; Marcer et al., 2021). The temperature – velocity relationships are complex and not fully understood, but two factors seem to play a key role.

As mentioned before, warmer ice is more ductile. Warmer air temperatures penetrate the rockglacier and increase the temperature of the ice. This mostly affects the ice-rich core, which is relatively close to the surface and where some deformation is known to take place (Arenson et al., 2002). The increased ductility of the ice facilitates deformation in the ice-rich core (Kääb et al., 2007; Marcer et al., 2021). The deformation in the ice-rich core is possibly also enhanced by higher amounts of liquid water. In the shear horizon, where the majority of deformation takes place and pore water is known to play a major role, a similar effect takes place. Especially under relatively warm ground conditions, it is expected that an increase of pore water leads to an accelerated deformation by destabilizing the ice-debris mixture (Cicoira, 2020).

Despite its importance in rockglacier kinematics and source of water in arid regions, the hydrological processes and water flow paths in rock glaciers are still poorly understood (Jones et al., 2019). Figure 5 shows a simple overview of the different possible water sources and flow paths in rock glaciers. Water in rock glaciers can originate from rain, snow melt, ice melt or ground water. The water in the rock glacier can flow above, below or even through the permafrost body when it is not continuous (Schaffer et al., 2019).

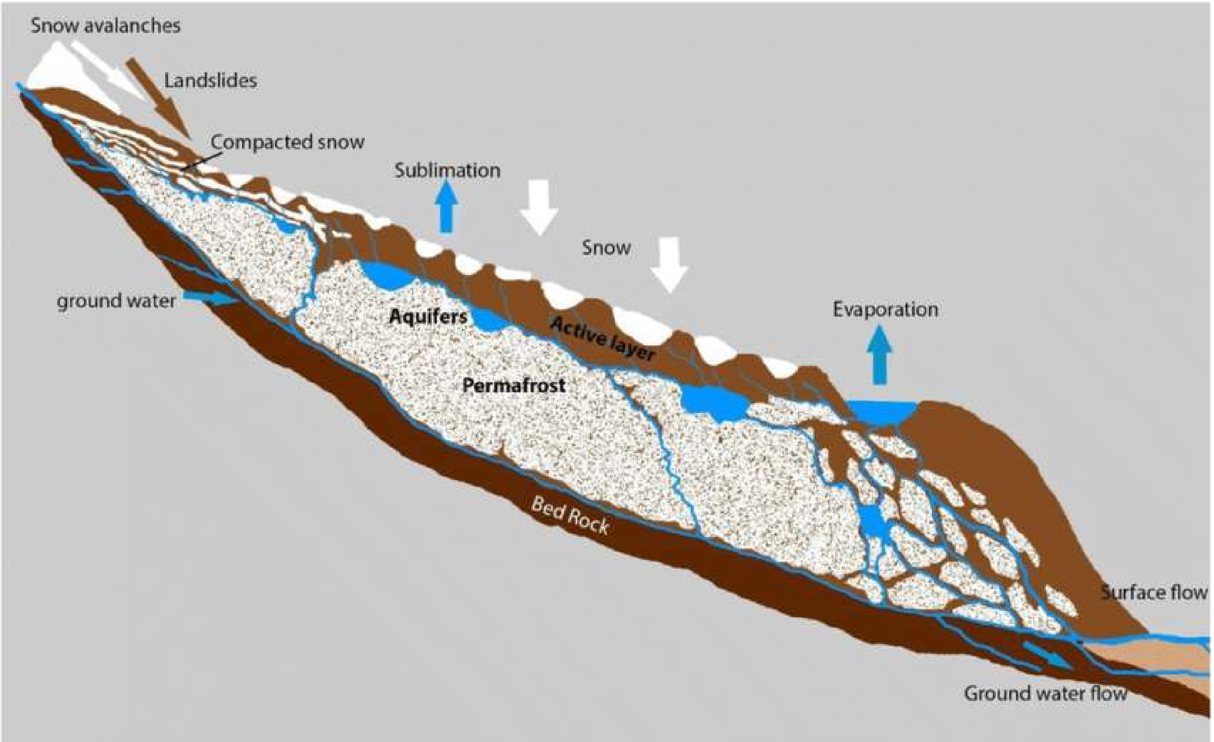

Figure 5: Schematic view of rockglacier structure, inputs, outputs and hydrological system, flow directions and mass movements are indicated by arrows (Schaffer et al., 2019, p. 1272)

Research methods on rockglacier hydrology includes the analysis of $\delta^{18}O$ in water sources (Del Siro et al., 2023; Jones et al., 2019; Krainer & Mostler, 2002; Reato et al., 2022; Williams et al., 2006). The observed trend is that $\delta^{18}O$ of rockglacier discharge increases from spring to fall. This can be explained by snow meltwater that is increasingly enriched due to isotopic fractionation in the snowpack (Taylor et al., 2001). Additionally, summer rainfall which tends to have high $\delta^{18}O$ values leads to $\delta^{18}O$ peaks in rockglacier discharge (Krainer et al., 2007). While exact values are heavily dependent on location and climate, it is known that summer precipitation generally has the highest $\delta^{18}O$ values of all water sources (Amschwand et al., 2025) and that the snowpack has lower values that rise during summer (Taylor et al., 2001).

There are knowledge gaps about how important ice melt is in the hydrology of rockglaciers and comparably little data is available on the $\delta^{18}O$ values of rockglacier ice in the Alps. Studies suggest that permafrost ice melt is not a significant component of rockglacier discharge (Amschwand et al., 2025; Krainer et al., 2007). Other sources support the theory that measured $\delta^{18}O$ in discharge can be explained by ice melt (Williams et al., 2006). It has been theorized that ice in rockglaciers gets enriched by melt-freeze cycles and contact with infiltrating liquid water. Through fractionation processes, light isotopes are preferentially left behind in the ice, through which the remaining ice gets enriched in $\delta^{18}O$ (Steig et al., 1998; Williams et al., 2006). By this process, rising $\delta^{18}O$ values in rockglacier outflow from early to late summer can also be explained by an increased share of ice melt. It is important to note that the importance of processes may vary largely depending on the structure of a rockglacier. $\delta^{18}O$ values of rock glacier ice exist for the Reichenkar (Krainer et al., 2007) and Lazaun (Bertolotti & Krainer, 2025) rockglacier in Austria. At Reichenkar values ranged from -16.7 ‰ to -12.2 ‰ and at Lazaun from -15 ‰ to -8.9 ‰. These values show that $\delta^{18}O$ of rockglacier ice varies both between rockglaciers and within a rockglacier, but are generally higher than snowmelt and lower than summer precipitation (Krainer et al., 2007).

2.2 Dendrogeomorphology

Geomorphological processes can be reconstructed and dated by the application of dendrogeomorphology. Ring-width measurements and wood anatomical analyses provide valuable insights into tree growth. Parameters such as cell size, cell structure, and the formation of reaction wood are closely associated with environmental changes and disturbances (Alestalo, 1971). Dendrogeomorphological methods can and have been used for a variety of processes, including the reconstruction of landslides (Fantucci & McCord, 1995; Paolini et al., 2005; Šilhán, 2021) or debris flows (Gärtner, 2001; Strunk, 1997), the examination of erosion rates (Heinrich et al., 2007; LaMarche, 1968) and to reconstruct the advance of rockglaciers by buried trees (Bachrach et al., 2004). Dendrogeomorphology has also been used to research permafrost-plant interactions (Nikolaev et al., 2009; Qi et al., 2023; Schweingruber et al., 2013; Zhu et al., 2024). While there have been studies connecting vegetation distribution to rockglacier movement (Burga et al., 2004; Cannone & Gerdol, 2003), the use of wood anatomy to gain insights into rockglacier dynamics is a relatively new approach and is largely understudied. A first time application by Gärtner-Roer et al. (2013) showed that vessel sizes in the roots of *Salix helvetica* shrubs are significantly smaller on an active rockglacier than on an inactive rockglacier. This result can be explained by different thermal soil conditions or differences in surface movement. In this thesis, a similar approach, combining vessel size and ring width analysis of shrub branches on rockglaciers of different activity levels, is used to further investigate the use of dendrogeomorphology as an indicator for rockglacier dynamics.

2.2.1 Vessel Size

Vessels in plants are responsible for the transportation of water, which makes them critical for shrub survival and growth (Fonti et al., 2010). Vessel size is connected to growth, because an increased amount of water transport allows for higher rates of growth (Hacke & Sperry, 2001). Vessel size and growth thus cannot be considered as independent. It has been suggested that vessel size primarily depends on stem length and plant size, and climatic conditions are not a relevant controlling factor (Olson et al., 2014). Vessel size variations have been related to various environmental disturbances and climatic trends. Large vessels are more likely to be damaged by cavitation caused by freezing or drought (Hacke & Sperry, 2001), which is likely to be of importance on rockglaciers. Vessel lumen area (VLA) was also shown to be altered in trees that were tilted (Heinrich et al., 2007). This effect can be explained by altered wood anatomy with smaller vessels in reaction wood. Followingly, reduced vessel sizes can be expected when there is surface movement. In arctic *Juniperus* shrubs, tracheid size was shown to be positively related to summer temperature (Lehejček et al., 2017). No age effect of tracheid size could be observed in these shrubs, which can be explained by the physiological adaptions necessary in harsh climates and a prostrate growth form. Another study analysing *Betula nana* shrubs in Greenland found that VLA is driven by spring and summer temperatures as well, concluding that the shrubs adjust their hydraulic capacity through vessel size to control radial growth (Nielsen et al., 2017). Again, no clear age trend for vessel size could be found. These studies indicate that shrub vessel size is a suitable indicator for climatic changes in arctic or alpine environments. Age seems to have little influence on vessel sizes in dwarf shrubs in cold regions. This effect is likely absent due to small size of these shrubs, so differences in stem length are far smaller during ontogeny than in other climates (Carrer et al., 2015). The age effect is caused by the height of a plant, which remains very limited in shrubs at any age.

The research by Gärtner-Roer et al. (2013) and analyses of arctic shrubs suggest that vessel size is different on rockglaciers of different activity levels. The mechanisms are still unclear, but it seems likely that differences are caused either by different temperatures or ground movement.

2.2.2 Ring-Width

The ring width in trees and shrubs represents the radial growth of the analysed plant. It has been widely used to reconstruct growing conditions and climate (Esper et al., 2002; Fritts, 1976; Treydte et al., 2006). As with vessel size, age-related trends in ring width have been reported. However, there is no general direction of an age trend in shrubs. Depending on the species and study, an age-related increase or decrease of ring width, or no trend at all, was reported(Myers-Smith, Hallinger, et al., 2015).

Various studies link ring width with climatic conditions in arctic regions (Blok et al., 2011; Cui et al., 2025; Dobbert et al., 2022; Iturrate-Garcia et al., 2017; Lehejček et al., 2017; Owczarek & Opała, 2016). It is often described that the main controlling factor of shrubs is spring and/or summer temperature. However, other factors such as nutrient availability (Iturrate-Garcia et al., 2017), soil moisture and winter snow conditions (Dobbert et al., 2022), or fast thawing/freezing and sunshine duration (Owczarek & Opała, 2016) have been identified as the main drivers of shrub growth. These divergent results highlight that growth limitation is highly dependent on location specific conditions.

Studies on alpine shrubs are more limited. Francon et al. (2021) found that shrub growth in the Alps used to be mainly limited by air temperature, but since the 1990s moisture limitation is increasingly frequent due to climate change. Looking only at vegetation at the high altitude treeline, it was found that the mean seasonal soil temperature in the root zone at locations all over the world was between 6°C and 7°C (Körner & Paulsen, 2004). This is a very narrow range and air temperatures at different treelines are much more divergent than soil temperatures. This observation has been tested on a low-lying permafrost island in the Swiss Jura, where soil temperature is the same as at the altitudinal treeline, but air temperature is higher. The dwarf trees at this location are considerably smaller than surrounding tree stands and have very low annual growth rates (Körner & Hoch, 2006). This study strongly indicates that especially at high altitudes and on permafrost, ground soil temperature is a very important limiting factor for plant growth.

2.3 Stable Isotopes

Isotopes are variants of elements with a different number of neutrons (Fry, 2006). Stable Isotopes are not radioactive, so they do not decay over time. The main elements in wood (carbon, oxygen and hydrogen) have more than one stable isotope in nature. The chemical properties of these elements are almost identical, but the mass of these isotopes varies depending on the number of neutrons. Because of this, chemical, physical and biological processes can discriminate against some isotopes (McCarroll & Loader, 2004). The ratio of isotopes is usually expressed by delta (δ) in reference to a standard isotopic ratio (Eq. 1). The ratio is expressed by parts per thousand (‰) so δ has to be multiplied by 1000 (Saurer et al., 2025).

$$\delta = \frac{R_{Sample} - R_{Standard}}{R_{Standard}} \qquad \textit{Eq. 1}$$

Isotopic ratios of all three main elements in wood ($\delta^{18}O$, $\delta^{13}C$ and $\delta^{2}H$) can be analysed, where the combination of multiple isotope ratios gives increased insights into plant processes. The dual approach with carbon ($\delta^{13}C$) and oxygen ($\delta^{18}O$) isotope ratios is most established and widely used. The inclusion of hydrogen ($\delta^{2}H$) is a recent trend and less established (Saurer et al., 2025). This thesis utilises the classic dual approach with the analysis of $\delta^{18}O$ and $\delta^{13}C$.

2.3.1 Oxygen

The stable isotope ratio $\delta^{18}O$ is the ratio of ^{18}O to ^{16}O. The original reference value is Standard Mean Ocean Water (SMOW) (Craig, 1961). The reference value has since been standardized as Vienna Standard Mean Ocean Water (VSMOW) to avoid confusion and inconsistency (Coplen, 1995).

The relationship between air temperature and $\delta^{18}O$ was first described by Dansgaard (1964) (Figure 6). This correlation is caused by a fractionation process during condensation. Heavier ^{18}O preferentially enters the liquid phase during condensation in the atmosphere. The heavy ^{18}O isotopes are proportionally overrepresented in the precipitation. Thus, the water vapour in the air gets increasingly depleted in ^{18}O as it moves to higher latitudes or altitudes which are more distant from the regions where the water originates (Dansgaard, 1964). The effect is not simply temperature driven. Other factors like the source of the moisture, atmospheric circulation patterns, season of the year, precipitation amounts or continentality play an important role in the ^{18}O-values of precipitation (Rozanski et al., 1993).

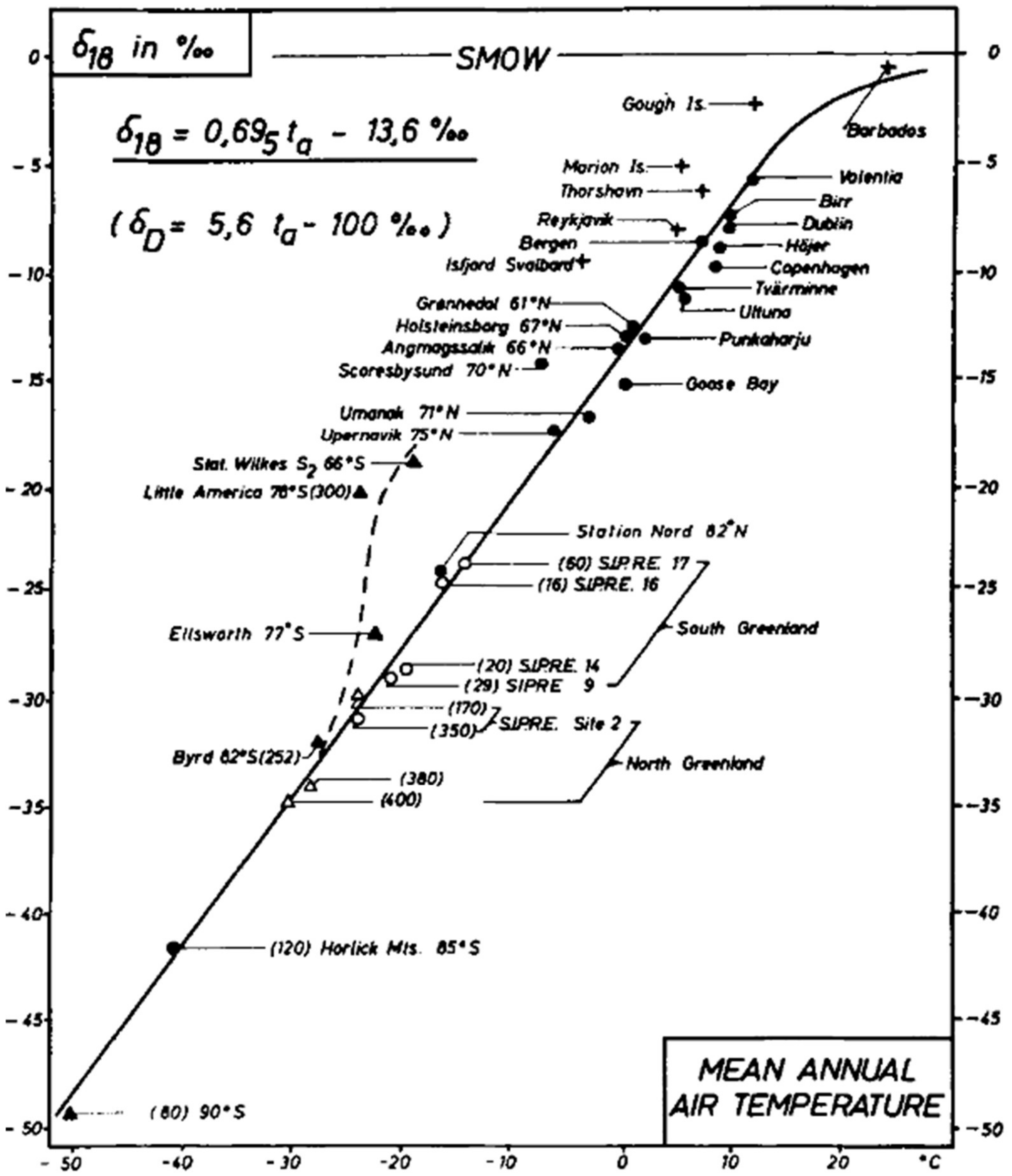

Figure 6: Annual mean δ18O of precipitation (y-axis) as a function of the annual mean air temperature (x-axis). Measurement points are indicated in the plot, and a line shows the connection between δ18O and temperature (Dansgaard, 1964, p. 443)

Plants take up water from soil water, which directly or indirectly results from precipitation. The ^{18}O-signature of the precipitation therefore gets absorbed by the roots into the plants (McCarroll & Loader, 2004). During the take-up of water there are no fractionation processes, which change $\delta^{18}O$ (Wershaw et al., 1966). However, the $\delta^{18}O$ in plant material is heavily enriched in ^{18}O, which is mainly due transpiration in the leaf, with enrichment of up to 20‰ (Saurer et al., 1998). $\delta^{18}O$ in wood is influenced by three main factors (Barbour et al., 2001; Roden et al., 2000):

1. $\delta^{18}O$ of source water
2. $\delta^{18}O$ enrichment in the leaf due to evaporation
3. Fractionation during synthesis of cellulose and lignin

Of those three factors, the impact on $\delta^{18}O$ is not on a comparable level. A study of temperate tree species found that between 96 and 99% of $\delta^{18}O$ variation could be explained by source water $\delta^{18}O$ (Roden & Ehleringer, 1999). Evaporative enrichment of leaf water through the stomata occurs during transpiration and depends primarily on the isotopic difference between the source water and atmospheric water vapour, as well as on the gradient in vapour pressure between the leaf interior and the surrounding air. This gradient is also known as vapor pressure deficit (VPD). Lower relative humidity increases this gradient and enhances evaporative enrichment, resulting in higher $\delta^{18}O$ values in leaf water and subsequently in plant organic matter (McCarroll & Loader, 2004). During carbohydrate and cellulose formation, part of the oxygen atoms can exchange with xylem water within plant tissues, which modifies the isotopic signal incorporated into plant biomass (Barbour, 2007). However this factor is considered relatively stable compared to environmental controls (Roden et al., 2000). Differences in $\delta^{18}O$ are therefore controlled mostly by source water $\delta^{18}O$ and evaporative enrichment in the leaf. The most important controlling environmental factors of $\delta^{18}O$ in wood are $\delta^{18}O$ of precipitation and air humidity during the vegetation period, while the relative share of these factors varies (McCarroll & Loader, 2004).

Because the δ^{18}O-signal in wood carries information about past environmental conditions, it is frequently used as a tool for climate reconstruction (Büntgen et al., 2021; Grießinger et al., 2019; van der Sleen et al., 2015). However, the reasoning that δ^{18}O in plants directly reflects the δ^{18}O of precipitation is an oversimplification in many cases. As is illustrated in Figure 7, δ^{18}O of the precipitation is only part of the source water signal.

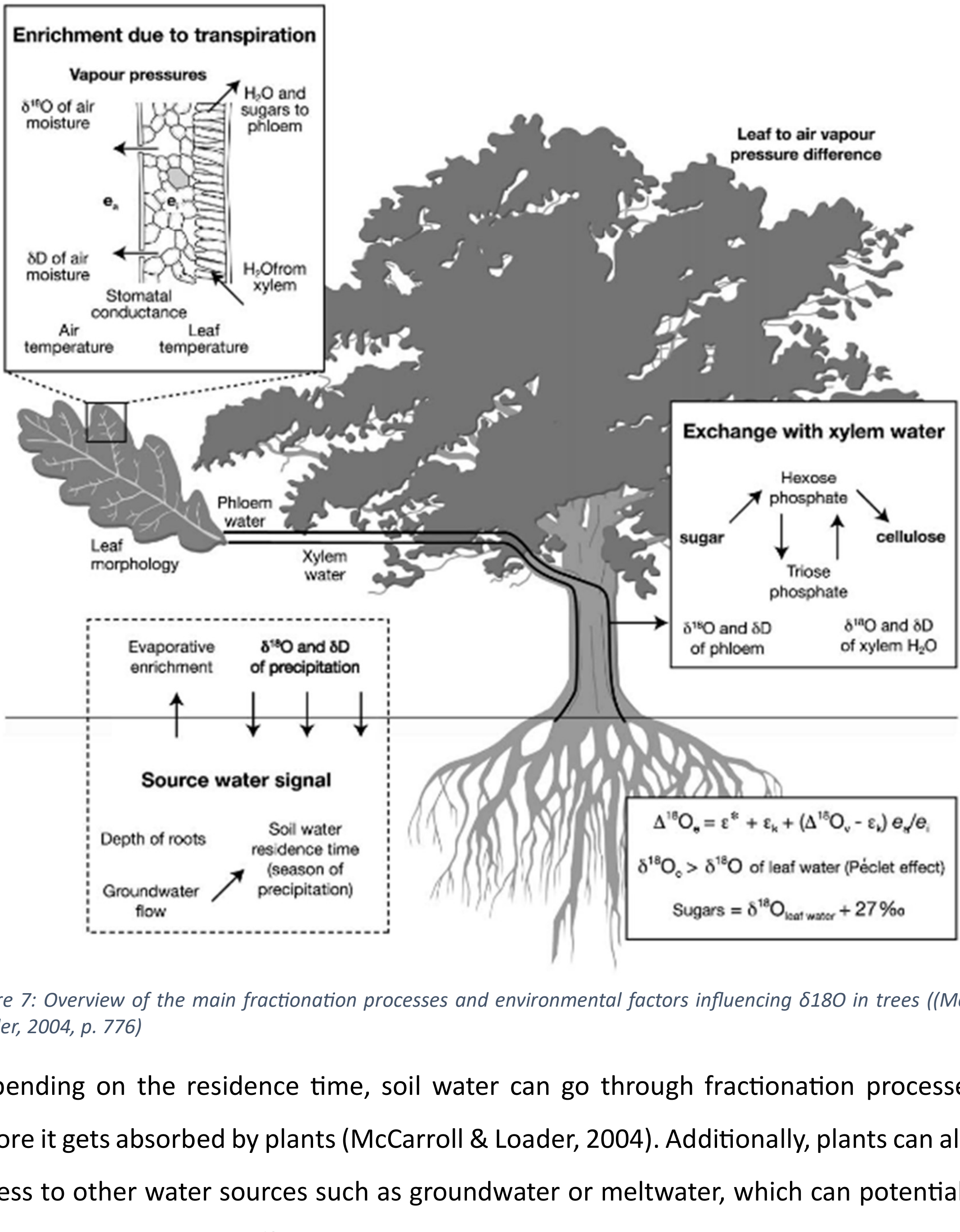

Figure 7: Overview of the main fractionation processes and environmental factors influencing δ18O in trees ((McCarroll & Loader, 2004, p. 776)

Depending on the residence time, soil water can go through fractionation processes even before it gets absorbed by plants (McCarroll & Loader, 2004). Additionally, plants can also have access to other water sources such as groundwater or meltwater, which can potentially have a completely different δ^{18}O signature to the local precipitation. This is effect must be considered, as the climate signal in wood can be disturbed or even completely lost when other water sources are available (Grießinger et al., 2021). Instances of other source water influencing $\delta^{18}O$ have been recorded numerous times. Especially relevant for this thesis are cases where the studies were performed on permafrost. There are multiple examples of arctic sites, where $\delta^{18}O$ in wood can be matched with the signature of permafrost meltwater (Bryukhanova et al., 2015; Churakova-Sidorova et al., 2020; Fan et al., 2023; Sugimoto et al., 2002). In these studies, $\delta^{18}O$ was used to identify the water source of shrubs and trees in permafrost regions and how meltwater can serve as an additional water source.

2.3.2 Carbon

The stable carbon isotopes analysed for $\delta^{13}C$ are the ratio of naturally occurring ^{13}C and ^{12}C. The standard relative value was originally Peedee Belemnite (PDB), a marine fossile, and got replaced by the standardized Vienna Peedee Belemnite (VPDB), when original PDB ran out (Coplen, 1995). The isotopic composition is expressed in the standard δ-notation. Other than oxygen isotopes in plants which have their origin in water (H_2O), the carbon in plants originates from the CO_2 of air. $\delta^{13}C$ of air has a value around -8‰ (VPDB) which is much larger than typical values found in the wood of plants (-20‰ to -30‰). $\delta^{13}C$ in plant tissue describes physiological processes in plants that control carbon uptake and fixation and is a widely used indicator of carbon assimilation dynamics. The depletion in wood is caused by two factors. The stomata through which CO_2 diffuses are very small, and the smaller ^{12}C enter the leaf more easily (McCarroll & Loader, 2004). The fractionation through diffusion is commonly expressed as *a.* The second fractionation takes place when internal CO_2 is used for photosynthesis. During carboxylation, which turns CO_2 into plant sugars, the photosynthetic enzyme RuBisCO tends to prefer ^{12}C over ^{13}C, which leads to further $\delta^{13}C$ depletion (McCarroll & Loader, 2004). The fractionation during carboxylation is expressed as *b*. The carbon isotope discrimination ($\Delta^{13}C$) in C_3 plants can be calculated as (Farquhar et al., 1982):

$$\Delta^{13}C = \frac{\delta^{13}C_{atm} - \delta^{13}C_{plant}}{1 + \delta^{13}C_{plant}/1000} \qquad \textit{Eq. 2}$$

The carbon isotope discrimination is mostly controlled by diffusion and carboxylation. Those discrimination processes can be expressed as the following formula (Farquhar et al., 1982):

$$\Delta^{13}C = a + (b - a)\frac{c_i}{c_a} \qquad \textit{Eq. 3}$$

The two discrimination factors *a* and *b* are normally treated as constants. The estimated values for *a* are 4.4‰ and for *b* ≈27‰. c_i and c_a are the intercellular and ambient CO_2 concentrations

(Farquhar et al., 1982). Because *a* and *b* are treated as constants, variation in $\Delta^{13}C$ primarily reflects changes in the c_i/c_a ratio. If stomatal conductance (g_s) is low relative to photosynthetic demand (A), the internal CO_2 concentration (c_i) decreases. As a result,the photosynthetic enzyme RuBisCO discriminates less against ^{13}C during carboxylation, leading to higher $\delta^{13}C$ values (McCarroll & Loader, 2004). The ratio of A to g_s is the internal Water Use Efficiency (iWUE). It describes the amount of carbon biomass produced per unit of water transpired, and can be approximated as follows (Farquhar et al., 1989):

$$iWUE = \frac{A}{g_s} = \frac{c_a(1 - c_i/c_a)}{1.6} \qquad \textit{Eq. 4}$$

The factor 1.6 is based on the ratio of binary diffusivity between water vapor and air, and CO_2 and air (Farquhar et al., 1989).

$\delta^{13}C$ in wood reflects the physiological response of a plant during the time of carbon fixation and thus carries information about the environmental conditions of that time. Due to $\delta^{13}C$ being largely controlled by c_i/c_a, less negative $\delta^{13}C$-values are commonly linked with increased stomatal closure due to water stress or an increase of photosynthesis. In dendrogeomorphological and dendrochronological applications, $\delta^{13}C$ and iWUE as a derived product are commonly used to reconstruct plant reactions to climatic and environmental changes. Next to the connection with drought stress, increasing iWUE has been widely observed in forest ecosystems and is often interpreted as a consequence of rising atmospheric global CO_2 concentrations and following stomatal adjustments in plants (Saurer et al., 2004).

3. Study Site

3.1 Location

The study area of this thesis lies in the Turtmann valley in the Canton Valais in Switzerland, which is a tributary valley of the Rhone valley in the south of Switzerland. At the end of the valley there are two glaciers, and several hanging valleys branch from both sides of the main valley. The Turtmann valley is in the region with the highest peaks of Switzerland reaching from the Rhone (620 m a.s.l) to the Bishorn (4151 m a.s.l) and Weisshorn (4506 m a.s.l) at its end. The Gruob rockglacier (46° 12′ 12 N, 7° 43′ 24 E) on which samples were taken for this thesis lies in the Gruobtälli above the seasonally inhabited village of Gruben (swisstopo, 2026). The Gruobtälli is a hanging valley on the east side of the Turtmann valley. The research area in the Gruobtälli is marked in Figure 8 and shown in the context of the greater region.

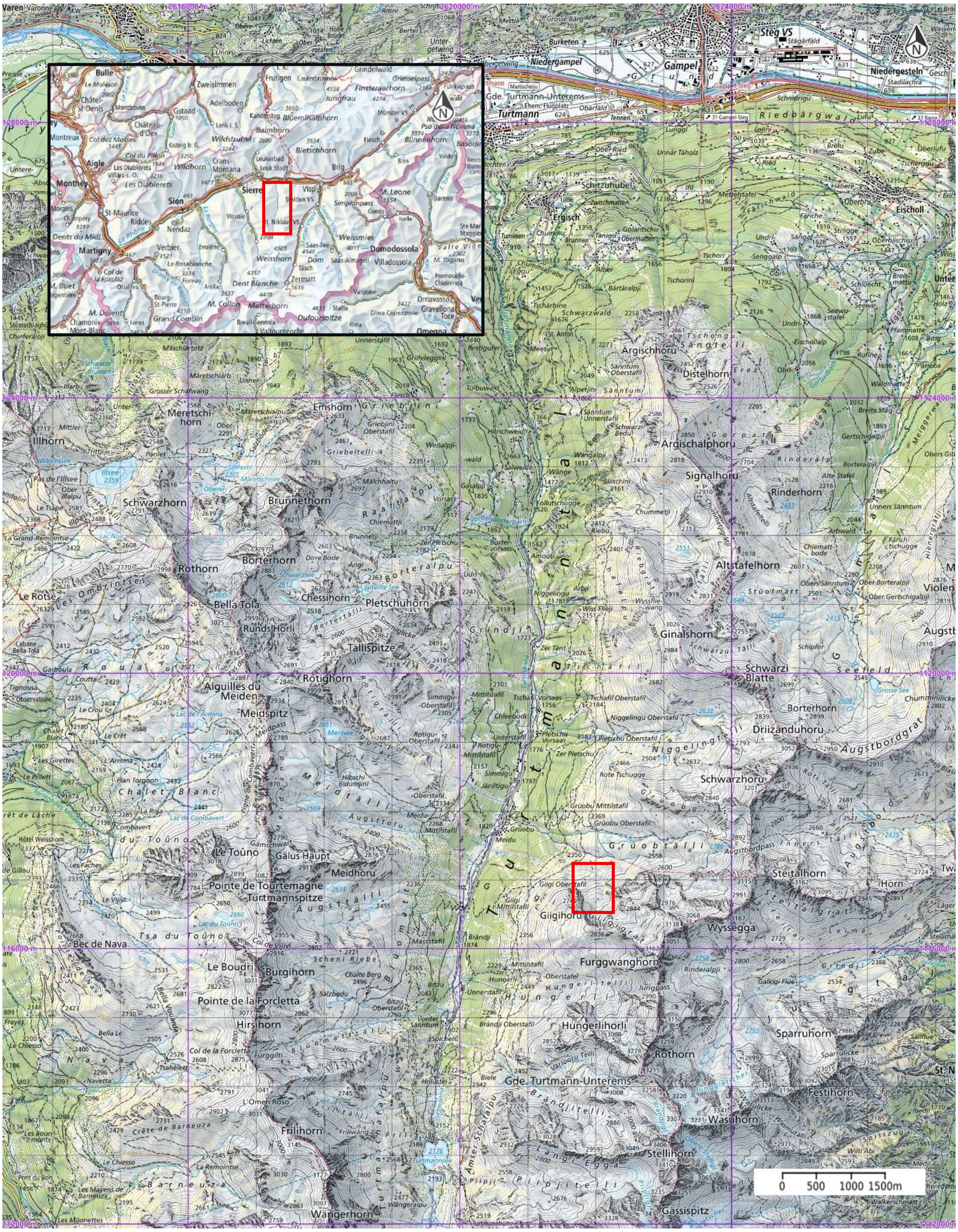

Figure 8: Map of the study area in the Turtmann valley, with an overview map of the canton of Valais. The location of the Gruob rockglacier is marked by the red square (basemap: swisstopo (2026))

3.2 Climate

There are no long-term climate observation stations in the Turtmann valley. There is only an automatic precipitation measurement station by MeteoSwiss at an artificial reservoir (Turtmannsee) at the end of the valley. The station lies at an altitude of 2180 m a.s.l, which is close to the altitude of the Gruob rockglacier (2419 – 2917 m a.s.l). Unfortunately, measurements only started in 2012, so changes over the last decades cannot be read from the data. The closest meteorological station that also measures temperature is in Grächen, one valley east of the Turtmann valley, at an altitude of 1605 m a.s.l. Precipitation and air temperature have been measured there since 1864, so the data is very well suited to observe climatic changes in the region since the beginning of the of the industrialization. Regarding precipitation, the data of the two stations can be compared for the years since 2012.

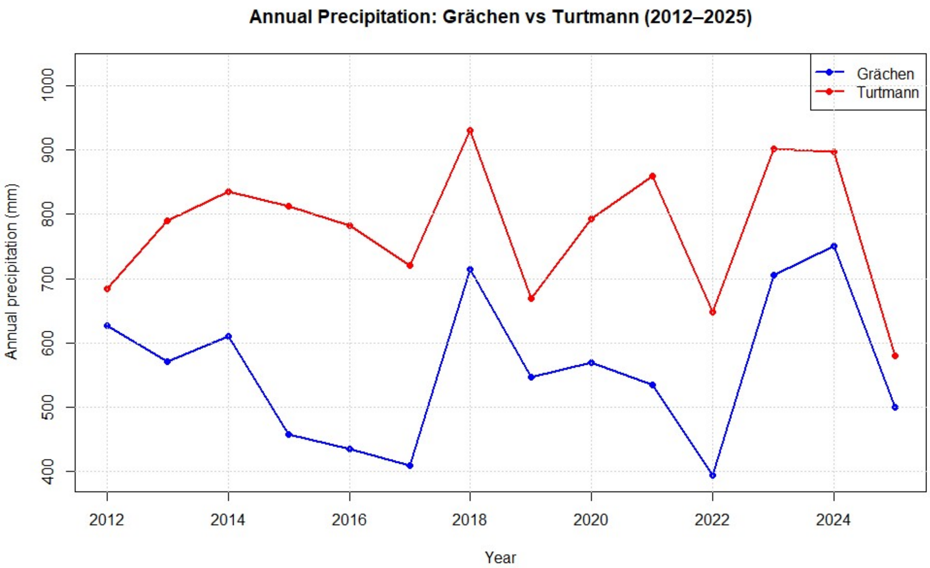

Figure 9: Comparison of the annual precipitation in the Turtmann valley (2180 m a.s.l) and Grächen (1605 m a.s.l) from 2012 - 2025

In Figure 9, it becomes visible that yearly values of the two stations follow a similar pattern, with the station in the Turtmann valley experiencing more precipitation every year, with values ranging from 600 mm to 900 mm per year. Comparing the values shows that general trends in precipitation are the same at both stations. The higher values at the Turtmann station can be partly explained by the higher elevation. The low annual precipitation of 600mm to 900 mm per year shows that the Turtmann valley experiences the typical continental climate of the region. The precipitation values in Figure 11 from Grächen show that annual precipitation has been relatively stable since 1900. There was rise of precipitation in the 1980s, but the values have been decreasing again since then. If only the precipitation of the vegetation period (May to September) is considered, there is no peak in the 1980s, but the last 10 – 15 years show lower average precipitation amounts.

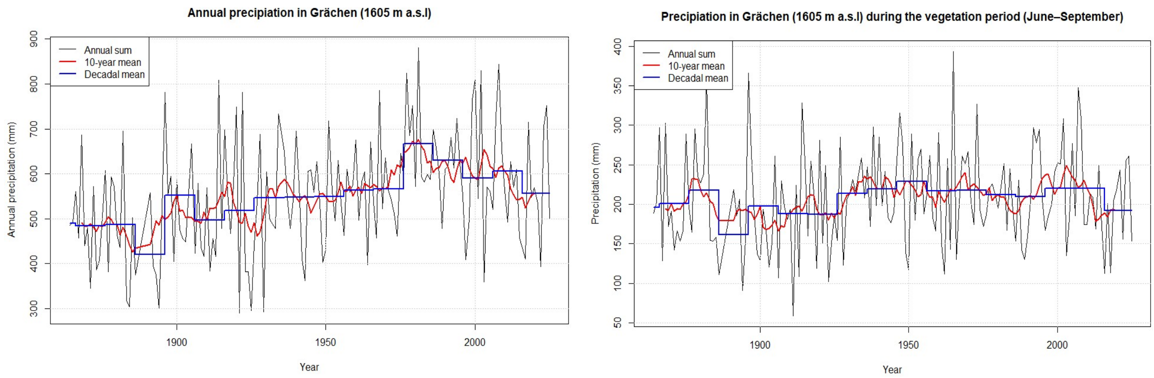

Figure 11: Annual precipitation in Grächen (left) and annual precipiaton per vegetation (June-September) period in Grächen (right), plot includes 10-year rolling mean in red and decadal means in blue

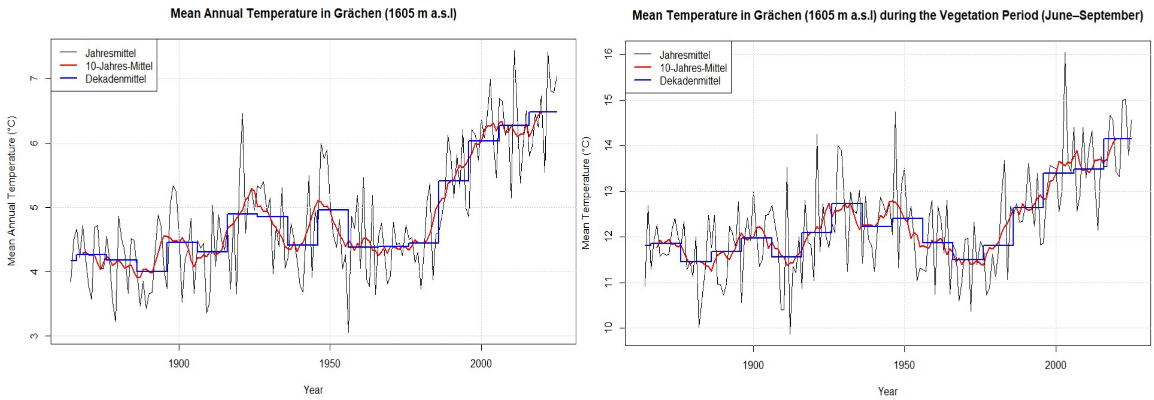

Figure 10: Mean annual temperature in Grächen (left) and mean annual temperature during the vegetation period (June-September) in Grächen (right), plot includes 10-year rolling mean in red and decadal means in blue

Regarding the mean temperature (Figure 10), there is a very clear trend since the 1980s, with steadily rising temperatures. The same trend can be observed for both annual temperatures and temperatures during the vegetation period. However, the trend is even stronger during the vegetation period with an increase of almost 3°C, while the annual temperature has risen around 2°C. This is consistent with the climatic trend introduced in Chapter 1.1, showing that Switzerland is affected more strongly by climate change than the global average. It also stands out that the last decade had a large increase in temperature, while the two decades before were on a similar level.

3.3 Geology

The Turtmann valley is part of the "Mischabel-Kristallin" complex, which makes up the bulk of the "Bernhard-Decke" between the Simplon and Val d'Anniviers. The geological profile of the valley is visible in Figure 12, with the study area located near the Furggwanghorn. The main material of the mountains above the Gruob rockglacier (Furggwanghorn, Giigihoru) is of metamorphic origin from the Paleozoic era. The main rocks are mica schist and gneiss, characterised by a felsic composition (Bearth, 1980). The debris rock material of the Gruob rockglacier originates from this bedrock on the Giigigrat above the rockglacier. Below the Gruob rockglacier, the ground was formed by older quaternary moraines during cold periods (Bearth, 1980). The Dufour map from 1845 does not show the presence of glaciers in the Gruobtälli during the Little Ice Age, except for small glaciers just below the Furggwanghorn and Wyssegga (swisstopo, 1845). These glaciers did not reach the valley floor or the sampling sites of this thesis.

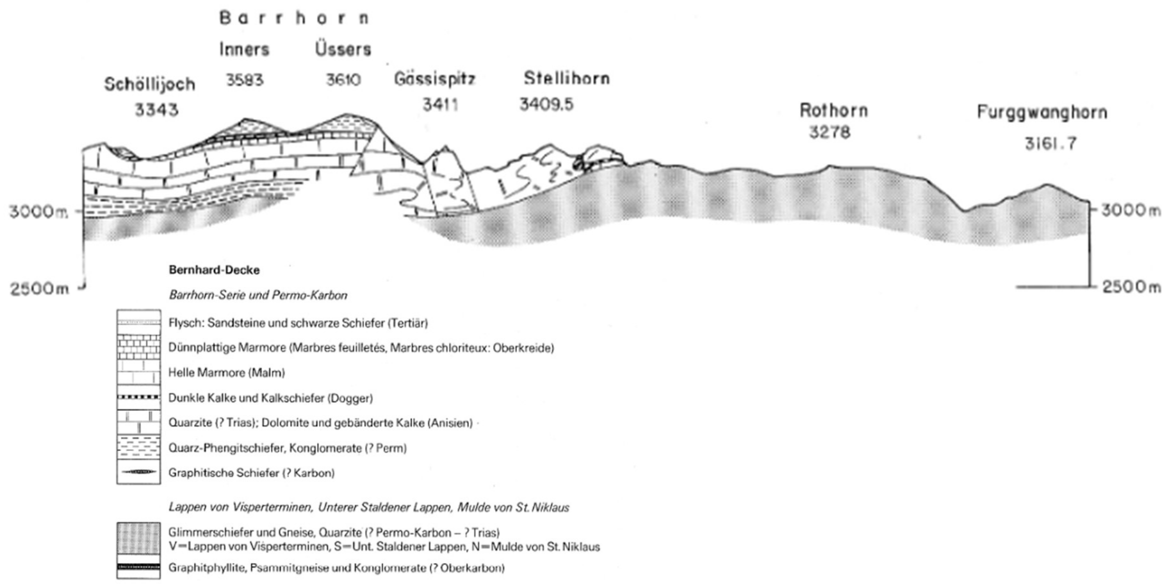

Figure 12: Geological profile along the east side of the Turtmann valley (Bearth, 1980)

3.4 Vegetation

The treeline in the Gruobtälli lies at an altitude of 2200 m a.s.l. It is not limited by climatic conditions, but by alpine pastures, where cattle are grazing in summer. The vegetation above the treeline mainly consists of grasses, shrubs and some small trees. Additional to the *Salix helvetica* shrubs analysed in this thesis, some other typical alpine shrub species like *Rhododendron* and *Juniperus* are present.

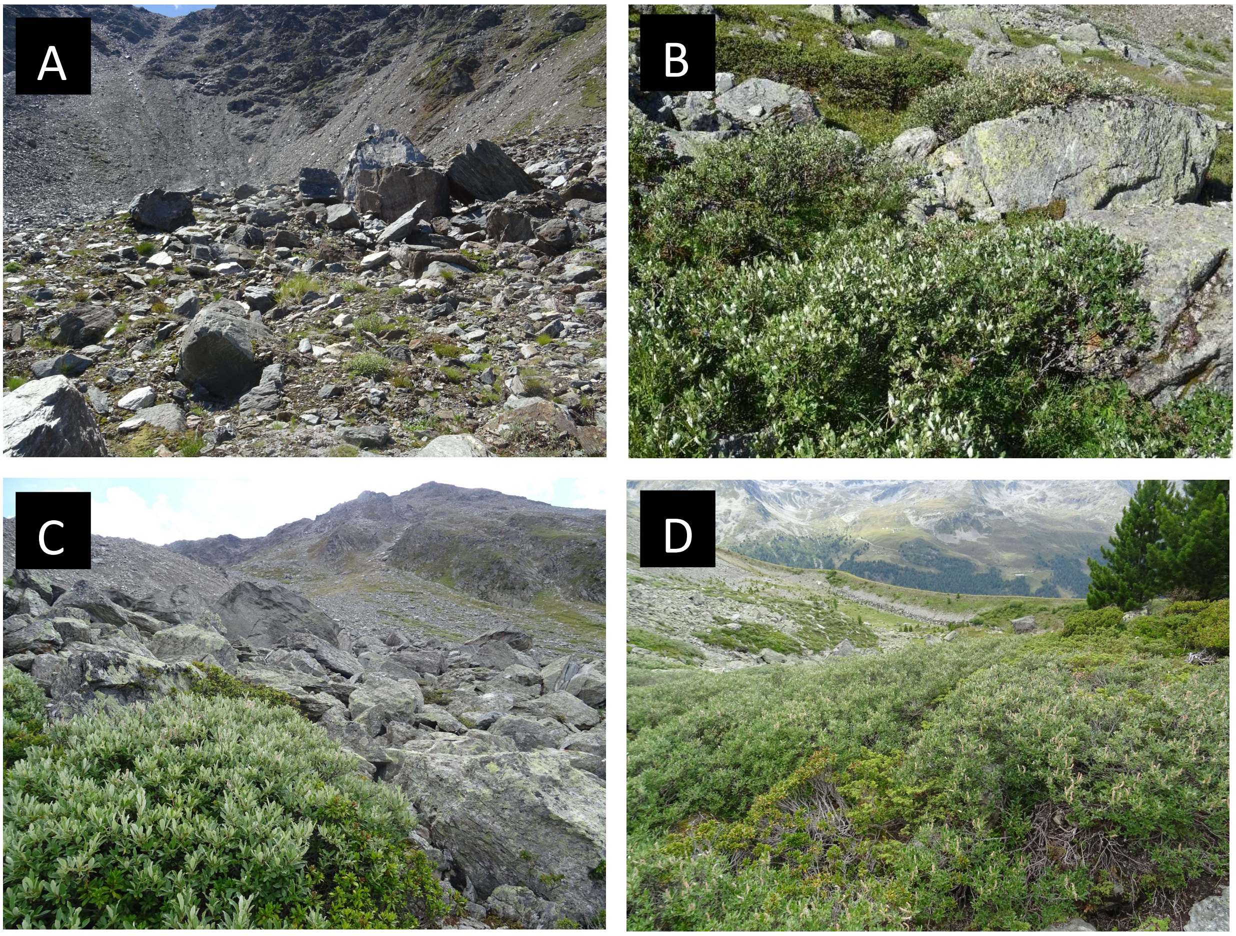

Figure 13: Vegetation on the active rockglacier (A), inactive rockglacier (B), middle site (C) and reference site (D), pictures represent typical conditions at the sampling locations

The different vegetation pattern between the four studied sites is noteworthy. Especially the active rockglacier is mostly vegetation free. Panel A in Figure 13 shows the only area where some vegetation is present and the samples for this thesis were taken. Apart from some very small *Salix Helvetica* shrubs*,* the only other vegetation consists of small tufts of grass, mosses and lichen. The other three sites are much more similar to each other. On the inactive and middle site, *Salix helvetica* shrubs are the most abundant shrub species and grow much larger than on the active rockglacier. The difference between those sites is mainly that on the middle site much of the area is not vegetated at all due to large boulders (Figure 13, Panel C). On the reference site, the *Salix helvetica* shrubs are also large, but there are more other shrub species like *Juniperus*.

3.5 Permafrost and Rockglaciers

The geomorphology of the Turtmann valley is characterized by an abundance of periglacial landforms. Rockglacier and other permafrost features cover a total area of 110 km^2 or about 4.4 % of the area in the Turtmann valley. There are rockglaciers of all activity states (active, inactive, relict) (Roer & Nyenhuis, 2007). Thanks to the high number of rockglaciers and periglacial processes taking place in the Turtmann valley, a number of rockglacier research has been conducted here (Buchli et al., 2013; Gärtner-Roer et al., 2013; Gärtner-Roer & Nyenhuis, 2010; Roer & Nyenhuis, 2007; van Tatenhove & Dikau, 1990). The rockglaciers in the valley were identified and classified by photgrammetric monitoring and geomorphologic mapping

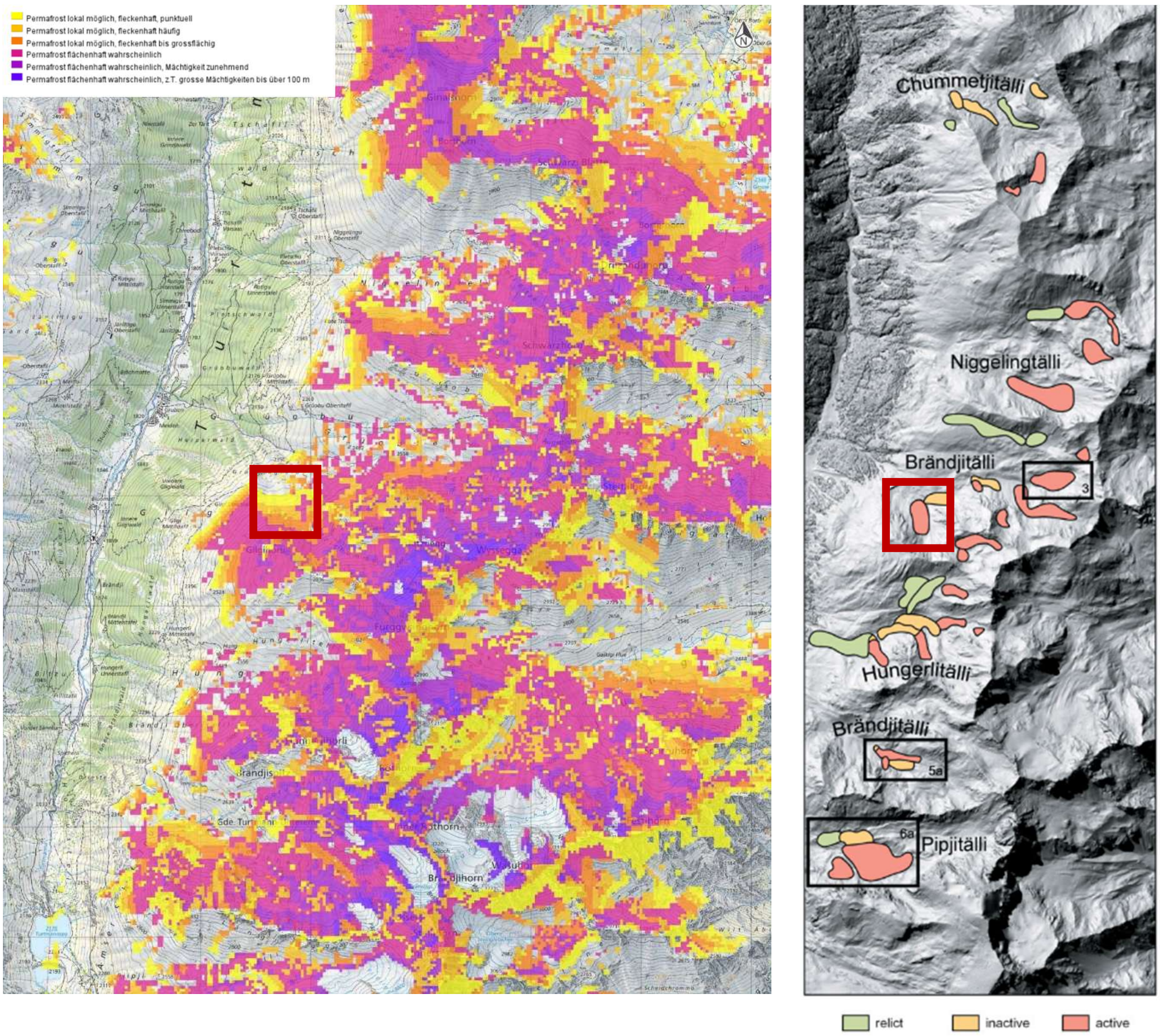

Figure 14: Modelled permafrost distribution in the Turtmann valley on the left (swisstopo, 2005), geomorphical mapping of the rockglaciers in the Turtmann valley on the right (Roer & Nyenhuis, 2007, p. 1753), research area of this thesis marked in red rectangle

(Roer & Nyenhuis, 2007). The modelled permafrost distribution in Figure 14 shows that permafrost in the study area (red square) is possible, but not continuous and at the lower distribution belt of permafrost presence (swisstopo, 2005).

3.5.1 Gruob Rockglacier

The Gruob rockglacier lies on a north-facing slope below the Giigigrat. It is the lowest active rockglacier in the Turtmann valley, lying between an altitude of 2419 and 2617 m a.s.l. It has a length of 348 m, a width of 214 m and a surface area of 86’400 m^2. The thickness is estimated to be between 11 and 19 meters, which leads to an estimated volume of 1’088’266 m^3 to 1’879’732 m^3 (Nyenhuis, 2005). The characteristic features of a rockglacier are well recognizable in Figure 15.

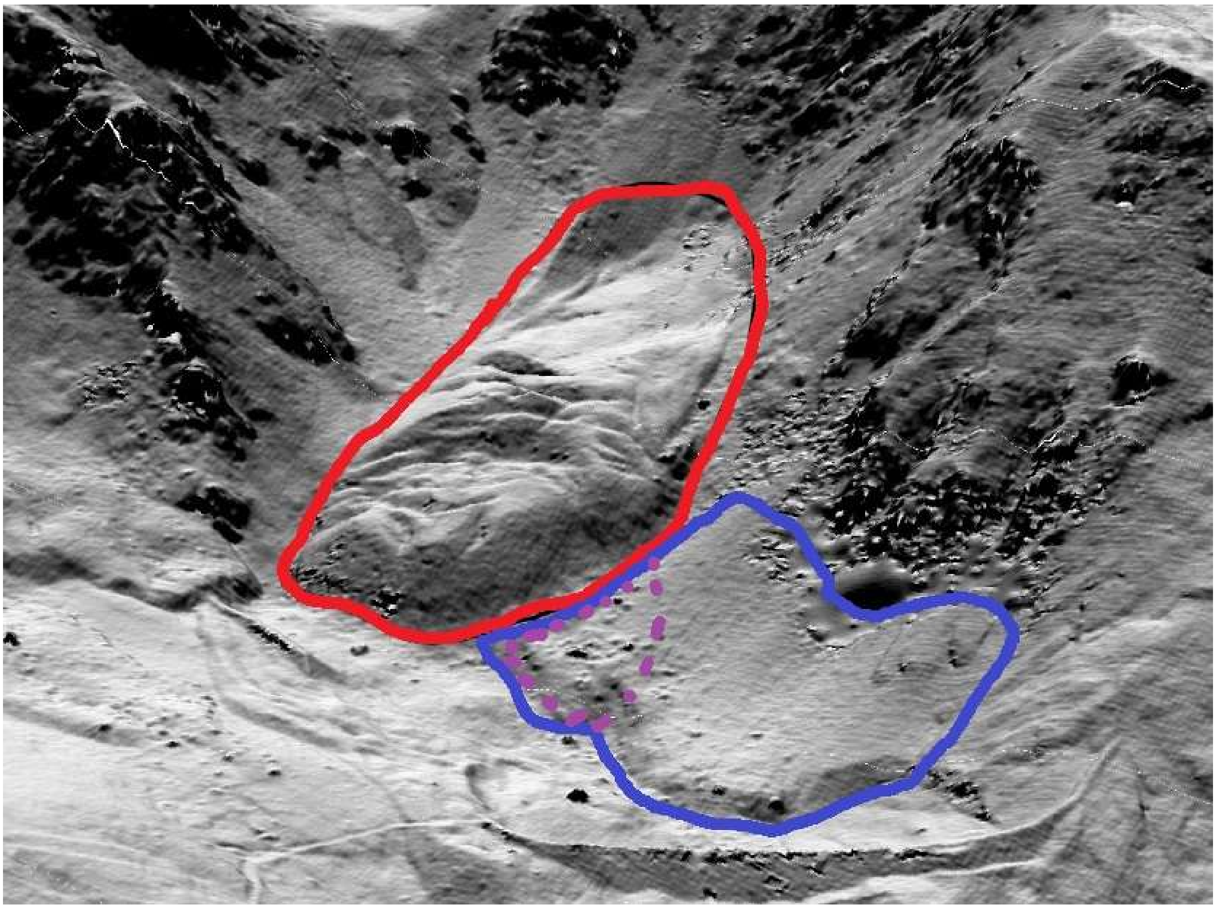

Figure 15: Digital terrain model (DTM) of the Gruob rockglacier. Active rockglacier highlighted in red, inactive rockglacier highlighted in blue, middle lobe highlighted in purple (based on: Nyenhuis, 2005, p. 36)

The active surface with ridges and furrows, and the steep front are in clear contrast to the surrounding area. Next to the active rockglacier there is also an inactive rockglacier (Gärtner-Roer et al., 2013). This inactive rockglacier is directly adjacent to the active rockglacier and can be split into two parts with separated fronts. In this thesis, the part closer to the active rockglacier is referred to as “middle site”. It is distinctive from the rest of the active rockglacier due to its location directly bordering the active rockglacier. Additionally, its geomorphic features with a steeper front and less vegetation indicate more intense or more recent activity than the other part of the inactive rockglacier.

With elevation models and orthoimages, the kinematics of the Gruob rockglacier were reconstructed over the past decades (Steffen, 2025). Like many other rockglaciers, the Gruob rockglacier was classified as destabilized due to thermal and hydrological reasons in this study. Still, the horizontal displacement values of the Gruob rockglacier are distinctly different from other rockglaciers in the area. From 1968, the rockglacier shows increasingly high horizontal displacement. However, there is a clear break between 2005 and 2011, when horizontal displacement is far lower than before (Figure 16).

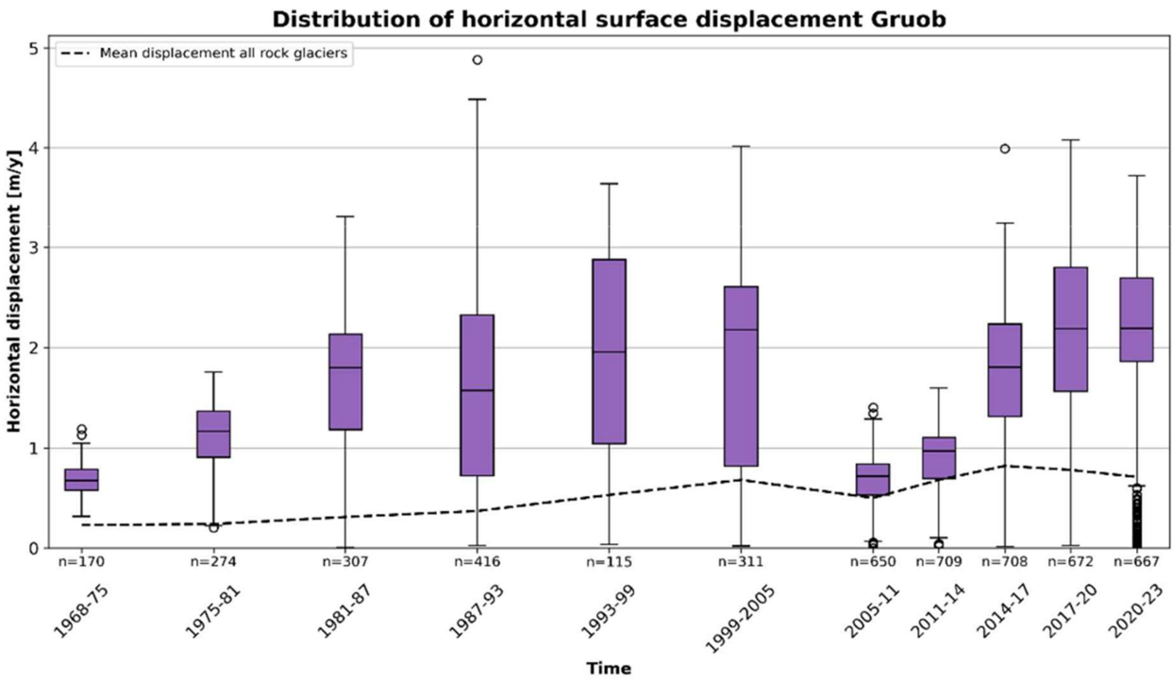

Figure 16: Horizontal displacement values of the Gruob rockglacier 1968 – 2023 (Steffen, 2025, p. 63)

After that, the displacement increases again and has reached the high levels from before this break again. This evolution over time is also visible in Figure 17. The same trend can be observed across the entire rockglacier, especially in the period of 2005 to 2011, when all regions of the rockglacier show very low displacement values. Generally, the upper part of the rockglacier, where the shrub samples were taken for this thesis, is less active than the lower parts of the rockglacier. The trend of high values before 2005, a period of comparably low displacement from 2005 – 2011, and acceleration afterwards is also clearly present in the upper parts of the rockglacier. The creep behaviour is unique compared to the other rockglaciers studied by Steffen (2025). No other rockglacier in the area has yearly creep values of 2 meters over such a long time. Also, the sudden deceleration of this magnitude, followed by an acceleration in creep again, is not found in any other rockglacier.

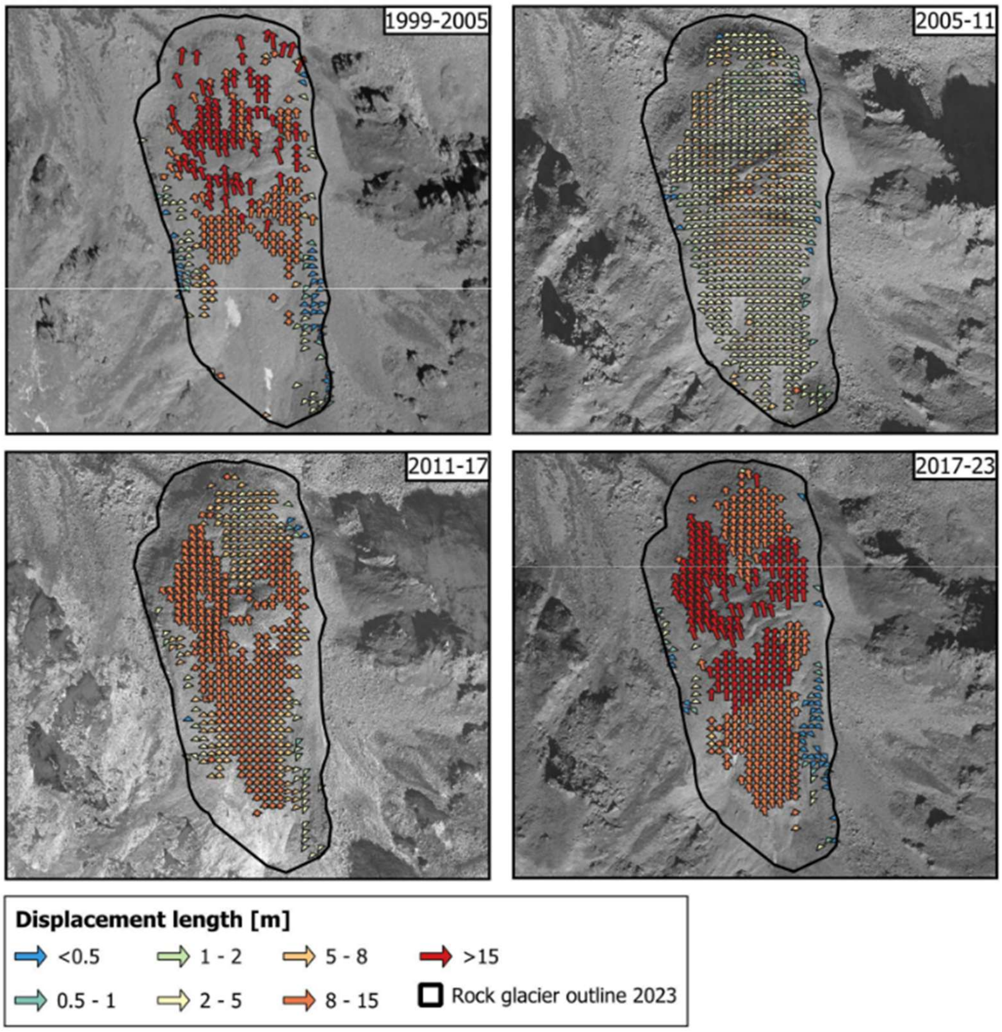

Figure 17: Horizontal displacement on the Gruob rockglacier for four periods since 1999 (Steffen, 2025, pp. 119–120)

4. Material and Methods

4.1 Study Site Selection

The study site was decided on in the early stages of the thesis. The Turtmann valley is known for its extraordinary abundance of rockglaciers (Chapter 3.5). The rockglaciers in the valley are studied well and a lot of information is available on them. For example, there exist analyses of the permafrost distribution (van Tatenhove & Dikau, 1990), comparisons of rockglacier monitoring methods (Roer & Nyenhuis, 2007), a catalogue of all the rockglaciers (Nyenhuis, 2005), monitoring of single rockglaciers (Buchli et al., 2013) and an assessment of rockglacier destabilization (Steffen, 2025). These studies all provide important context for the analysis of the shrub samples in this study. However, the crucial point in the selection of the rockglacier was the presence of shrubs on the rockglacier. Ideally, the rockglacier complex would include rockglacier structures of different activity status (active & inactive). Rockglacier research rarely focuses on the vegetation growing on rockglaciers, so it is not frequently recorded if shrubs are present on a rockglacier. The study by Gärtner-Roer et al. (2013) was the first to apply wood anatomical techniques to detect rockglacier creep. This paper was based on *Salix helvetica* shrub samples taken on active and inactive parts of the Gruob rockglacier. While published over ten years ago, it provides crucial information that shrubs were present on both active and inactive parts of the Gruob rockglacier. Apart from the high likelihood that shrubs are still present on the Gruob rockglacier, it also opens the possibility to compare the results of this thesis with the findings of Gärtner-Roer et al. (2013). While the exact conditions still had to be verified in the field, the Gruob rockglacier was chosen as the primary candidate for the sampling location of this thesis.

4.2 Sampling Strategy

The available data was not sufficient to decide on the exact sampling locations prior to the first field day. Especially on the active rockglacier, it was unclear where and in what quantity *Salix helvetica* shrubs are present. The first field day took place on the 22 July 2025 and was accompanied by my supervisor Dr. Holger Gärtner, Dr. Isabelle Gärtner-Roer and Prof. Dr. Jussi Grießinger.

The aims were to get an overview of the site, decide on the sampling strategy and collect first samples. Before the field day, it was decided to take samples on the active and inactive part of the rockglacier. Additionally, reference samples from a location next to the rockglacier without permafrost influence would be needed. In the field, we also discovered a middle lobe between the active and inactive rockglacier, whose activity state is not entirely clear. The four sampling sites are more closely presented in Chapter 3.1. We decided to include the middle lobe as a fourth site, as it could give insights in transformational activity processes on the rockglacier. With the overall four sites of interest, we decided to sample twelve shrubs per site, which results in a total of 48 shrubs included in the thesis. This number is large enough to show statistical differences between the sites, while maintaining a manageable number of samples to be processed and analysed in the scope of this thesis. At the four sites, samples were taken in three subgroups of four shrubs each (Figure 18). This strategy would offer some potential subgroups in the analysis if differences in the sites themselves would show up. It also ensured that samples would be taken at different spots at the four sites and potential disruptive factors due to micro location influences remain limited.

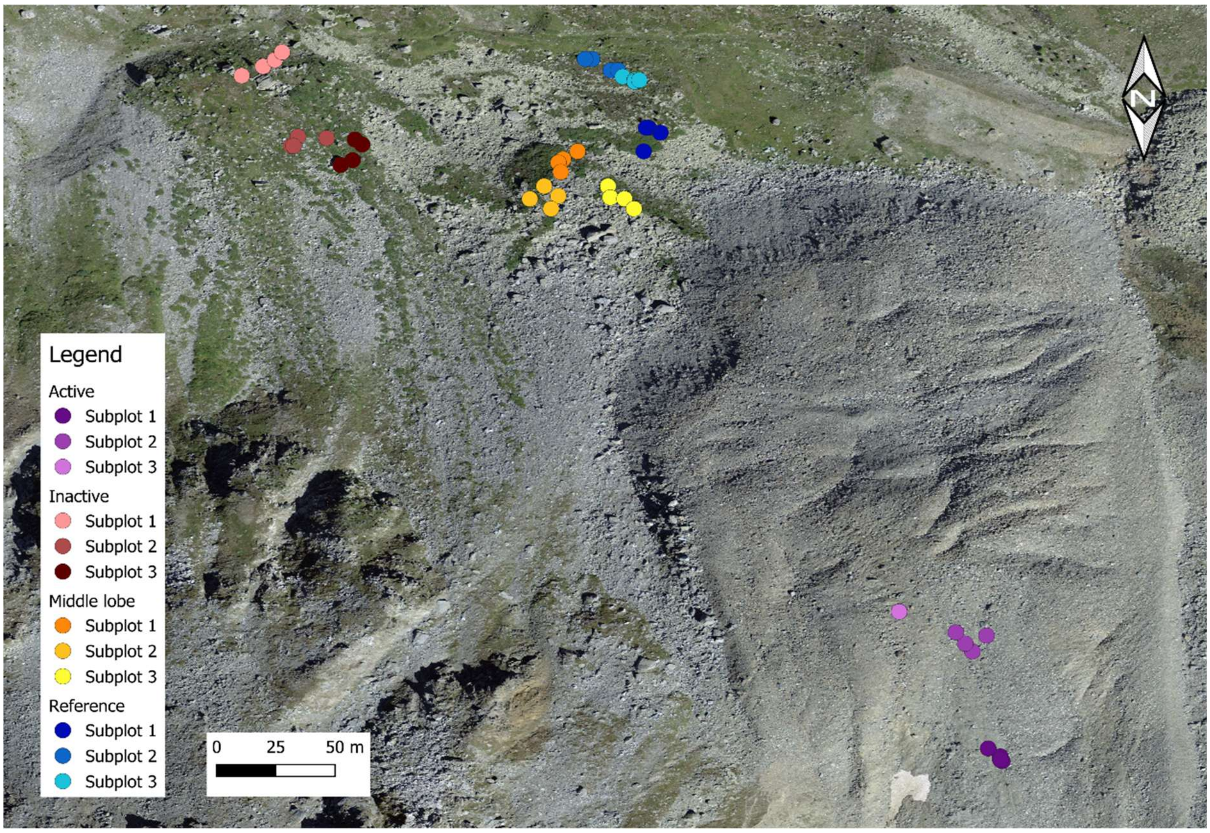

Figure 18: Map of the location of all the sampled shrubs on and around the Gruob rockglacier (Basemap: swisstopo (2026))

The individual shrubs were chosen due to their size and representativeness of the other *Salix helvetica* shrubs in the area. Larger shrubs are expected to be older and of better health than smaller shrubs. Older shrubs offer data further into the past and data from healthy shrubs is not skewed by disturbances. It was decided to collect as much material from the shrubs as possible, so the option remained to analyse different parts of the same shrub later. The collected material would include the main shoot of the shrub, with the main branches and also the main root.

A focus lay on the sampling on the active rockglacier on the first field day, as working on an active rockglacier alone or in a small group can be dangerous due to the unstable surface. The examination of the active rockglacier showed that shrubs and other vegetation are only present on the upper central part of the rockglacier. Compared to the lower parts, the surface is more even there with less ridges and furrows. The material is finer compared to the large rocks and boulders that could be found on other parts of the rockglacier. The different surface structure of this area is well visible in Figure 18. While the active rockglacier has a large area of 86'400 m^2 (Nyenhuis, 2005), the sampling was restricted to this smaller upper section, where shrubs were present. Due to this restriction, the distance to the other sampling location is largest for the active rockglacier site, and they lie at a slightly higher altitude. The active rockglacier sampling site lies at an altitude between 2533 m a.s.l and 2579 m a.s.l, the other sites between 2351 m a.sl. and 2390 m a.s.l. Also, the number of shrubs on the active rockglacier was limited and the choice of suitable shrubs was limited.

The samples at the inactive, middle and reference site were taken during a second field trip starting on the 3. August 2025. On the inactive rockglacier and middle site, *Salix helvetica* shrubs are much more abundant, and it was possible to distribute the subgroups around different places on the rockglacier lobe. Subplots are distributed at different distances from the rockglacier front. However, the shrubs here were considerably larger than the shrubs on the active rockglacier. Identifying the main shoot of the shrub was more challenging and it is possible that the main shoot was not collected in all cases. Additionally, it was not possible to gain access to the roots in all cases. As is visible in Figure 18, the locations of the shrubs for the reference site are all close to each other. The number of suitable shrubs was also limited here for multiple reasons. Compared to the other sites, more other species shrubs and small trees are present here, so *Salix helvetica* shrubs are not the dominant species like at the other sites. Additionally large areas around the Gruob rockglacier were influenced by the construction of artificial dams below the rockglacier. Either directly, where the dams were built, or indirectly, through material transport and the stationing of construction equipment. The areas with visible influence of the construction were excluded, because shrubs growing likely established there after the dam construction in 1999 and the modified ground might influence growth. Additionally, areas further away from the rockglacier are used as pastures for cows, which leads to disturbances that are not present at the other sites, and had to be excluded as well. Due to these restricting factors, only a small area was defined to be suitable as a reference site. Its position close to the rockglacier ensures comparable environmental conditions. However, the possibility that the reference site is also exposed to influences from the rockglacier to some extent through water flow paths or air circulation remains. It must be accepted that the reference site does not represent shrubs growing under controlled or stable conditions. The shrubs growing there are expected to experience the same environmental pressures and changes, while the differing factor to the other sites is the presence of a rockglacier and permafrost.

4.3 Sample Preparation

Most of the shrub samples got cut into disks in the laboratory. Only the largest shrubs were already processed in the field, because they were too large to transport back as a whole. The strategy was to extract multiple disks per shrub, to have more flexibility in later stages of the preparation and analysis. Disks were taken along the main branch and side branches or roots if possible. The most important disk to extract was the one closest to the root, as it is most reliably reflects the age of the shrub (Myers-Smith, Hallinger, et al., 2015). Additionally, sections with bends, emerging side branches or damages were excluded, as it could complicate preparation and distort results. Figure 19 shows two examples of shrubs, where the places to extract disks are marked by tape.

Figure 19: Examples of two shrubs before disks were cut out, the location and label of disks are marked by tape

4.4 Wood Anatomy Analysis

For further analysis, micro-sections of the disks were prepared. For most disks the full cross-sections could be taken because of the small diameter of the disks. The other disks were cut to a processable size, always including the side with the longest radius. A sledge microtome was used to prepare micro-sections with a thickness of about 20 µm (Gärtner et al., 2015). To facilitate the process, the samples were soaked in water before cutting the microsections.

The micro-sections were stained with a combination of Safranin and Astra-blue, which increases contrast and distinguishes between non-lignified and lignified parts of the sample. Further, the micro-sections were rinsed with ethanol and xylol, embedded in Canada-Balsam and dried in an oven for at least 24 hours. Then the slides were taken out to cool down and to ensure the hardening process of the Canada Balsam.

The prepared micro-sections, which were fixed on microscope slides, were scanned by a AXIO Scan.Z1 (ZEISS) scanner. After the scanning, high resolution images of all prepared cross-sections were available for the analysis of wood anatomy (Figure 21). In Figure 20 the main steps in the preparation of micro-section images are shown.

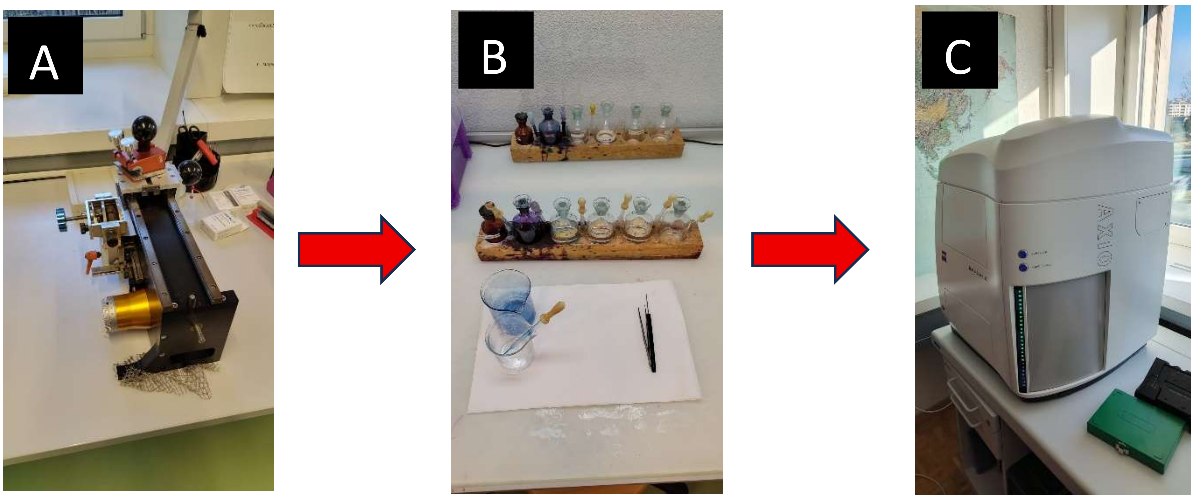

Figure 20: Main steps in the preparation of the micro-sections: A) sledge microtome B) staining station C) slide scanner

Figure 21: Example of one of the micro-section scans on which wood-anatomical measurements were performed

4.4.1 Ring Width

Ring width was measured on the scanned micro-sections of all shrubs. The program CooRecorder (Cybis) was used to manually mark the borders of the annual rings (Figure 22). Ring width was measured on the side with the largest radius. Ring distinction is easiest there and often wedging rings are not present on other sections of the cross-section. Thanks to the thin cross-sections, staining and high resolution of the scans, the tree rings were visually mostly easily distinguishable, despite there being some very thin rings.

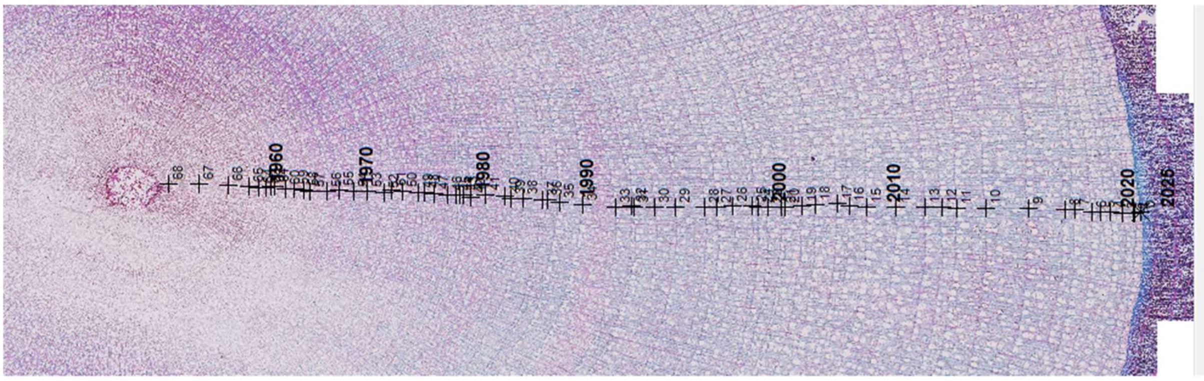

Figure 22: Example of a ring-width measurement in CooRecorder, crosses indicate borders between two rings and the numbers indicate the year the ring was grown

Ring width series are often detrended to account for age-related trends, which are commonly present in trees (Fritts, 1976). For arctic and alpine shrubs different trends have been observed. However, these trends vary greatly between locations and species. It has followingly been suggested that detrending of ring-width measurements in arctic or alpine shrubs should only be applied when trends are clearly evident in the data (Myers-Smith, Hallinger, et al., 2015). The ring-width data of all samples was analysed on a yearly basis, but also in periods and age blocks. The same 10-year blocks were used for the VLA-measurements and to assure comparability between the parameters. The age blocks were used to check for evident age trends. No consistent age trend could be found across sites and followingly, no detrending was conducted.

4.4.2 Crossdating

As a basis for the further analysis, the samples were dated by crossdating. Crossdating ensures that data collected from tree rings can be assigned to specific years or periods across samples from different shrubs or trees. The crossdating was done in TSAP-Win^{TM} (RINNTECH). In the crossdating process, the ring widths of all shrubs are compared to look for similar trends in right width, which can be matched across samples to accurately date the tree rings. Important marker years are especially wide or narrow, and can are caused by environmental or climatic factors all shrubs experienced (Myers-Smith, Hallinger, et al., 2015). The ring width for all samples was collected by the process described in Chapter 4.4.1. Because all samples in this thesis were collected from living shrubs in the summer of 2025, the date of the outermost ring was known for all samples. However, partial or missing rings can be present in alpine shrubs, and by crossdating, they are accounted for. Due to the different conditions at the four studied sites, which lead to different growth patterns, the crossdating was done separately per site.

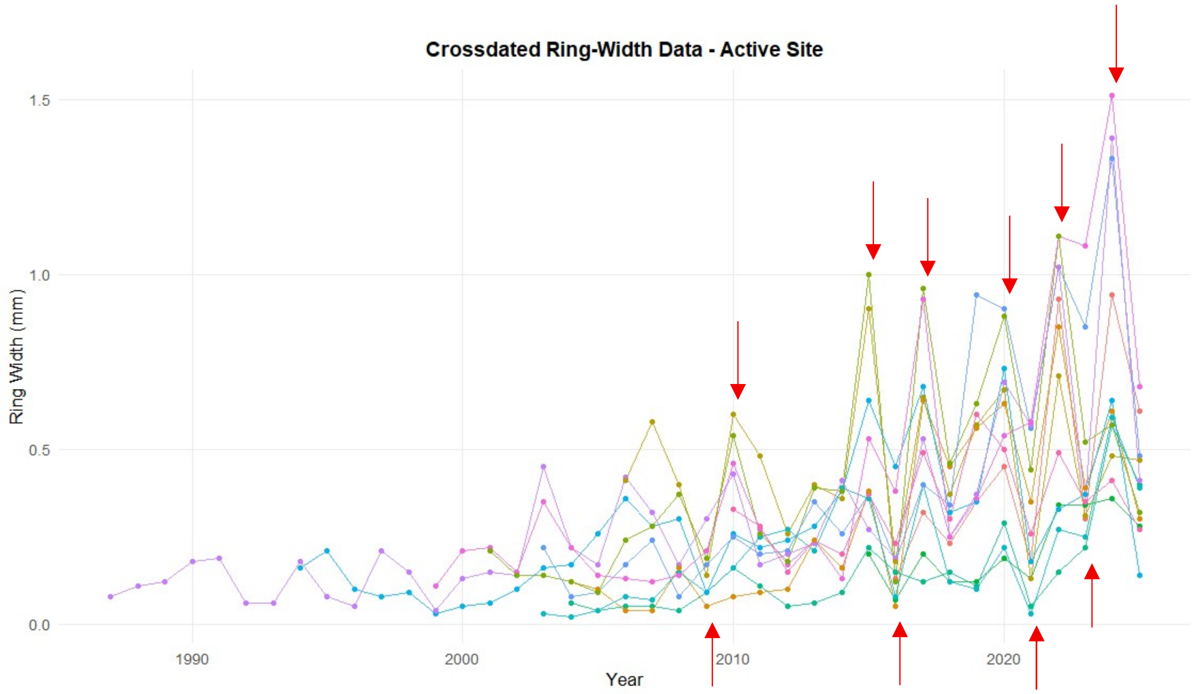

Figure 23: Crossdated ring-width data of the active site, including the data of all shrubs over time, each line represents one shrub, marker years indicated with a red arrow

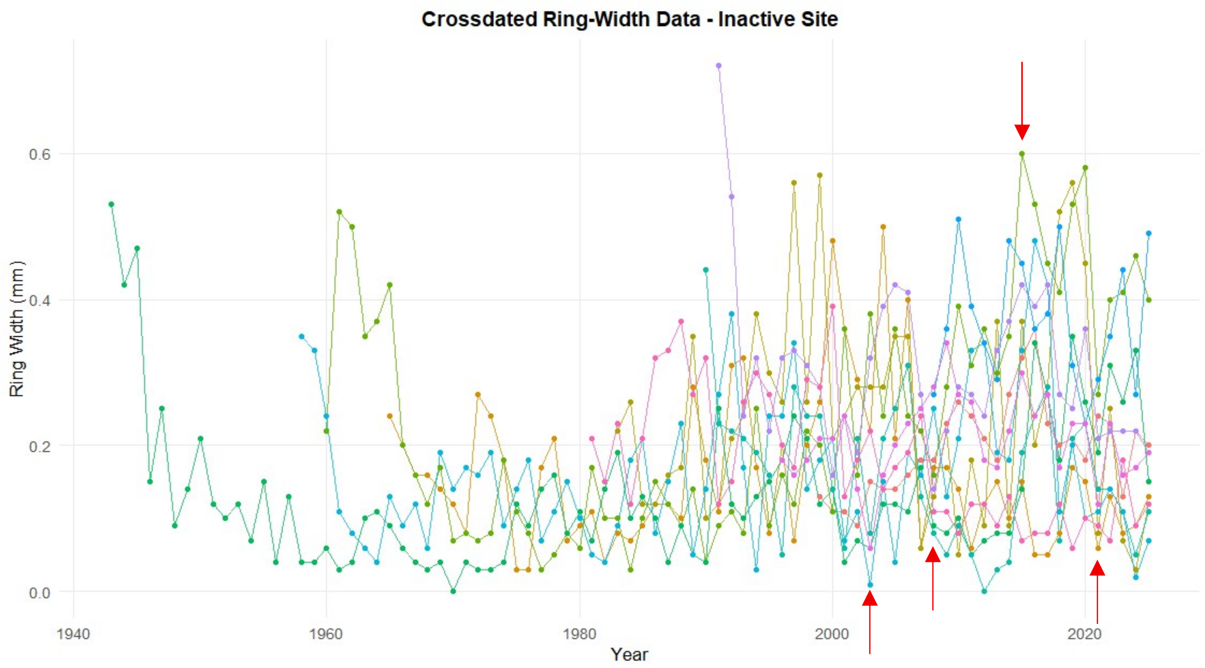

Figure 24: Crossdated ring-width data of the inactive site, including the data of all shrubs over time, each line represents one shrub, marker years indicated with a red arrow

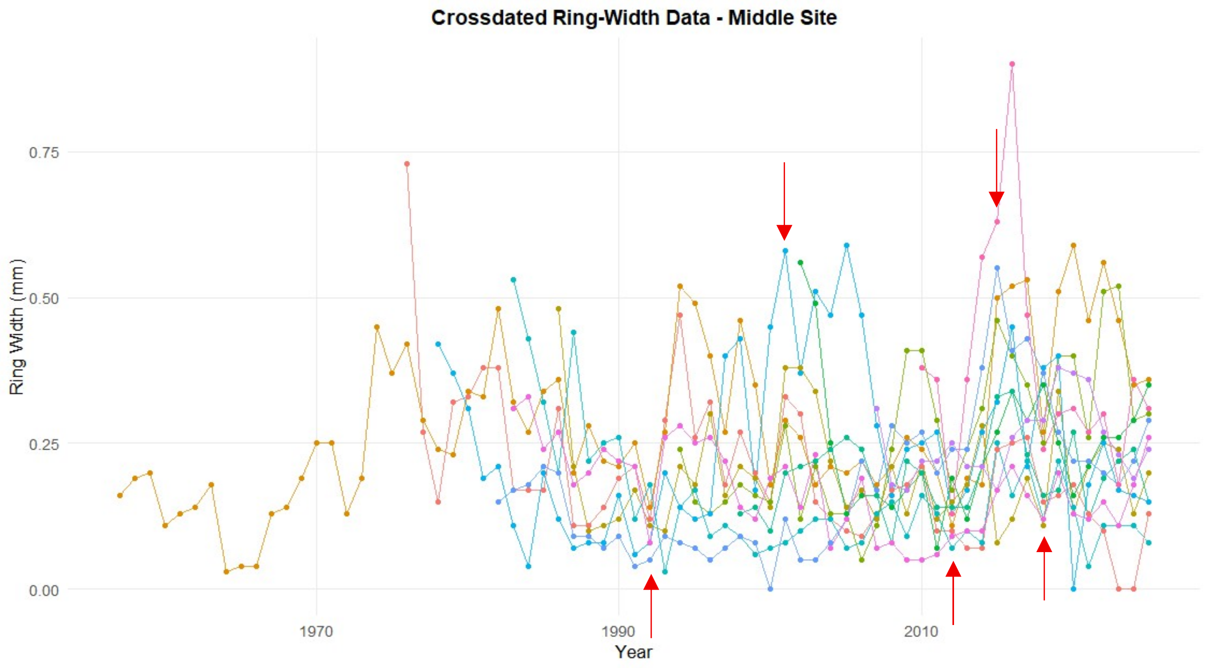

Figure 25: Crossdated ring-width data of the middle site, including the data of all shrubs over time, each line represents one shrub, marker years indicated with a red arrow

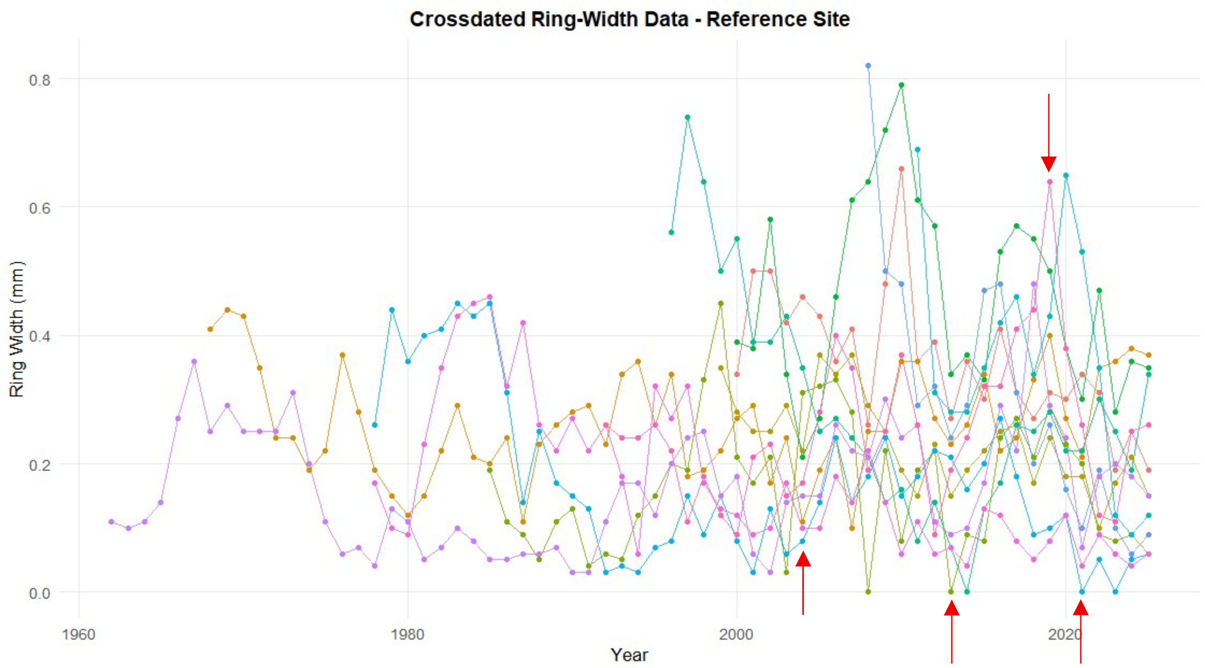

Figure 26: Crossdated ring-width data of the reference site, including the data of all shrubs over time, each line represents one shrub, marker years indicated with a red arrow

At all sites some marker years could be identified, but the above plots show that the different sites behave differently in multiple aspects. The marker years with low or high growth are not the same at the four sites, and the sites show different levels of correlation between individual shrubs. At the active site (Figure 23), practically all years could be identified as marker years, and the growth trends of the shrubs are mostly identical. Consequently, crossdating was very easy at this site, and the dating is of a high accuracy. For the middle site (Figure 25) and reference site (Figure 26), some clear marker years could be identified and matched across all shrubs. Especially the inactive site (Figure 24) was challenging to crossdate as very few common trends can be identified across shrubs. In some cases, mismatching patterns of single shrubs could be resolved with adjustments in the ring identification (Chapter 4.2.2). In cases of unclear ring borders, additional rings could be added when the general pattern pointed towards an additional ring. Completely missing rings are also possible in alpine shrubs, but rings were only added with caution, when not visible in the cross-section. These plots represent the best attempts of crossdating for the four sites, but especially for the inactive site, some uncertainty remains.

4.4.3 Vessel Size

The vessel size measurements were made with the image analysis program WinCELL (Regent Instruments). With this program, different parameters of cells can be automatically measured (Figure 27). A scan of the whole micro-section was not possible, because the program could not compute the large size of the scans. Instead, the widest part of the scan was scanned as a whole, as well as in 10-year blocks defined by the tree rings. The 10-year blocks were calculated by two methods, starting at the outermost and at the innermost ring. Through this method, there were average VLA values for the whole sample, for defined time periods, and for age periods of the shrub. The chosen thresholds were a minimum of 200 μm^2 and a maximum of 10’000 μm^2. The lower threshold of 200 μm^2 was already used in a previous study of VLA on rockglaciers (Gärtner-Roer et al., 2013). This way, the results of this study would be comparable to earlier results, and this threshold proved to be reasonable by testing different values. The upper threshold was only included to prevent measuring mistakes, as no vessels of that size were present. Because of the huge quantity of vessels measured in each cross-section only a superficial quality control was required. Small measurement errors (splitting vessels, counting multiple vessels as one) likely occurred but are insignificant considering the thousands of vessels measured. Average VLA-values were calculated for all measured samples and sections, and boxplots were created to visualize differences between sites, periods and age groups. In Gärtner-Roer et al. (2013) It is mentioned that differences are larger when only looking at the 10 % to 35 % largest vessels. This approach has also been checked with this data, but showed no changes and was thus not followed up on.

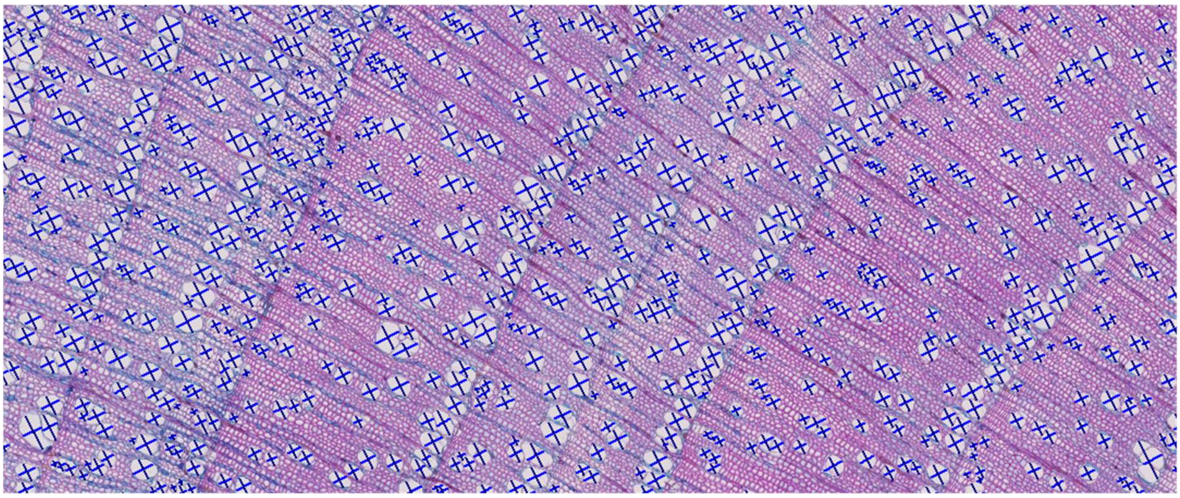

Figure 27: Example of automated vessel-size measurement of a micro-section in WinCELL, recognized vessels are indicated by the blue crosses

4.5 Stable Isotope Analysis

Wood is composed of the three main components cellulose, hemicellulose and lignin. These components all have a different ratio of stable isotopes (Kagawa et al., 2015). In current studies of stable isotopes of trees or shrubs, the common method is to extract cellulose. The climatic signal in cellulose is expected to be clearer, especially when comparing samples of different species and locations, where the ratio of wholewood components can differ (Gray & Thompson, 1977; McCarroll & Loader, 2004). However, this method requires cellulose extraction as an additional time-consuming step in the sample preparation. It has been suggested that the information loss by analysing wood alone is very small, and the advantage to be able to analyse more samples outweighs the slight information loss (Barbour et al., 2001; McCarroll & Loader, 2004). In this study, all the analysed shrubs grow at the same site and are of the same species. Additionally, no individual tree rings were analysed but were rather pooled in samples of at least 10 tree-rings. Analysing every individual ring was not possible due to the time and cost reasons. This method reduced the number of samples and still offered insights in temporal trends. As pooled samples of very similar origin were analysed in this thesis, it was decided that using wholewood samples is sufficient for the aims of this thesis.

4.5.1 Sample Preparation

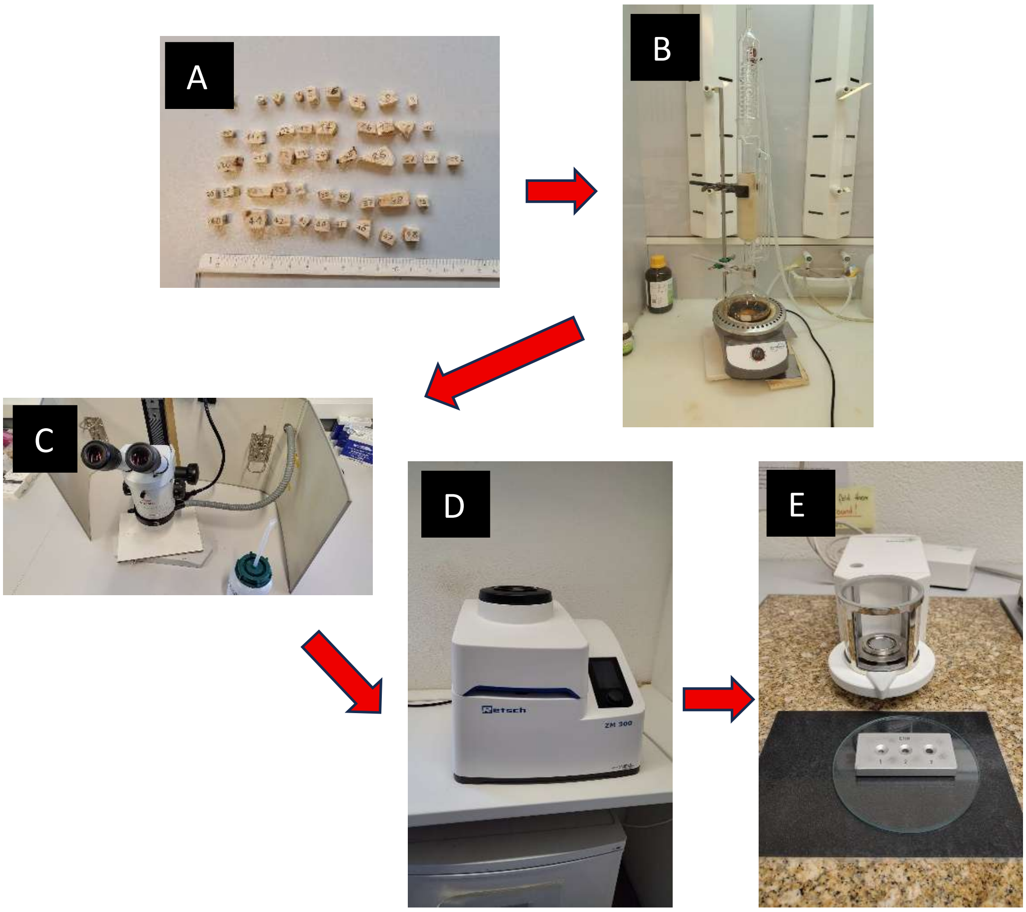

Figure 28: Main steps in the preparation of isotope samples: A) prepared wood wedges of all shrubs; B) Soxhlet for the removal of impurities; C) splitting the sections under a microscope; D) milling to homogenize samples; E) weighing and filling into silver capsules

For the analysis of the stable isotopes in the wood, the same disks were used as for the wood-anatomical analysis. After the micro-sections were cut, the disks were cut in wedges that included all tree-rings on the side with the longest radius. The wedges were cleaned of impurities in a Soxhlet extractor. After this step, the wood material was only touched with nitrile gloves and all surfaces and utensils that came in contact with the samples were cleaned with ethanol before use. After the removal of impurities, the wedges were cut into small chips with a blade. The samples were divided into up to three sections, depending on the number of rings present. The 10 most recent rings, the following 10 rings and the remaining rings were separated. This resulted in maximally three isotope samples per shrub. The wooden chips were then milled into fine powder by a centrifugal mill ZM 300 (Retsch). Between all samples, the machine was cleaned of any remaining powder. The milling was necessary to produce fine powder but also ensured homogenization of the samples. As a final step, 1 mg of powder of each sample was weighed with a MT 5 analytical Microbalance (Mettler-Toledo). The 1 mg of wood powder was inserted into a silver capsule and folded into a small ball, which was the final step in the sample preparation of the stable isotope analysis. Figure 28 shows an overview of the main steps to prepare samples for stable isotope analysis.

4.5.2 Sample Analysis

The stable isotope analysis of the wood samples was conducted at the Stable Isotope Research Centre (SIRC) at the Swiss Federal Institute for Forest, Snow and Landscape Research (WSL) in Birmensdorf according to the method described in Saurer et al. (2025). The previously prepared silver capsules first underwent a high temperature conversion. A Pyrocube (Elementar) with a tube-in-tube reactor and a CO trap that collects the CO at 40°C and releases it at 150°C were used. The isotope ratio mass spectrometer (IRMS) used was a MAT253 (Thermo). $^{18}O/^{16}O$ and $^{13}C/^{12}C$ were calculated from $^{12}C^{18}O/^{12}C^{16}O$ and $^{13}C^{16}O/^{12}C^{16}O$ analysis. $\delta^{18}O$ and $\delta^{13}C$ are calculated followingly:

$$\delta = \frac{R_{Sample} - R_{Standard}}{R_{Standard}} 1000 \qquad \textit{Eq. 5}$$

This results in $\delta^{18}O$ and $\delta^{13}C$ as ratios in permille (‰). The standard reference values SMOW for O and VPDB for C were used. The analytical error (standard deviation) is reported to be less than 0.3‰ for $\delta^{13}C$ and less than 0.2 ‰ for $\delta^{18}O$ (Saurer et al., 2025).

4.5.3 Data Analysis

4.5.3.1 Oxygen

The raw $\delta^{18}O$ values from the laboratory analysis were not processed further for the analysis. Mean values were calculated per shrub, because up to three wood sections consisting of different tree rings were measured per shrub.

4.5.3.2 Carbon

The raw $\delta^{13}C$ data from the laboratory analysis is not corrected for atmospheric change yet. Due to the combustion of fossil fuels, the ratio of ^{13}C to ^{12}C has changed in the past decades. This led to a decrease in atmospheric $\delta^{13}C$, which is known as the Suess Effect (Keeling, 1979). To correct for the change, the following calculation was performed:

$$\delta^{13}C = \delta^{13}C_{wood} - \left(\delta^{13}C_{atm(year)} - \delta^{13}C_{atm(ref)}\right) \qquad \textit{Eq. 6}$$

As a reference point, δ^{13}C of the year 1850 was chosen, which interpolates the data to a pre-industrial atmosphere. The wood samples that were analysed in this thesis include material from multiple tree rings. Correcting the raw δ^{13}C values for a single year is not possible. Instead, averaged values of all years that were represented in a block were calculated. Data series from different sources show minor discrepancies in the values per year. To obtain a consistent dataset, the interpolation method from Ferrio et al. (2005) was used. The data for the interpolation consists of datasets by Cleveland (1978), Indermühle et al.(1999), Leuenberger et al. (1992) and White et al. (2015). The trends of atmospheric CO_2 and atmospheric δ^{13}C over time are visualised in Figure 30.

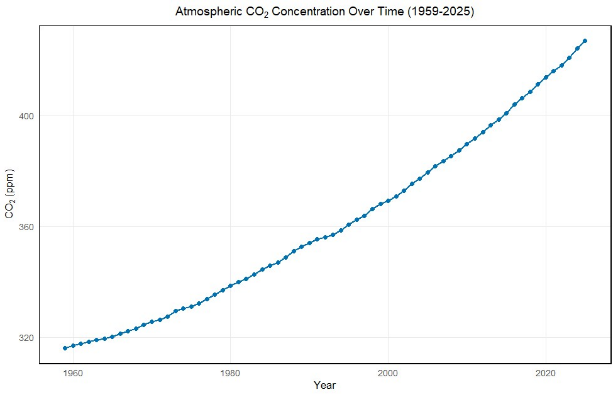

Figure 30: Atmospheric CO_2 in parts per million (ppm) over time (1959-2025), data used for atmospheric correction (Keeling et al., 2001)

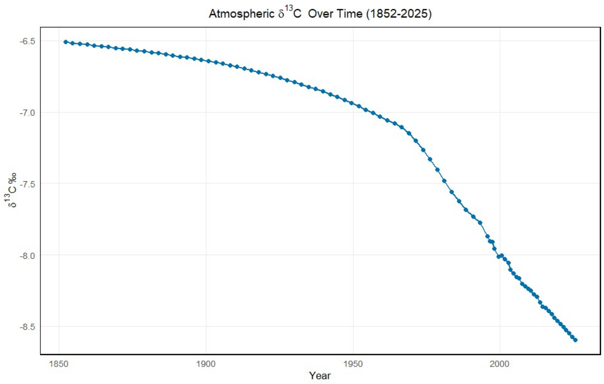

Figure 30: Atmospheric δ^{13}C over time (1852-2025), data used for atmospheric correction (Ferrio et al., 2005)

To calculate iWUE and related parameters, the equations introduced in Chapter 2.3.2 were used.

$$\Delta^{13}C = \frac{\delta^{13}C_{atm} - \delta^{13}C_{wood}}{1 + \delta^{13}C_{wood}/1000} \qquad \textit{Eq. 7}$$

To calculate $\Delta^{13}C$, the atmospheric δ^{13}C averages for the blocks were used again. With $\Delta^{13}C$ known for all samples, c_i/c_a can be calculated with the following formula. As introduced in Chapter 2.3.2, *a* and *b* are treated as constants with values of 4.4‰ and 27‰ respectively.

$$\frac{c_i}{c_a} = \frac{\Delta^{13}C - a}{b - a} \qquad \textit{Eq. 8}$$

Given c_i/c_a, iWUE can be calculated. However, c_a has to be known. As with the atmospheric δ^{13}C, also CO_2 concentration in the atmosphere has changed due to fossil fuel emissions. Due to its long data series, the measurements on Mauna Loa were chosen for correction (Keeling et al., 2001). Yearly average of seasonally adjusted monthly data was calculated and the averages of the same yearly blocks as described earlier were calculated.

$$iWUE = \frac{A}{g_s} = \frac{c_a(1 - c_i/c_a)}{1.6} \qquad \textit{Eq. 9}$$

By rearranging Equation 9 c_i can be calculated with the followingly:

$$c_i = c_a \frac{\Delta^{13}C - a}{b - a} \qquad \textit{Eq. 10}$$

4.6 Visualization and Statistical Analysis

All measured and calculated parameters are checked both visually with the help of boxplots and with statistical tests. RStudio (Posit PBC) was used for the creation of all plots and to calculate statistical values. The data was generally visualized as mean values of 10-year blocks to facilitate comparisons between wood anatomy and stable isotopes. To avoid assumptions of normality, non-parametric tests were used throughout. Differences between sites during the same time period were assessed using Kruskal-Wallis tests and followed by pairwise Dunn post hoc tests to compare sites pairwise. Temporal differences within sites to compare periods were analysed using paired Wilcoxon signed-rank tests. This test compares values of the same individual shrubs and accounts for changes in individual shrubs across time. The sample size is restricted by the period with the lowest number of observations, which can limit significance. Visual interpretation of temporal trends is critical alongside the statistical values to account for small samples sizes. Significance is reported through p-values with a significance level of $p < 0.05$. The colour scheme used in plots was proposed by Okabe and Ito (2008) and is designed to be colour-blind friendly.

Due to the given time resolution of 10 years in the pooled stable isotope samples, VLA and right width are also analysed as mean values in the same time periods. As the number of periods was not restricted by the methodology, data from before 2006 could still be split in periods of 10 years. Due to this these slightly different approaches all years before 2006 are summarized in the group <2006 for the stable isotopes, but VLA and ring width is still visualized in 10-year periods. Additionally, VLA and ring width were also analysed in age groups of 10 years, where the innermost ring was chosen as zero point instead of the outermost.

5. Results

5.1 Wood Anatomy

5.1.1 Vessel Lumen Area

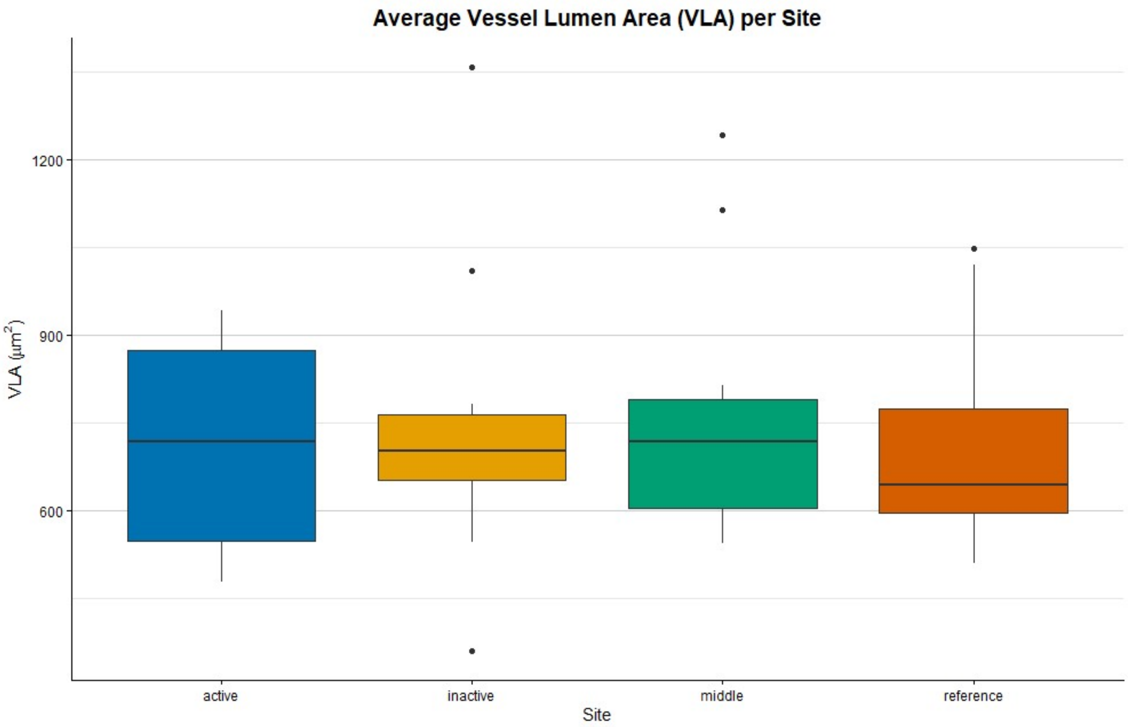

Figure 31: Boxplot of the average Vessel Lumen Area (VLA) per shrub at the four study sites

The average VLA of the studied shrubs over all periods is similar at all sites (Figure 31). The median values are close together at all four sites, with the reference site showing the lowest median. The active site has a median value of 718 µm², the inactive 703 µm², the middle 717 µm² and the reference 643 µm². The differences are not statistically significant, and all the sites have overlapping ranges. At all sites the bulk of values lies between 600 and 900 µm². The active site shows the largest differences between the lower and upper quartile.

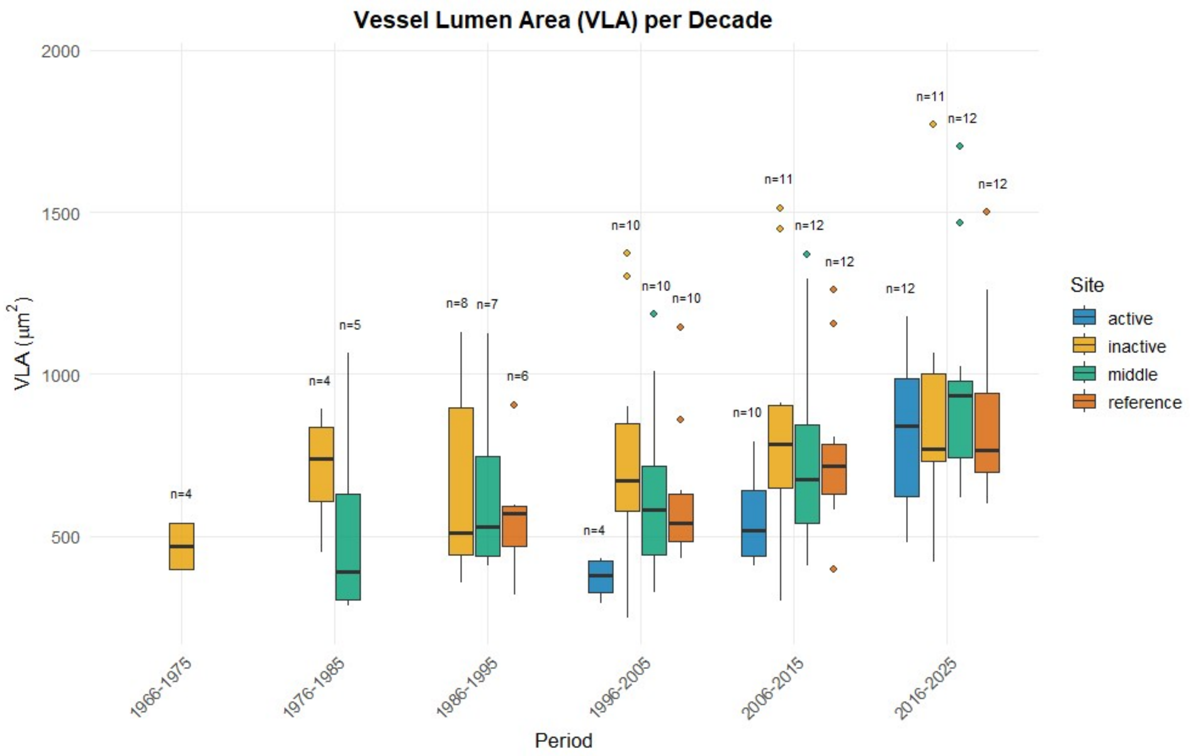

Figure 32: Boxplot of the average Vessel Lumen Area per decade for all four study sites, sample size indicated above each box

Figure 32 visualizes the VLA values of the four examined sites for the different time periods. Sample size for the different sites varies, because it is dependent on the age of the shrubs at the respective site. Boxes where less than four datapoints (shrubs per site) exist are not displayed in the figure, because the sample size is too small to draw valuable conclusions. All sites display widespread data, and outliers are frequent. Despite that, over the last three decades, a clear visual trend to higher values is present at all sites. This increase over time is significant at all sites, except for the inactive site between 2006 – 2015 and 2016 – 2025. The trend exists at all sites, but the gradient is visually steepest at the active site. Due to the small sample size of the active rockglacier in period 1996 – 2005, the increase is not statistically significant. However, at the active site, the increase of the median value from 380 µm² in the period 1996 - 2005 to 841 µm² in the period 2016-2025 is an increase of 121%. The maximum increase at any other site is 61% at the middle site. Also, in the earlier periods a trend to higher values is visible when looking at the median values of the sites with sufficient data. The high median of 738 µm² at the inactive site in the period 1976 - 1985 is an outlier in this trend. In the period 1996 – 2005, the VLA values are significantly lower than the three other sites. In the period 2006 – 2015, the box of the active site already shows an overlap with the middle site but is still significantly different to the inactive *(p= 0.0095)* and reference *(p=0.035)* sites.

In the most recent period 2016-2025, all four sites exhibit a similar range of values and no significant differences between sites are present. This period resembles the aggregated data in Figure 31 the most.

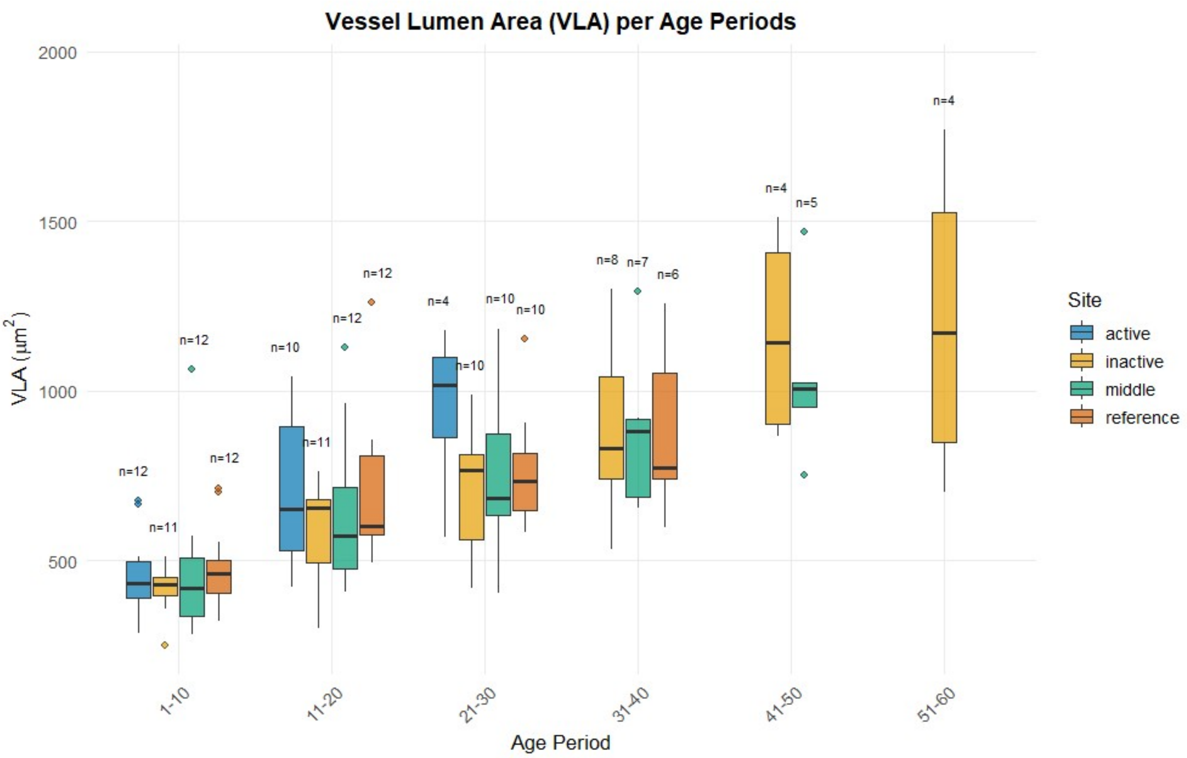

Figure 33: Boxplot of the average Vessel Lumen Area (VLA) per shrub age for all four study sites, sample size indicated above each box

Figure 33 visualizes how VLA changes based on the age of the plants. The x-axis indicates the age groups. All periods include the vessel data of ten annual rings. While containing the same data as Figure 32, this figure does not compare vessel sizes of the same decades, but related to their relative age group in years instead. The age groups have been created starting at the innermost ring, while the decadal groups start at the outermost ring and are created backwards. There is a clear positive trend at all sites, with linearly rising values over time. The increase per period in the first three age groups is significant at all sites. An exception is the period 21 – 30 at the active site, where no significant level could be reached due to the sample size. The sites generally remain in similar ranges, with increasing ranges of values. The outlier site is the active site. The first period is in accordance with the other sites. The second period already shows a trend to higher values in the upper percentiles, while not being significantly different. At period 21 – 30, the values on the active site do not follow the linear trend of the other sites anymore. The VLA-values are visually clearly higher than the other three sites.

Surprisingly, the Dunn-test does not show any significant differences between sites at any of the first three periods, including the active site in period 21 – 30. It must be considered that the sample size has an impact on the p-value. Other metrics like the median, upper and lower quartile are clearly the highest at the active site in the age period 21-30. For example, the median value of 1017 µm² is only surpassed by the inactive site at the age brackets 41 – 50 and 51 – 60. This is higher than any median values in Figure 32. Due to the different data structure in Figure 33, sample size decreases in the upper age groups, and high-VLA samples have relatively more weight than in Figure 14.

5.1.2 Ring Width

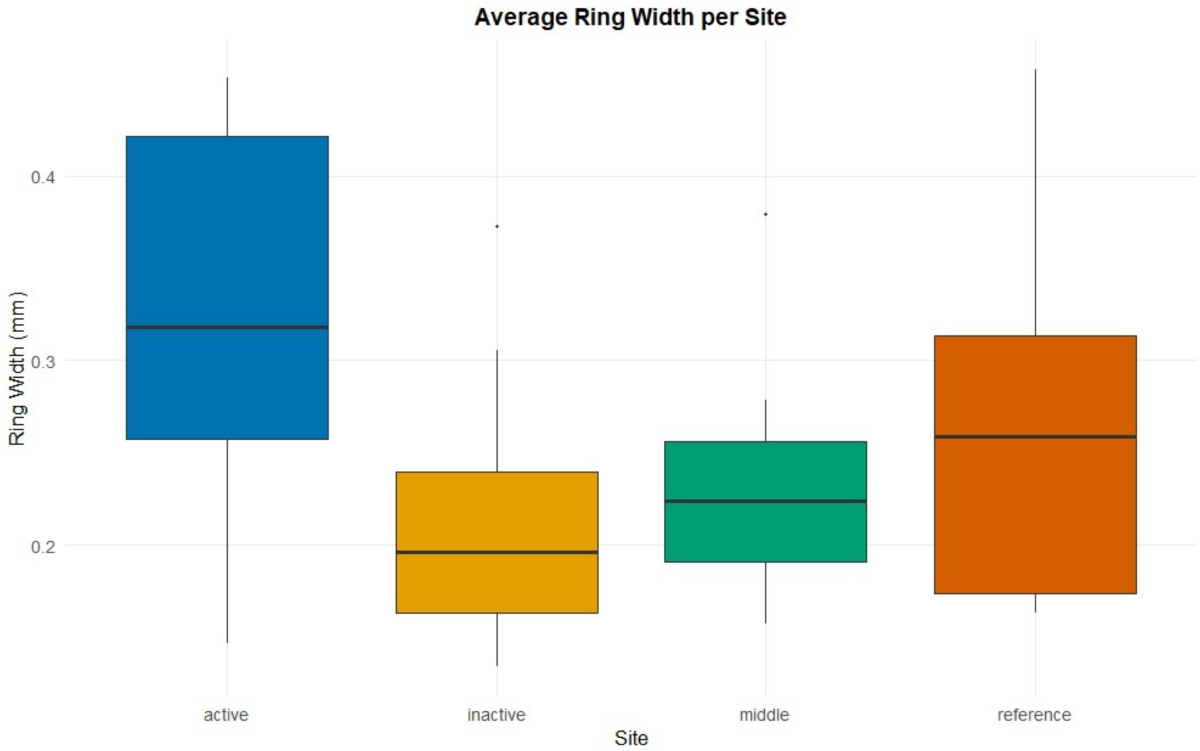

Figure 34: Boxplot of average ring width at the four study sites

Figure 34 shows the average ring width of the sampled shrubs per site. It clearly indicates that the median ring width of 0.32 mm is larger on the active rockglacier compared to all other sites. The difference is significant compared to the inactive *(p=0.0021)* and middle *(p= 0.013)* sites. While the maximum value at the reference at active site is almost the same, the upper quartile at the active site has a value of 0.42 mm, compared to only 0.27 mm at the reference site and even lower values at the other two sites. The minimum values are close to 0 at all sites, as very thin rings are present at all sites. The inactive, middle and reference site have overlapping values, with the reference site having the largest range of values and the highest absolute values of these three sites.

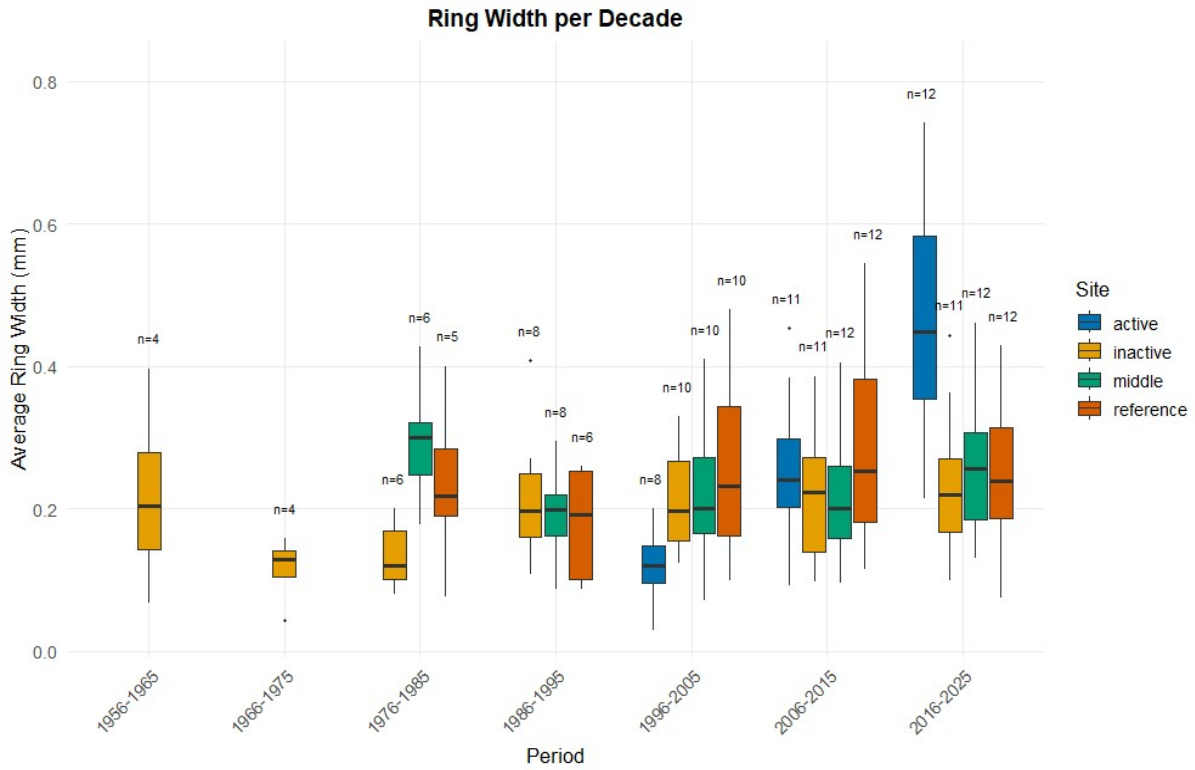

Figure 35: Boxplot of average ring width at the four study sites over time, sample size indicated above each box

Figure 35 visualises the average tree-ring width of the samples at each site for 10-year periods. Values are only visualized if data from at least four shrubs is available for the site during this period. The inactive, middle and reference site all behave comparable over time. In the latest four periods, no differences are visible between those sites or between the different periods. Looking the earlier periods, some common trends are visible. The first visualized period of all these three sites has higher values (1956 – 1965 for inactive site, 1976 – 1985 for middle and reference site) than the decade afterwards. Afterwards, a small but gradual increase of values is observable at all those sites. For the early periods, it must be considered that less datapoints are available, so the uncertainty in those early periods is higher. The whiskers indicate large variance of data for all sites during the later periods. For the active, site no values could be displayed for the earlier periods because none or too little data is available due to younger shrubs. The most striking observation in Figure 35 is the evolution of the tree ring width at the active site. During the period 1996 – 2005, it has the lowest values of all sites, but the difference is only significant for the reference site *(p= 0.036)*. Taking an isolated view at period

2006 – 2015, no differences between any site are observable, with mean, maximum and minimum ring width being close together at all sites. A big shift then takes place from period 2006 - 2015 to period 2016 - 2025. The active site now clearly has the highest values of all sites, and significantly higher values than during the previous two periods. The median value is 0.44 mm, compared to 0.13 mm during period 1996 - 2005. This is an increase of 213 %. However, the range is very broad, with a minimum value of 0.22 mm and a maximum value of 0.74 mm. Despite that, the active site is significantly different to all other sites in that period. The other sites also have a large range of values during period 2016 - 2025, but not to the same extent as the active site. As with the VLA data (Chapter 5.1.1), it must be considered that the active site has less values (n=8) during the period 1996 - 2005 than in the period 2016 – 2025, when all sites have the maximum number of values. Comparing the averaged values of Figure 34 with the more detailed values of Figure 35, it becomes clear that while differences are present between the active site and the other sites, those mainly arise in the most recent 10 years. The trend has existed before, but to a lesser extent.

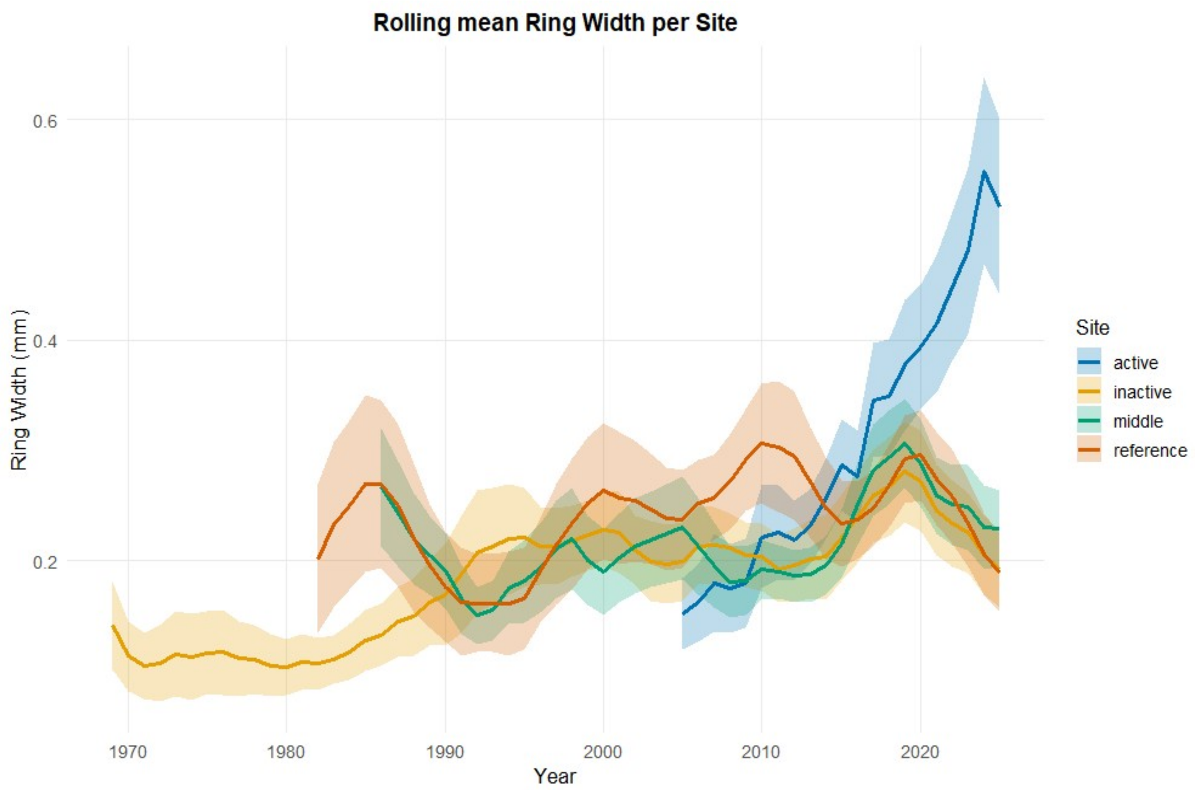

Figure 36: Rolling 5-year mean of tree ring widths at the four sites for years with n ≥ 4 with standard deviation buffer

The same trend is visible in Figure 36, where the rolling 5-year mean of tree-ring width is displayed. The rolling mean was calculated as an average of the current and the four preceding years of each site. It must be considered that the samples were taken during the vegetation period of 2025, so the tree rings of that year were not fully developed yet. In the last 10, years the active, inactive and middle site show the same trend of first rising and then falling values. The active site is not following the same trend but is rising continuously and strongly. Figure 36 also shows that tree-ring width has not been as constant at any site as Figure 35 might suggest. There are regular phases of higher and lower growth, which are often synchronous at multiple sites. The aggregation in 10-year blocks in Figure 35 led to an evening out of these variations. The extent of these variations is also overshadowed by the huge increase of growth at the active site in the past decade.

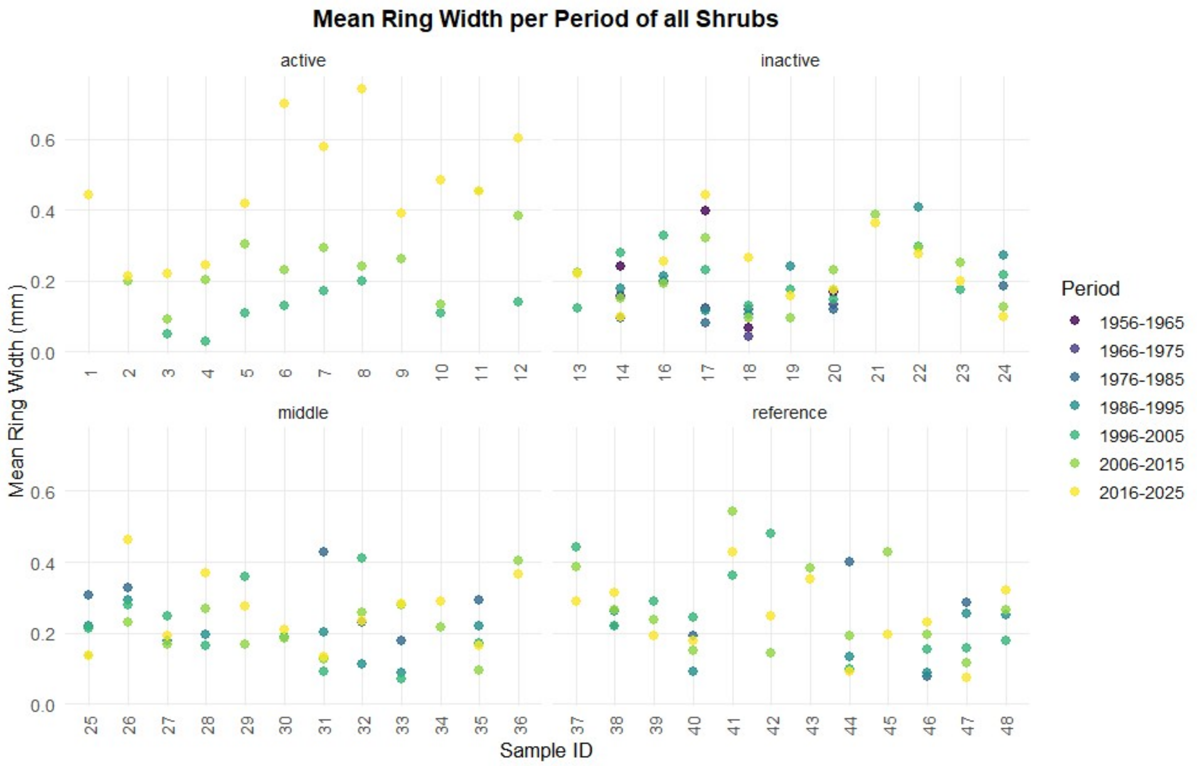

Figure 37: Point plot of mean tree-ring width per decade of all sampled shrubs, Sample ID indicates the individual shrubs

Figure 37 visualizes mean values for each decade in all sampled shrubs. This visualization gives an insight how values behave in individual shrubs. The inactive, middle and reference site have more points because the shrubs there tend to be older (Figure 38). While being very close together sometimes (shrubs 3 and 7), the data points at the active site are without exception in the same order, with increasing average ring width over time. This clear ordering cannot be seen at any other site, even when only looking at the data from the most recent three decades. The order visually seems random, without recurring patterns between sites or shrubs.

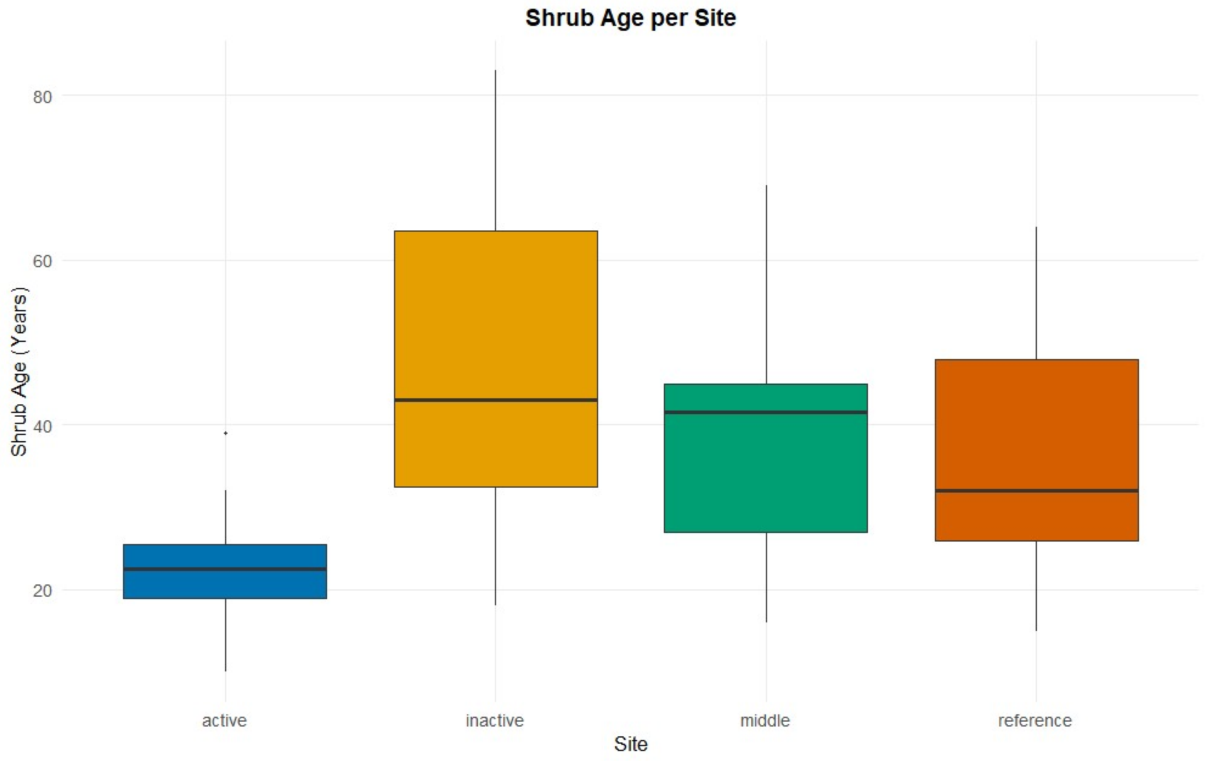

Figure 38: Boxplot of the number of rings per shrub at the four sites

The different age of the shrubs must be considered in the analysis of the results. Figure 38 visualises how big age differences between sites are. The active site clearly has the samples with least amount of tree rings. The median number of tree rings is 22 at the active site, 32 at the reference site, 41.5 at the middle site and 43 at the inactive site. Also, the maximum values differ largely between the sites. Even with an outlier of 39 tree rings, the active site has the lowest maximum value by far. The absolute maximum is reached at the inactive site, where a shrub with 83 tree rings was recorded. The middle and reference site reach maxima above 60 as well. The active site does not only have the shrubs with the least tree rings, but the standard deviation is also the lowest.

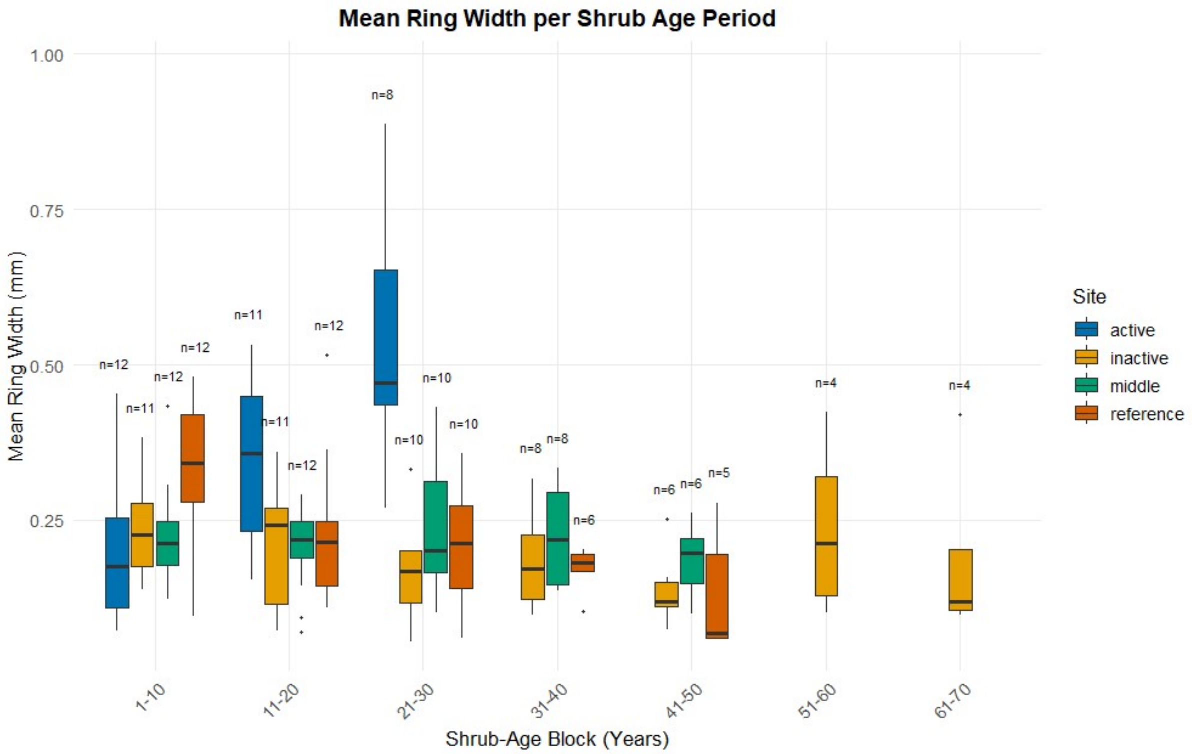

Figure 39: Boxplot of the mean ring width of shrubs in age brackets at the four sites, sample size indicated above each box

Figure 39 serves as a different visualization of the same data as in Figure 35. Because the number of tree rings varies a lot between the sites, the periods in Figure 35 include data of differently aged shrubs. Figure 39 can show if the trends over time could also be influenced by an underlying age effect, which has varying effects on the sites because of the different age distribution. Again, the active site behaves differently from the other sites. The values are rising significantly with each period, and it clearly has the highest values of all sites during the age periods 11-20 and 21-30. The other sites do not show any indices that would point towards a general age trend. The values are stable or slightly declining with time at the inactive and the middle site. Variation is small, with median values ranging from 0.14 mm to 0.24 mm at the inactive site, and 0.2 mm to 0.22 mm at the middle site. The reference site shows a decline of average ring width over time. Especially from age period 1-10 to 11-20, the difference is considerable. After that, the ring width is still decreasing, but at a lower rate. Overall, Figure 39 mostly mirrors the values from Figure 35, with some shifts on the x-axis due to differences in the number of tree rings at the four sites.

5.2 Stable Isotopes

5.2.1 Oxygen

5.2.1.1 $\delta^{18}O$

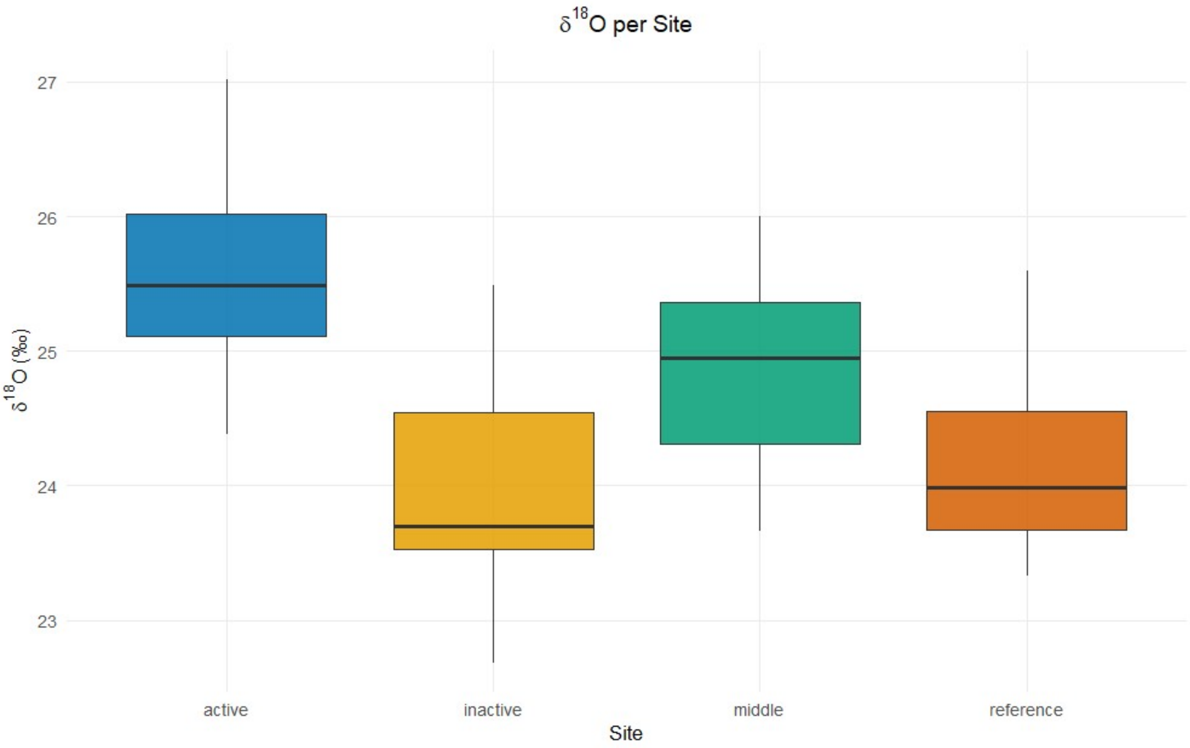

Figure 40: Boxplot of the mean $\delta^{18}O$-values of shrubs at the four studied sites

$\delta^{18}O$ was measured in all samples for all three periods, provided the shrubs had enough tree rings. Figure 40 visualizes the mean $\delta^{18}O$ values of each shrub. The inactive site and the reference site have very similar median values, with 23.70 ‰ for the inactive site and 23.99 ‰ for the reference site. Also, the value ranges at these two sites are almost the same. The active site has significantly higher values compared to the inactive site *($p=0.00027$)* and reference site *($p=0.00072$)*. The middle site is only significantly different to the inactive site *($p=0.034$)*. However, it seems visually clear that the middle site has values which lie in the gap between the high values of the active site and the low values of the inactive and reference site. The spread of values is comparable at all sites with similarly sized boxes and whiskers.

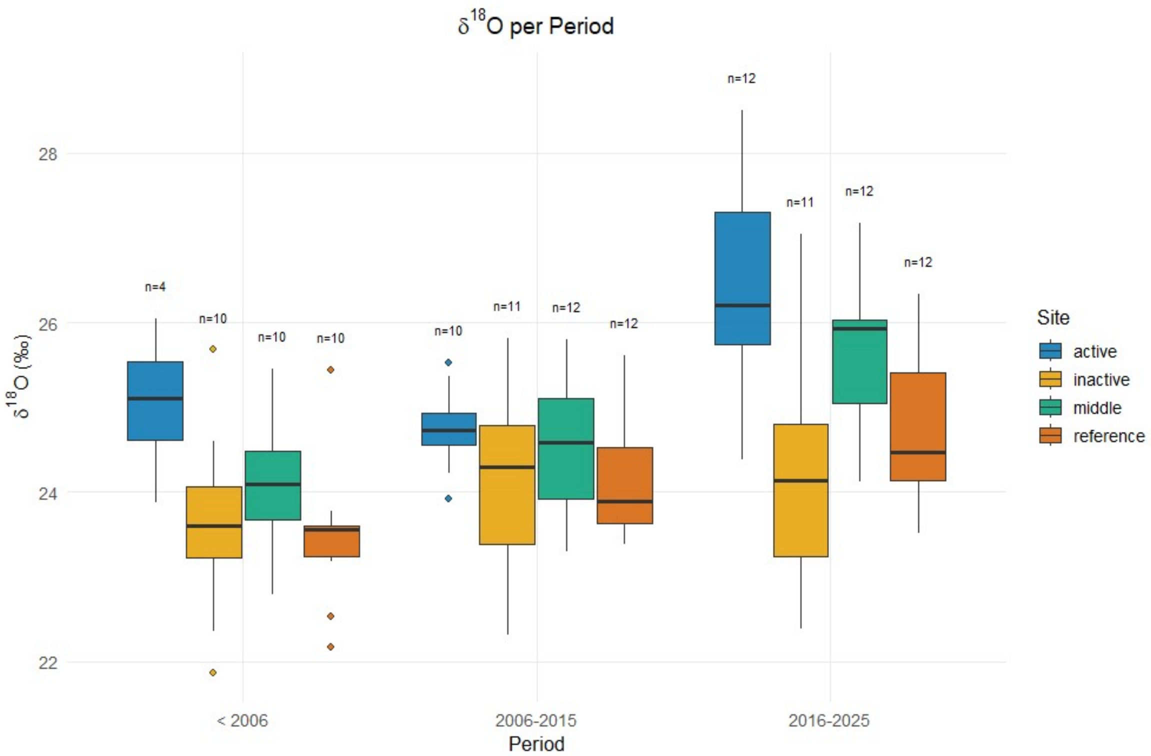

Figure 41: Boxplot of $\delta^{18}O$ values at the four sites during the three analysed periods, sample size indicated above the respective boxes

Looking at the distribution of the data across different time periods shows additional differences and trends. Overall, the mean values rise over time at all sites, with a few exceptions. At the active site, the values fall slightly from the period < 2006 to the period 2006 - 2015, before they rise significantly in the period 2016 - 2025. At the inactive site, there is a rise between the earlier two periods, before there is a slight decrease in the period 2016 – 2025. As the aggregated data in Figure 40 suggested, the active site also has the highest mean values across all individual periods. However, the magnitude of the difference varies highly. In the period < 2006, the active site has significantly higher values than the inactive site *($p=0.026$)* and reference site *($p=0.0085$)*. The middle site also has lower values, but significance is not reached. During the period 2006 – 2015, all sites move closer, and the only difference that remains significant is between the active and reference site *($p=0.049$)*. The most differences between sites can be observed during the period 2016 – 2025, where the active site has considerably higher values than the inactive *($p=0.0001$)* and reference site *($p=0.0016$).* The middle site clearly has higher values than the reference and especially inactive site, but is not significantly different from the active site. Also, the other sites differ more with significant differences between the inactive and middle site *($p=0.0057$)*, and between the middle and reference site *($p=0.041$)*. During all three periods, the active site has the highest median value, and the middle site has the second highest mean values, so the order observed in Figure 40 remains consistent during all three observed time periods, but with different magnitudes of differences. In the period 2016 – 2025, differences between sites are the largest, and in the period 2006 – 2015, the values of all sites are close together. The first period < 2006 lies between those two extremes considering the magnitude of differences between sites. The reference site shows the smallest change over time, with no significant differences between periods. The reference site has a significant rise of values between the first and middle (p=0.0019) and between the middle and most recent (p=0.012) period. For the active and middle site, significant rises only happen towards the most recent period 2016 – 2025.

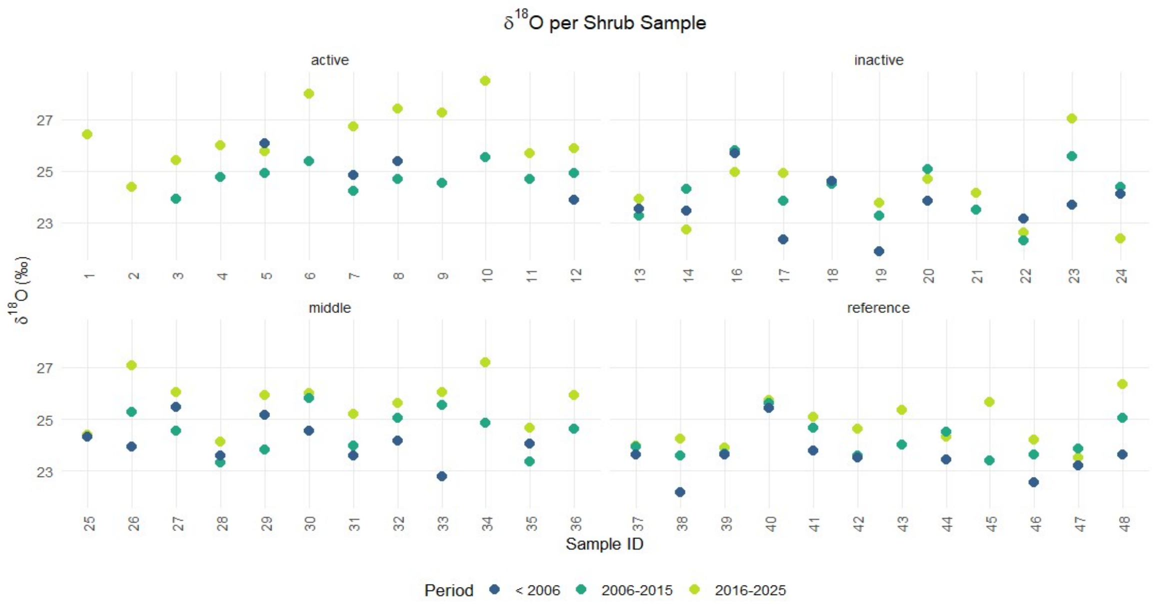

Figure 42: Point plot of δ^{18}O-value per decade of all sampled shrubs, Sample ID indicates the individual shrubs

The positive trends at different sites are confirmed in Figure 42. At the active site, the period 2016 – 2025 has higher values than the periods 2006 – 2015 and < 2006 for all shrubs with multiple values except shrub 5, where < 2006 has the highest value. Also, at the middle and the reference site the period 2016 – 2025 consistently has the highest values. At the inactive site, the temporal order of the values per shrub is least observable, which underlines again that the inactive site does not show a clear trend to higher values over time like the other sites.

5.2.2 Carbon

5.2.2.1 $\delta^{13}C$

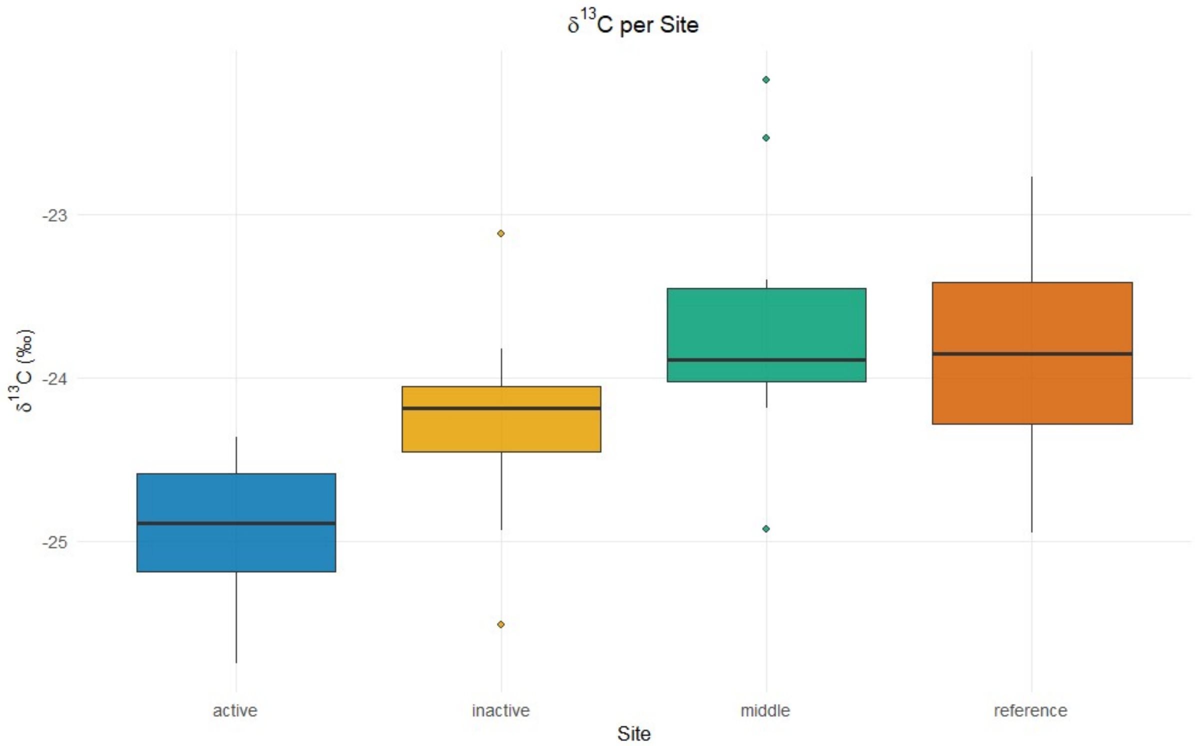

Figure 43: Boxplot of the average $\delta^{13}C$ values at the four analysed sites

Figure 43 gives an overview of the average $\delta^{13}C$ values per shrub at all sites. The median values lie in the range of a minimum of -24.89 ‰ at the active site and a maximum of -23.85 ‰ at the reference site. The active site has lower values than the other three sites. The differences to the middle *(p= 0.00004)* and reference site *(p=0.0004)* are highly significant, and the difference to the inactive site (p=0.026) is also significant. The inactive site has the second lowest values, but it is not statistically significant to the middle or reference site. Generally, the differences between sites are not very large, with a maximum of 1 ‰ difference in median values.

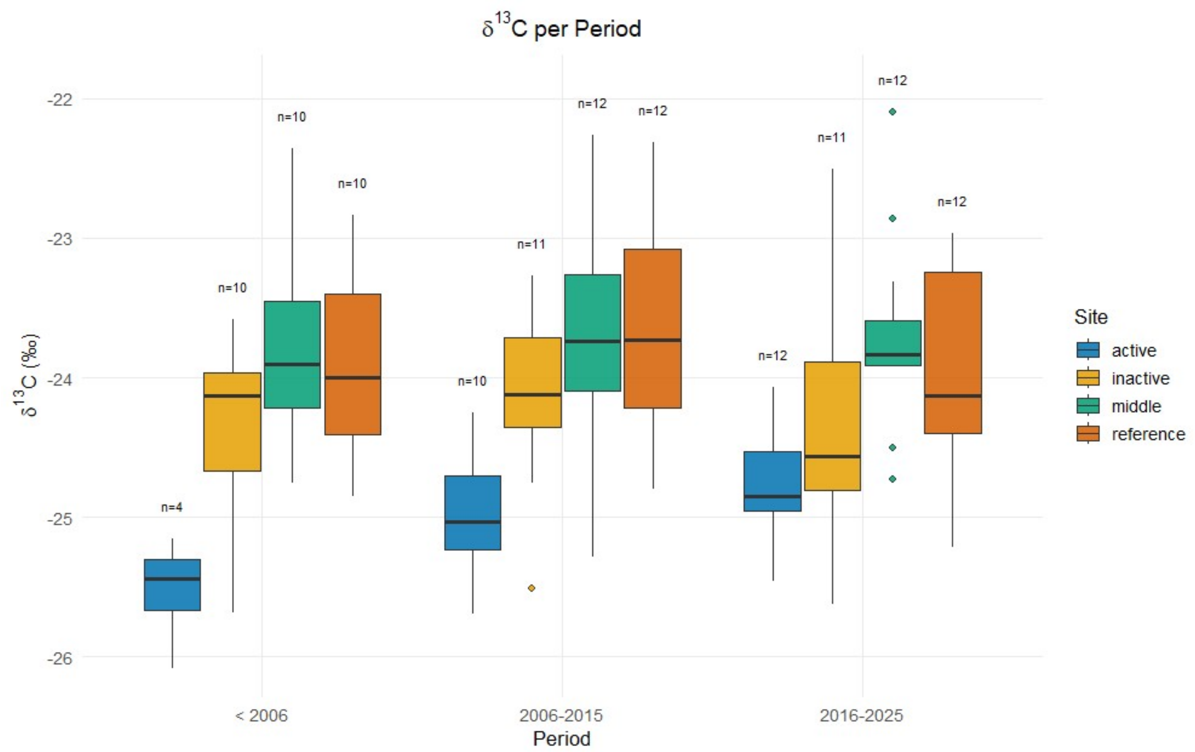

Figure 44: Boxplot of $\delta^{13}C$ values at the four study sites during the three analysed periods, sample size indicated above the respective boxes

Figure 44 gives insight into the evolution of $\delta^{13}C$-values over time at the four sites. The strongest trend can be observed at the active site. During the first period, the active site clearly has lower values than the inactive *(p=0.033)*, middle *(p=0.0015)* and reference *(p=0.0034)* sites. The median values rise from -25.44 ‰ at the period < 2006, to -25.03 ‰ at the period 2006 – 2015, and to -24.85 ‰ at the period 2016 - 2025. In the earliest period, the difference to all other sites is considerable. The difference lies between 1.24 ‰ compared to the inactive site and 1.44 ‰ at the reference site. During the period 2006 – 2015, the difference is still significant compared to the inactive *(p=0.013)*, middle *(p=0.00019)* and reference *(0.00022)* sites. During the most recent period, the active site has overlapping values with the inactive site, but still has significantly lower values than the middle *(p=0.00028)* and reference *(p=0.01)* site. The only significant difference between other sites is between the inactive and the middle site during the period 2016 – 2025 *(p=0.027)*. The other sites do not mirror the trend of rising values at the active site. The inactive, middle and reference site have a slight rise in $\delta^{13}C$ from the period < 2006 to the period 2006 – 2015 and fall again to period 2016-2025, when these sites have the lowest median values. The differences between periods are very small at these three sites, especially considering the large span of values, visualized by the long whiskers.

Generally, the δ^{13}C values on the active rockglacier are less spread with less outliers than at the other sites.

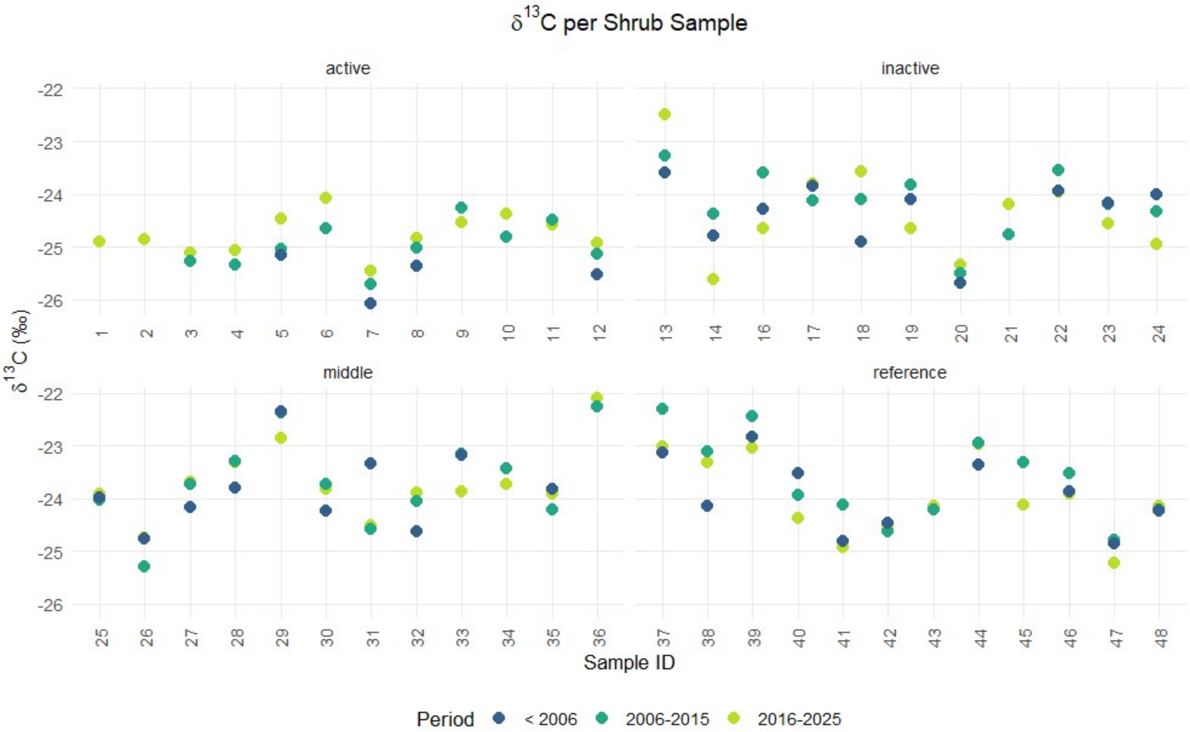

Figure 45: Point plot of δ^{13}C values per decade of all sampled shrubs, Sample ID indicates the individual shrubs

The distribution of individual values visible in Figure 45, which displays the period values of all analysed shrubs, gives further insights. The shrubs on the active rockglacier barely differ in their value distribution and range. Statistically, the values on the active site only rise from 2006 - 2015 to 2016 - 2025 *(p=0.049)*. This is supported by the observation that the values of the period 2016 - 2025 are highest for all shrubs, except two, where multiple measurements could be taken. Differences between periods are small at all shrubs at the active site, but usually the same order of periods can be observed for all shrubs. During the period < 2006, where only four datapoints are available, this value is lower than the other periods in all cases. This pattern was not captured by the Wilcoxon-test due to the small sample size. Such a pattern is not present at the other sites, where the ordering seems random. Additionally, differences in the absolute values between the individual shrubs are much larger, which leads to the long whiskers in Figure 44.

5.2.2.3 iWUE

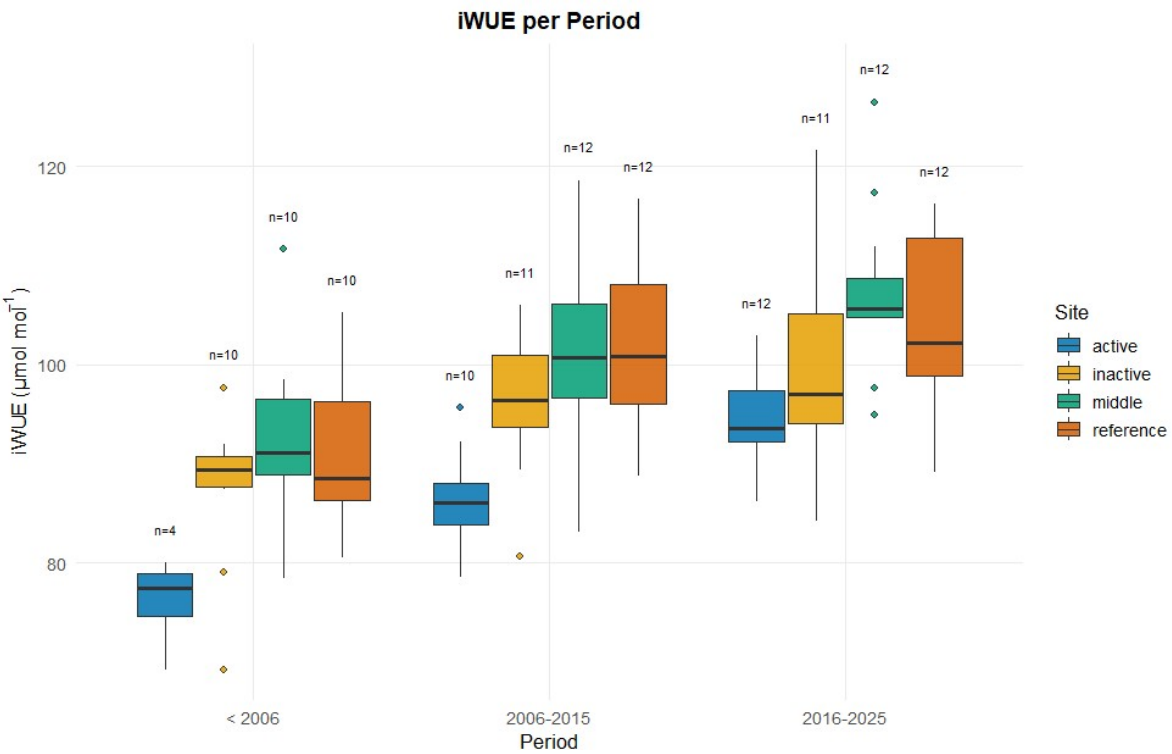

Figure 46: Boxplot of iWUE values at the four study sites during the three analysed periods, sample size indicated above the respective boxes

iWUE is directly derived from $\delta^{13}C$ and the pattern of distribution closely resembles the data described in Chapter 5.2.2.1. The median values range from 77.47 µmol mol^{-1} (active site, < 2006) to 105.67 µmol mol^{-1} (middle site, 2016-2025). The differences between periods at the same sites are larger than for $\delta^{13}C$, and there is a clearer positive trend at all sites. The rate of increase is strongest at the active site, where the median increases from 77.47 µmol mol^{-1} to 93.52 µmol mol^{-1}. This trend is consistently significant across all sites with some exceptions. The increase from 2006 – 2015 to 2016 – 2025 is not significant at the inactive and reference site. Due to the small simple size (n=4), the rise from the period < 2006 at the active site is statistically not significant, but the trend seems visually very clear. The active site has significantly lower values compared to all other sites during the periods < 2006 and 2006 – 2015. During the period 2016 – 2025 the active site is still significantly different to the middle *($p= 0.00028$)* and reference *($p= 0.01$)* sites. Notably the active site has the lowest standard deviation of all sites during all periods.

5.2.2.4 c_i/c_a

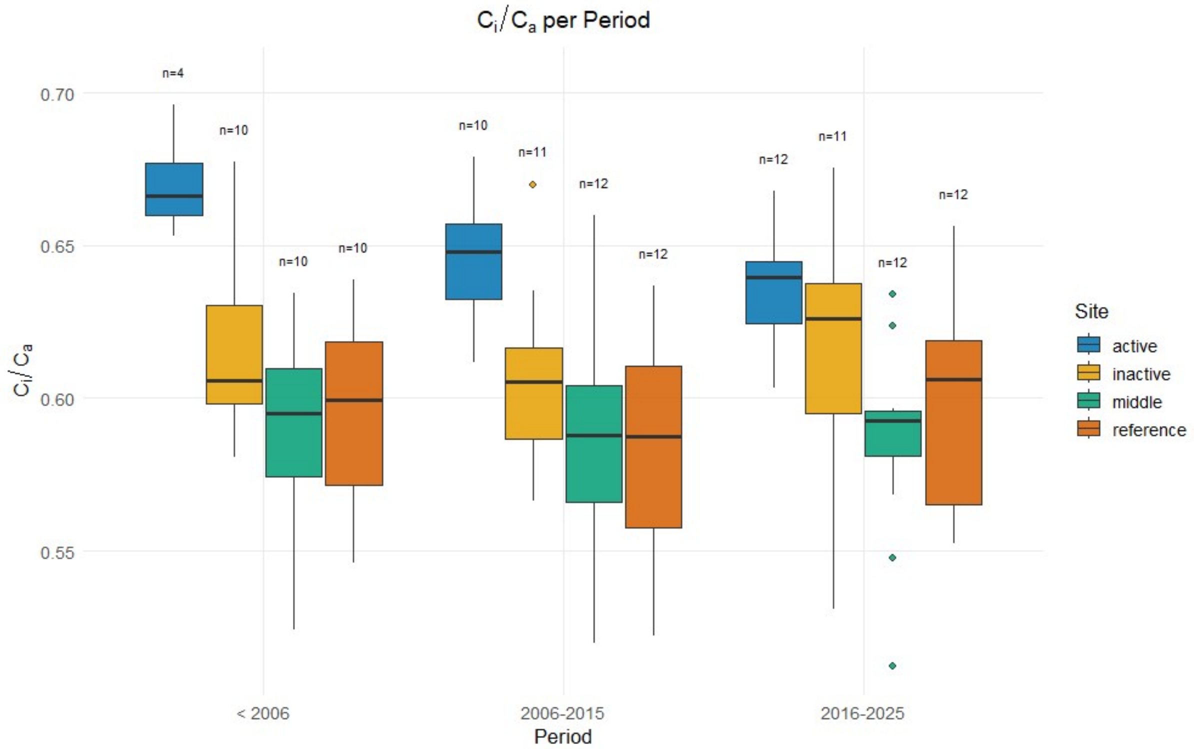

Figure 47: Boxplot of the estimated c_i/c_a -ratio values at the four study sites during the threeanalysed periods, sample size indicated above the respective boxes

c_i/c_a has the same pattern over time as $\delta^{13}C$. The difference is that the y-axis is inverted. This leads to a decline in values over time at the active site, while the other sites remain relatively stable. The median values range from 0.59 to 0.67, with the active site having the highest values at all periods. This difference is significantly different to all other sites during the periods < 2006 and 2006 – 2015. During the period 2016 – 2015, the difference is significant at the middle *(p= 0.00028)* and reference *(p= 0.01)* site. The median values suggest slightly rising values at the inactive site, whereas at the middle and reference site, values first fall and then rise again. However, differences at these sites are very small from period to period especially when considering the large range of data indicated by the whiskers and outliers. The only significant trend is present at the reference site from 2006 – 2015 to 2016 – 2025 *(p= 0.016)*. As a consequence of the small sample size in the period < 2006, the decrease on the active site is only significant from 2006 – 2015 to 2016 – 2025 *(p= 0.016).* Visually, the decreasing trend at the active site is clearly recognizable in Figure 47.

5.2.2.5 C_i

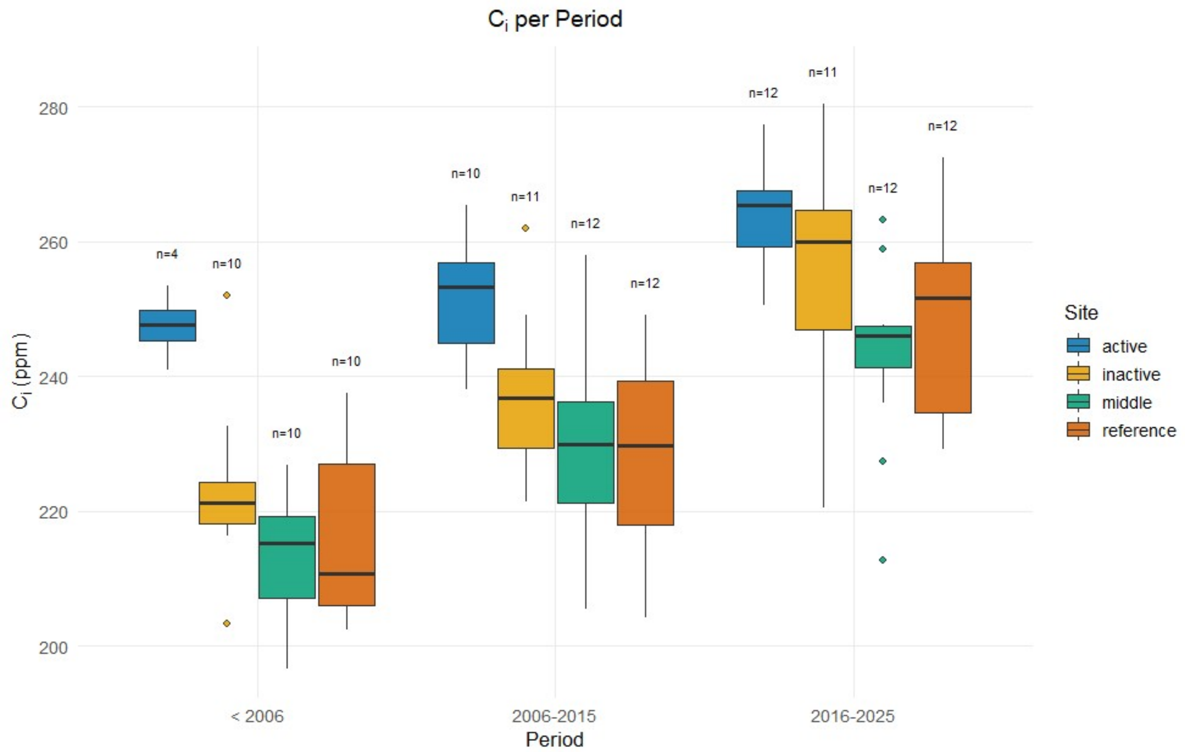

Figure 48: Boxplot of estimated C_i values at the four study sites during the three analysed periods, sample size indicated above the respective boxes

C_i is derived from the parameters presented before ($\delta^{13}C$, c_i/c_a). Thus, the structure of c_i resembles the data presented there. C_i rises at all sites, and the active site has the highest values during all periods. Only during the period 2016 – 2025, the difference is not significant compared to the inactive site. The median values range from 210.7 ppm at the reference site to 247.6 ppm at the active site during the period < 2006. During the period 2016-2025 the range is narrower, with medians of 246 ppm at the middle site and 265.5 ppm at the active site. The positive trend is weaker at the active site, which leads to a convergence of values between the sites. The positive trend is significant between all periods at the inactive, middle and reference site. At the active site the trend is significant between 2006 – 2015 and 2016 – 2025 *($p= 0.0019$)*. It must be considered that the sample size for the period < 2006 is only four at the active site.

6. Discussion

	Active Site	Inactive Site	Middle Site	Reference Site
VLA	↑	↗	↗	↗
Ring Width	↑	→	→	→
$\delta^{18}O$	↗	→	↗	↗
$\delta^{13}C$	↗	→	→	→
iWUE	↑	↗	↗	↗
c_i/c_a	↘	→	→	→
c_i	↗	↑	↑	↑

Table 1: Simplified overview of how the measured and calculated values change over time at all four sites. → = constant, ↗ = increase, ↑ = strong increase, ↘ = decrease

Table 1 serves as a simplified overview of the trends at the four sites presented in Chapter 5. It only compares how parameters behaved over time, but does not include absolute differences between sites. It also only captures very general trends, and the data presented in Chapter 5 is more complex. Despite its simplicity, Table 1 already shows the following three key observations in the data:

1. The active site changes (strongly) over time in all measured parameters
2. The changes at the active site are almost always stronger than at the other sites (exception is C_i)
3. The general trends observed at the inactive, middle and reference site are mostly similar (exception is $\delta^{18}O$ at the inactive site)

These observations are explored in the following chapter in more detail. By looking at the meaning of individual parameters, it is possible to gain insights into the processes causing these main observations.

6.1 Wood Anatomy

6.1.1 Vessel Lumen Area

The first impression of the aggregated VLA data (Figure 31) suggests that no differences between the study sites exist. When measuring the VLA of whole cross-sections, average values reach very similar numbers at all sites. One indication that there are some differences between the sites is, that the VLA data on the active rockglacier is spread over a larger range. When looking at the different periods (Figure 32) it becomes clear, that the average VLA of the shrubs growing on the active rockglacier has not always been on the same level as at the other sites. In the earliest analysed period (< 2006), values are much lower on the active rockglacier. That these differences get lost when aggregating the values, can be explained by the data structure. As not all samples have the same age, not all samples cover the earlier periods. This is mostly relevant for the active site which includes the youngest shrubs and only has a sample size of 4 during the period 1996 - 2005. Because of the smaller sample size, the aggregated data of Figure 32 does not show this signal directly. Even though VLA increases at all sites, the trend of the last three decades is especially remarkable on the active rockglacier. As all sites lie geographically close together, it is likely that the unique conditions on an active rockglacier have a major impact on VLA values. The convergence of the VLA values of the active rockglacier site with the other sites also implies that whatever factor has been limiting VLA in the shrubs on the active rockglacier has diminished steadily over the last decade.

Gärtner-Roer et al. (2013) showed, that VLA in roots of *Salix helvetica* shrubs on active rockglaciers is lower than in shrubs on inactive rockglaciers. Comparing the results from Gärtner-Roer et al. (2013) with the results presented in this study is insightful on multiple levels. In Gärtner-Roer et al. (2013) the vessels in the roots have been analysed over the whole cross section. While a VLA analysis of the whole branch cross section does not show any differences between sites in this study, that does not necessarily mean that the observed differences in roots are absent in above-ground growth. When excluding the last period, which starts after the sampling time of the study by Gärtner-Roer et al. (2013), the VLA on the active rockglacier is significantly lower in above-ground parts of the shrubs. The data from this analysis therefore suggests that the differing results are not due to the sampling of different shrub components (root vs. branch), but are caused by the sampling year instead. In Gärtner-Roer et al. (2013) it has been suggested that differences in VLA between sites may arise due rockglacier creep or different thermal conditions on the active and inactive rockglacier. Vessel size in plants can be reduced by the formation of reaction wood caused by mechanical stress (Heinrich et al., 2007). Other site conditions like topography and climate can be assumed to be comparable.

Therefore, it can be deduced that either rockglacier movements or thermal conditions on the active rockglacier must have changed in the time since 2007, when these samples were taken, so that they are now much more similar on the active and inactive rockglacier. Thanks to the work of Steffen (2025), an overview of surface displacement on the Gruob rockglacier is available. While there was a period of much lower horizontal displacement around 2005 – 2014, surface movement has been at high and comparable levels before and after this period. In this thesis, the middle period covers the years 2006 – 2015, which closely matches the low displacement period of the Gruob rockglacier. In the VLA data there is no break in the positive trend, which can be observed over the three periods. If rockglacier movement was an important limitation for vessel size, VLA could not reach increasingly high values over the last decade when displacement is still high. It would be expected that VLA decreases in the most recent period 2016 – 2025. Therefore, it can be assumed that surface displacement is not the main inhibitor of vessel sizes, and any differences between sites and periods cannott be explained by this factor. The possibility that thermal conditions in and near the ground have changed, seems much more likely. It is known that large vessels are more likely to be damaged by cavitation due to drought or freezing (Hacke & Sperry, 2001). The increase in VLA could thus be a reaction to fewer freezing events in the last decades, which allows the shrubs to build larger vessels with less danger of freezing damage. It is important to note that this does not mean that surface movement and instability do not influence plant presence and survival. It is well documented that plant growth on the unstable surface of rockglaciers is heavily impaired in some cases (e.g. Burga et al., 2004; Cannone and Gerdol, 2003). In the case of VLA of established shrubs however, surface movement does not seem to be the driving factor.

As VLA also increases at the other sites, underlying trends that affect all sites must be considered. Vessel size is functionally linked to plant water transport capacity, which scales strongly with diameter (Hacke & Sperry, 2001). In woody plants, VLA is therefore closely tied to hydraulic demand and growth conditions. An increase in VLA over time is expected as shrubs develop, because larger plants require greater hydraulic capacity (West et al., 1999). Accordingly, a positive age-related trend in VLA is likely across all sites, independent of environmental conditions. In this study, average ring width did not increase clearly at three of the four sites (Chapter 5.1.2). Nevertheless, VLA showed a consistent positive trend across all sites, indicating that age-related development plays a dominant role in vessel enlargement. At the active rock glacier site, however, VLA increased more strongly over time. This pattern coincides with an increase in ring width, suggesting that enhanced radial growth amplified the ontogenetic trend in vessel size at this site. This is consistent with the observation that the sampled shrubs on the active rockglacier are considerably smaller but produced vessels of similar size compared to the other sites. In this observed case, VLA can therefore not simply be seen as a function of plant size.

6.1.2 Ring Width

The ring width of shrubs reflects the radial stem growth of the plant (Dobbert et al., 2022). Relatively wider rings can indicate better growing conditions. Especially in arctic or alpine environments, where growth is often limited by temperature, a warming climate can lead to increased growth (Blok et al., 2011). When comparing the sites, it is important to consider, that shrubs of different ages are compared during the same time period. Due to this, the data was also checked for underlying age trends that might influence the interpretation. This was especially important because the age distribution is different between sites. Comparing tree ring sections of the same shrub age (Figure 39) shows that there is no clear age trend with increasing ring width at the inactive, middle or reference site.

It was observed that *Salix* shrubs in harsh arctic conditions do not exhibit age trends in ring width like tree species, but rather react to environmental factors (Owczarek & Opała, 2016), which also seems to be the case in the *Salix helvetica* shrubs on and around the Gruob rockglacier. The younger age and lower number of tree rings at the active site not only need to be considered in the interpretation of tree-ring widths, but also provide information about past conditions at the different sites. As has been introduced in Chapter 4.2, there were not many shrubs available on the active rockglacier. It is unlikely, that many other shrubs on the active rockglacier are older and the sampled shrub should show a representative age distribution. This indicates that there are no or only very few shrubs with an age over 30 years present on the active rockglacier. This does not match the age pattern observed at the other sites. An explanation for this could be the surface movement, which can damage or crush plants (Burga et al., 2004; Cannone & Gerdol, 2003). A large part of the sampled shrubs on the active rockglacier have an age of around 20 years (Figure 38). According to Steffen (2025) there was a period of comparably small surface displacement from 2005 to 2011. The age clustering of shrubs around that period on the active rockglacier could indicate that the emerging *Salix* *helvetica* shrubs on the active rockglacier profited from the relatively stable surface in their first years, when they are most susceptible to damage (Körner, 2003).

Especially during the most recent period 2016 – 2025, the ring-width values of the inactive, middle and reference site are similar, while the active site has much higher values (Figure 35). Before, all other sites show a relatively stable pattern, while the active site already has a positive trend from period < 2006 to period 2006 - 2015. In other words, growth remains mostly stable at all sites with the exception of the active site, where growth has been rising slowly at the beginning, and very strongly in the last 10 years. This trend is not only present in aggregated data like in Figure 35 but also on an individual level for each shrub (Figure 37). In each shrub on the active site the average ring width increases from one period to the next. The shrubs with the highest values in period 2016 - 2025 are mostly those which also have data for period 1996 – 2005. The absolute highest values are reached by older shrubs on the active rockglacier. This means that age could have an influence on the maximally possible radial growth per year. None of the other sites have such visibly clear sorting, and the order of the data points does not follow a pattern at any period. This underlines the exceptional trends on the active site once more.

While an age effect could be present on the active rockglacier, there is no evidence that it is a generally present mechanism at the other sites. No other site has experienced such an increase in growth at any time. As it only comes into play on the active rockglacier, where very high values are recorded, it could mean that age is only a restricting factor when exceptionally high increases of growth happen.

Ring width increases in the most recent 10 years, but rockglacier movement is high during this period with up to 4 meters per year (Steffen, 2025). Followingly there is no correlation between rockglacier movement and shrub growth. Despite rising temperatures during the last decades due to a warming climate (Figure 31, Chapter 3.2), explaining increased growth as a direct consequence of air temperature falls short. As all sites are in close distance with a maximum of 540 meters between two sampling locations, all the four sites have experienced the same change in climate. Increased growth has only taken place at the site on the active rockglacier. With overall air temperature and surface movement being unlikely factors for the discrepancy between sites, other microsite differences must be considered. Regularly mentioned factors limiting growth in alpine environments are nutrient availability (Iturrate-

Garcia et al., 2017) and soil temperature (Cui et al., 2025). Cui et al (2025) found that radial growth of coniferous trees in an alpine environment is controlled by soil temperature rather than by air temperature. Another study by Francon et al. (2021), showed that snow-free growing degree days are the most important factor of growth for shrubs in the Alps, which is also a mostly temperature driven factor. As introduced in Chapter 2.2.2, soil temperature is a strong limitation of growth at altitudinal limits (Körner & Hoch, 2006; Körner & Paulsen, 2004). No measurements of soil temperature were taken during this thesis, but due to the frozen permafrost core of the active rockglacier it can be expected that soil temperatures tend to be lower on the active rockglacier compared to the other sites. Being the lowest lying active rockglacier in the Turtmann valley with an altitude of 2414 m a.s.l (Nyenhuis, 2005), it is likely that that the permafrost core of the Gruob rockglacier has been melting during the last decades because of climate change. The assessment of destabilization of rockglaciers in the Turtmann valley has also led to the conclusion, that Gruob rockglacier is destabilized because of thermal and hydrological conditions due to warming (Steffen, 2025). Thereby, the active layer of the rockglacier has increased in depth. This would have multiple impacts on the shrubs growing on the rockglacier. Generally higher soil temperatures are to be expected due to an increased active layer. Additionally, a longer vegetation period seems likely, because the thicker active layer thaws earlier in spring and freezes later in fall. Further, roots of the shrubs could have more space available due to the deeper permafrost horizon. This can increase water and nutrient availability for the shrubs.

In general, a thicker active layer could increase average soil temperature in summer, enable a longer vegetation period and make access to additional resources possible for shrubs growing on active rockglaciers. All these factors can increase growth in shrubs and can explain the strong positive trend in tree ring-width on the active rockglacier. Myers-Smith et al. (2015) stated that sensitivity of shrub growth to climate variation is higher for sites with greater soil moisture and for shrubs growing at northern or elevational limits. The highest sensitivity could be found in regions where permafrost is thawing. The continuously increasing growth rate of shrubs over the last decades at the active rockglacier can be explained by thawing permafrost and an active layer of increased thickness. This is a factor that is unique to the site on the active rockglacier, because no permafrost or even more degraded permafrost is expected at the other analysed sites.

However, some questions remain when comparing the ring widths on the active rockglacier to the other sites. It is surprising that ring width has gotten significantly wider in the last decade. Growth conditions on the active rockglacier may have improved while the conditions at the other sites were more stable, but it is hard to imagine that the active site now offers better conditions than neighbouring sites. Soil development on the active rockglacier is still clearly in early stages compared the other sites from visual impressions, and air temperature is also expected to be slightly lower due to the higher altitude of the site. A possible explanation is that alpine plants have larger root systems and more carbohydrate reserves (Körner, 2003). While all studied shrubs are of the same species and in an alpine environment, storage is generally more developed in low-resource environments (Chapin et al., 1990). The harsh conditions on the sparsely vegetated and the small growth form of shrubs on the active rockglacier point towards it being an environment with limited resources. The shrubs on the active rockglacier could have profited from these storages and well-developed root system when the growth limitation factor is removed.

Ring width has only really diverged between the sites in the last 10 years. Figure 36 even shows that ring width has decreased at the inactive, middle and reference sites. A possible reason for this could be that while shrubs on the active rockglacier profit from higher temperatures and the resulting permafrost melting, the other sites suffer from increased water stress due to warmer and drier climatic conditions. Another observation from the data is that no site apart from the active site has shown such clear positive trends at any period. At the inactive site, and especially the middle site, it is expected that there was or is still some permafrost presence. Considering this, it would be expected that an increase in ring width has taken place at those sites at some point in the past as well. The tree-ring data reaches back to 1966 - 1975 at its maximum at the inactive site, and data points get scarcer in the early periods. It is possible, that the data is not reaching back far enough to cover these developments in the past.

6.2 Stable Isotopes

6.2.1 Oxygen

$\delta^{18}O$ values in wood are often used to investigate the source water of the plants. This process is described in Chapter 2.3. The higher $\delta^{18}O$ values of the active rockglacier (Figure 41) could indicate that they have access to different source water than the inactive and reference sites (Bryukhanova et al., 2015; Churakova-Sidorova et al., 2020; Fan et al., 2023; Sugimoto et al., 2002). This interpretation is supported by the values of the middle site. As stated in the research questions, it was hypothesized that shrubs growing on the active rockglacier have access to meltwater from permafrost. This water could also be available to the shrubs on the middle lobe, although to a lesser extent. The middle lobe is closest to the active rockglacier of the three lower sites, and its geomorphological form suggests some recent activity.

Although the $\delta^{18}O$ results from the sites do not contradict that hypothesis, it is difficult to draw clear conclusions from the data. As no water, snow or ice samples have been taken for this thesis, it is difficult to estimate what the $\delta^{18}O$ values of the different potential water sources are. All the sites are in close proximity, so it can be assumed that $\delta^{18}O$ values in rain and snow are not significantly different between the four sites. The sampled shrubs on the active rockglacier grew at a slighter higher altitude, and $\delta^{18}O$ in precipitation is altitude-dependent, with more depleted values at high elevations (Barbour, 2007; Dansgaard, 1964). However, this effect cannot be the reason for the difference, as in the present data of this study, the wood is enriched with $\delta^{18}O$ compared to the lower sites. The difference in values could therefore arise from an additional water source at the active and middle sites that is not available at the other sites. Studies on $\delta^{18}O$ values of permafrost mostly show more depleted values for permafrost in comparison to precipitation (e.g, Amschwand et al., 2025; Fan et al., 2021; Krainer et al., 2007). While not abundant in alpine regions, there have been studies that showed that vegetation on permafrost carries a lower $\delta^{18}O$ signal in the cellulose (Grießinger et al., 2021). Direct measurements of $\delta^{18}O$ in rockglacier ice are scarce, and the hydrology of rockglaciers is complex and poorly understood, but it cannot be assumed that the ice of the Gruob rockglacier has such a different isotopic composition compared to other permafrost bodies without conducting direct measurements.

It has been reported that melt-freeze cycles can lead to an enrichment of $\delta^{18}O$ in snow and rockglacier ice (Steig et al., 1998). When water infiltrates the rockglacier and comes into contact with rockglacier ice, isotopic fractionation will preferably remove light isotopes and thus the remaining ice will be enriched in $\delta^{18}O$ (Williams et al., 2006). This indicates that $\delta^{18}O$-enriched ice in rockglaciers can be present, especially under warming conditions, where ice comes into contact with liquid water. It is also widely known that $\delta^{18}O$ in rainfall increases between spring and autumn (Del Siro et al., 2023). The higher $\delta^{18}O$ values on the active rockglacier could be an effect of a later start of the vegetation period compared to the other sites, where the vegetation period starts later and the low $\delta^{18}O$ rainfall of early summer only gets absorbed by the shrubs at the lower sites. Further, as also the snowpack is enriched in $\delta^{18}O$ over time because of fractionation processes, it has been widely reported that early season snowmelt has lower $\delta^{18}O$ values than late season snowmelt, which is isotopically enriched (Beria et al., 2018; Dietermann & Weiler, 2013; Taylor et al., 2001).

As described, explanations for the high $\delta^{18}O$ values on the active rockglacier by source water can be made, but without $\delta^{18}O$ measurements of the potential water sources they remain speculative. Source water is generally considered the most important factor for the oxygen isotope composition in plant material, with up to 96-99% $\delta^{18}O$ variation reportedly explainable by source water (Roden & Ehleringer, 1999). Still, $\delta^{18}O$ in plants can also be influenced by evaporative enrichment in the leaves (Barbour, 2007). With the warming climate, a rise in VPD can be expected, which increases evaporation in the leaf and leads to $\delta^{18}O$ enrichment in the leaf. Additionally, there is a trend towards higher $\delta^{18}O$ in precipitation due to a warming climate, albeit relatively small and not observable at all measuring stations (Vystavna et al., 2020). These trends could serve as an explanation to the general positive trend observed at all sites and periods except for the active rockglacier site from < 2006 to 2006 – 2015, and at the inactive rockglacier site from 2006 – 2015 to 2016 – 2025. However, for the generally higher values at the active and middle sites, the differences seem to be too large to be explained by evaporative enrichment. Likely, the differences in these baseline values are caused by different water sources and hydrological processes. Unfortunately, they remain difficult to disentangle from the present data.

The break in the positive trend on the active site in the middle time period leaves room for speculation about what processes might influence $\delta^{18}O$ of shrubs. The values rise strongly again towards the period 2016 – 2025, and the period 2006 – 2015 is clearly the time frame when the active site has the most similar values to the other sites. This is also the period when lower surface movement was observed on the Gruob rockglacier (Steffen, 2025). It is a possibility that hydrological flow paths in the active rockglacier were different in this phase of stability, which led to a different combination of water sources in the water available to shrubs than in phases of greater movement.

6.2.2 Carbon

An atmospheric correction of the $\delta^{13}C$ was made (Chapter 4.5), so the presented data does not show the increasing trend of the atmospheric CO_2 in past decades. Similar to the $\delta^{18}O$ values, the $\delta^{13}C$ values on the active rockglacier behave much differently than at the other sites, which all follow a similar and more constant pattern (Figure 44). The $\delta^{13}C$ values on the active rockglacier are rising over time, which is an indicator of changing environmental factors. Rising $\delta^{13}C$ is a widely established indicator for drought stress (Farquhar et al., 1982). In this case, drought stress as a lead factor for rising $\delta^{13}C$ values on the active rockglacier raises the question why the same cannot be observed at any other site. Drought stress would be caused by rising temperatures or lower precipitation. Such climatic trends are present in the region due to climate change (Chapter 3.2), but it would affect all four sites similarly, as they are geographically very close. At the other three sites, no rise of the same extent in $\delta^{13}C$ can be observed. The soil on the active rockglacier, which is in early stages of development, could potentially be a factor for reduced water availability, due to a lower water storage capacity. However, the analysis of the ring width (Chapter 5.1.2) showed rising growth over time on the active rockglacier. The combination of these two factors does not point to increasingly stressed shrubs. On the contrary, it indicates that changes in the isotopic composition in wood likely are influenced by accelerated growth.

$\delta^{13}C$, c_i/c_a and iWUE are all based on the same uncorrected $\delta^{13}C$ values with the addition of atmospheric change of ^{13}C and CO_2. The analysis of these different factors helps in understanding the underlying plant processes and environmental trends. iWUE estimates water-use efficiency in plants, defined as the amount of carbon fixed per unit of water lost. Therefore, high values indicate more closed stomata and low values indicate that stomatal conductance is increased. However, this is under the assumption that the photosynthesis rate is stable. When the photosynthetic rate is increased and stomatal conductance remains stable, water use efficiency will rise. iWUE is inversely related to the c_i/c_a ratio. Because of atmospheric CO_2 increase, the estimated Ci and iWUE values also rise without physiological change. This can be observed in Figure 46, where iWUE rises at all sites. The positive trend is strongest at the active site. The reason for this can be found in Figure 47. c_i/c_a remains constant over time at the inactive, middle and reference sites. This means that photosynthetic demand increases proportionally to stomatal supply. As there is no change in c_i/c_a at these sites and iWUE still rises, it can be concluded that the rise in iWUE is mainly driven by higher atmospheric CO_2. At the active site the scaling is not proportional, as can be seen by the declining c_i/c_a ratio in Figure 47. c_i does not increase in the same way as c_a at the active site (Figure 48). At the other sites, the atmospheric increase of c_a is directly translated to increasing c_i values. At the active site, the atmospheric signal is reduced by another factor, indicating an additional physiological constraint beyond atmospheric forcing. Potential factors include a lowered stomatal conductance or increased photosynthetic demand. The ring-width data indicates that growth has strongly increased at the active site, which likely means, that increased photosynthetic demand is the driving force of the trends observed for c_i, c_i/c_a and iWUE. With higher growth, plant processes and photosynthesis are also accelerated. Consequentially, the photosynthetic demand is increased. The CO_2 concentration inside the leaf (c_i) decreases because of the increased demand. Because of this lower concentration, RuBisCo discriminates less strongly against the heavy ^{13}C than before (Farquhar et al., 1989). The assimilated carbon is less depleted, which translates to an upward shift of $\delta^{13}C$ in the wood. This process takes place without a change in stomatal opening and does not point to a drought effect (Scheidegger et al., 2000). How an increased assimilation rate without equivalent changes in stomatal conductance reduces c_i/c_a and increases $\delta^{13}C$ is described by the equations presented in Chapter 2.3. (Farquhar et al., 1982).

The negative $\delta^{13}C$ trend at the inactive and reference sites is not significant, and while the mean value decreases, the range of the values stays almost the same. From those small differences, it is not possible to assign any climatic or physiological influences on this trend with the present data. However, the values on the active rockglacier converge with the other sites over time and have almost reached the same levels in period 2016 - 2025. This is an additional indicator that conditions and plant processes on the active rockglacier site continuously align with the other sites.

7. Conclusion

The measurements conducted for this thesis present a diverse picture that allows a lot of interpretations and speculations. It is important to remember the context of this study. Rockglaciers in the Alps are systems under pressure, which constantly have to adapt to new conditions. The ecosystem which is researched in this thesis is highly dynamic, and processes and relationships might change considerably over time.

Connecting individual measurements to physical processes poses a challenge due to unknown factors and the volatile environment. Nonetheless, the key observations presented in Chapter 6 allow some clear conclusions, additional to the more uncertain speculations.

For most of the analysed parameters, the site on the active rockglacier always shows the most change over time and behaves distinctly from the other sites. At the sites on less active ground or without permafrost influence, values are mostly stable and trends are far less pronounced than on the active rockglacier. These sites also behave much alike. These key observations clearly show that shrubs on active rockglaciers are exposed to processes that are less relevant at neighbouring sites. While climatic changes are the same at these sites, the direct consequences are more severe for shrubs on the active rockglacier. By being situated on the lower edge of the permafrost belt, the Gruob rockglacier faces the full consequences of global warming. It appears that the Gruob rockglacier has been in a dynamic state of change in the last decades and continues to do so today, which is reflected in the wood anatomy and isotopic composition of shrubs growing on the Gruob rockglacier. The data presented can be explained by a degrading rockglacier, which results in a thicker active layer and increased soil temperature. As an important limitation for growth at high altitudes, the increasing soil temperature has immediate effect on shrub growth, which is reflected in the data.

Changes in available source water are also possible, but it is difficult to describe the concrete changes with the present data. Interestingly, surface movement does not seem to be a highly relevant factor for shrub properties and growth once they are established. While some mechanisms are still unclear, this study shows that shrubs on rockglaciers carry information about changes in rockglacier structure and dynamics.

The results of this study strongly support the hypothesis that *Salix helvetica* shrubs growing on active rockglaciers have different wood-anatomical and isotopic properties than shrubs at neighbouring sites, which answers the overarching research question of this thesis. Differences could be found both for vessel size and ring width (Research Question 1), and for oxygen and carbon stable isotopes (Research Question 2). These differences vary over time and are sometimes not recognizable when analysing aggregated data or short time periods. This emphasises how the analysis of shrubs allows the capturing of information about a volatile environment over time. While the shrubs on the active rockglacier differ largely from the other sites, the shrubs on the other sites are much alike. The used methods could not capture differences between shrubs on rockglaciers of reduced activity levels and a site without permafrost influence. A key limitation is that it is not entirely clear whether and to what extent these sites are, or have been, active in recent decades due to a lack of information. Research Question 3 aimed to explain the isotopic and wood-anatomical differences to environmental factors. An argument has been made that soil temperature, influenced by the thickness of the active layer, is very influential. Further studies on shrubs growing on rockglacier including soil temperature measurements could support this claim.

The analysis of shrubs on rockglaciers offers multiple advantages compared to more established rockglacier monitoring methods, such as boreholes. Traditional methods often include the use of heavy and expensive equipment in the field, which can be challenging in high mountain environments. For the analyses conducted in this thesis, only small branch sections of shrubs had to be collected in the field. Another benefit of shrubs is that they carry information about past events or trends thanks to tree rings, which portray the situation during the year of ring formation. This is especially useful in regions where no long-term monitoring exists, as a reconstruction of past activity is possible. Additionally, the field of plant-permafrost research is of great interest as especially studies on alpine rockglaciers are scarce and interactions between rockglaciers and shrubs growing on them are poorly understood.

While insightful conclusions can be drawn from the present data, further research is needed. Connecting wood anatomical growth reactions and isotopic compositions reliably with processes in rockglaciers requires further data. Especially the isotopic signature of all potential water sources is important to calculate their share in shrub source water. Important measurements include precipitation, snowpack and permafrost and water flowing through and out of the rockglacier. Additionally, the monitoring of soil temperature and active layer depth could confirm the finding of this study, that an increased active layer thickness and consequently higher soil temperatures are the driving force for the trends observed in the data. While surface movement data is present, closer monitoring could give insights about yearly fluctuations, and connections to single tree ring properties could be made. Also, from a wood anatomical perspective, further measurements will increase the understanding of mechanisms. Analysing the isotopic properties of each single tree ring instead of blocks results in a higher resolution of data with data points for each single year. To reconstruct source water, even differentiating between early and late wood could be useful.

While offering a new approach to rockglacier research, it must be noted that its field of application is limited to rockglaciers where shrubs are growing. This excludes rockglaciers at a higher elevation, or rockglaciers where surface movement or soil material does not allow the growth of vascular plants. Furthermore, processes in shrubs or trees are complex, and their properties are only a potential proxy for rockglacier dynamics but not a direct observation or measurement. This study was conducted only on one rockglacier with one species of shrub (*Salix helvetica*), and results might differ on rockglaciers in other regions and with other species.

This study clearly highlights the potential of dendroecological methods on rockglaciers. Wood anatomy and stable isotope signatures of shrubs growing on an active rockglacier is unique and can be explained by physical processes. By further research the conclusions of this thesis can be confirmed and knowledge gaps can be closed.

8. Bibliography

Alestalo, J. (1971). Dendrochronological interpretation of geomorphic processes. *Fennia - International Journal of Geography*, *105*(1). https://fennia.journal.fi/article/view/40757

Amschwand, D., Tschan, S., Scherler, M., Hoelzle, M., Krummenacher, B., Haberkorn, A., Kienholz, C., Aschwanden, L., & Gubler, H. (2025). Seasonal ice storage changes and meltwater generation at Murtèl rock glacier (Engadine, eastern Swiss Alps): Estimates from measurements and energy budgets in the coarse blocky active layer. *Hydrology and Earth System Sciences*, *29*(9), 2219–2253. https://doi.org/10.5194/hess-29-2219-2025

Arenson, L., Hoelzle, M., & Springman, S. (2002). Borehole deformation measurements and internal structure of some rock glaciers in Switzerland. *Permafrost and Periglacial Processes*, *13*(2), 117–135. https://doi.org/10.1002/ppp.414

Arenson, L., Springman, S. M., & Sego, D. C. (2007). The Rheology of Frozen Soils. *Applied Rheology*, *17*(1), 12147-1-12147–14. https://doi.org/10.1515/arh-2007-0003

Bachrach, T., Jakobsen, K., Kinney, J., Nishimura, P., Reyes, A., Laroque, C. P., & Smith, D. J. (2004). Dendrogeomorphological assessment of movement at Hilda rock glacier, Banff National Park, Canadian rocky mountains. *Geografiska Annaler: Series A, Physical Geography*, *86*(1), 1–9. https://doi.org/10.1111/j.0435-3676.2004.00209.x

Baillarget, D., & Scaringi, G. (2025). Permafrost Degradation: Mechanisms, Effects, and (Im)Possible Remediation. *Land*, *14*(10). https://doi.org/10.3390/land14101949

Barbour, M. M. (2007). Stable oxygen isotope composition of plant tissue: A review. *Functional Plant Biology*, *34*(2), 83–94. https://doi.org/10.1071/FP06228

Barbour, M. M., Andrews, T. J., & Farquhar, G. D. (2001). Correlations between oxygen isotope ratios of wood constituents of Quercus and Pinus samples from around the world. *Functional Plant Biology*, *28*(5), 335–348. https://doi.org/10.1071/pp00083

Barsch, D. (1996). *Rockglacier Taxonomy* (D. Barsch, Ed.). Springer. https://doi.org/10.1007/978-3-642-80093-1_5

Bearth, P. (1980). *1308 St. Niklaus* [Map]. Schweizerische Geologische Komission. https://www.swisstopo.admin.ch/de/geologischer-atlas-der-schweiz-1-25000-pixel

Beria, H., Larsen, J. R., Ceperley, N. C., Michelon, A., Vennemann, T., & Schaefli, B. (2018). Understanding snow hydrological processes through the lens of stable water isotopes. *WIREs Water*, *5*(6), e1311. https://doi.org/10.1002/wat2.1311

Bertolotti, G., & Krainer, K. (2025). *Oxygen isotopes from the rock glacier core Lazaun I* [Data set]. PANGAEA.

Blok, D., Sass-Klaassen, U., Schaepman-Strub, G., Heijmans, M. M. P. D., Sauren, P., & Berendse, F. (2011). What are the main climate drivers for shrub growth in Northeastern Siberian tundra? *Biogeosciences*, *8*(5), 1169–1179. https://doi.org/10.5194/bg-8-1169-2011

Bryukhanova, M. V., Fonti, P., Kirdyanov, A. V., Siegwolf, R. T. W., Saurer, M., Pochebyt, N. P., Churakova (Sidorova), O. V., & Prokushkin, A. S. (2015). The response of δ13C, δ18O and cell anatomy of *Larix gmelinii* tree rings to differing soil active layer depths. *Dendrochronologia*, *34*, 51–59. https://doi.org/10.1016/j.dendro.2015.05.002

Buchli, T., Kos, A., Limpach, P., Merz, K., Zhou, X., & Springman, S. M. (2018). Kinematic investigations on the Furggwanghorn Rock Glacier, Switzerland. *Permafrost and Periglacial Processes*, *29*(1), 3–20. https://doi.org/10.1002/ppp.1968

Buchli, T., Merz, K., Zhou, X., Kinzelbach, W., & Springman, S. M. (2013). Characterization and Monitoring of the Furggwanghorn Rock Glacier, Turtmann Valley, Switzerland: Results from 2010 to 2012. *Vadose Zone Journal*, *12*(1), 1–15. https://doi.org/10.2136/vzj2012.0067

Büntgen, U., Urban, O., Krusic, P. J., Rybníček, M., Kolář, T., Kyncl, T., Ač, A., Koňasová, E., Čáslavský, J., Esper, J., Wagner, S., Saurer, M., Tegel, W., Dobrovolný, P., Cherubini, P., Reinig, F., & Trnka, M. (2021). Recent European drought extremes beyond Common Era background variability. *Nature Geoscience*, *14*(4), 190–196. https://doi.org/10.1038/s41561-021-00698-0

Burga, C. A., Frauenfelder, R., Ruffet, J., Hoelzle, M., & Kääb, A. (2004). Vegetation on Alpine rock glacier surfaces: A contribution to abundance and dynamics on extreme plant habitats. *Flora - Morphology, Distribution, Functional Ecology of Plants*, *199*(6), 505–515. https://doi.org/10.1078/0367-2530-00179

Cannone, N., & Gerdol, R. (2003). Vegetation as an Ecological Indicator of Surface Instability in Rock Glaciers. *Arctic, Antarctic, and Alpine Research*, *35*(3), 384–390. https://doi.org/10.1657/1523-0430

Carrer, M., von Arx, G., Castagneri, D., & Petit, G. (2015). Distilling allometric and environmental information from time series of conduit size: The standardization issue and its relationship to tree hydraulic architecture. *Tree Physiology*, *35*(1), 27–33. https://doi.org/10.1093/treephys/tpu108

Chapin, F. S., Schulze, E.-D., & Mooney, H. A. (1990). The Ecology and Economics of Storage in Plants. *Annual Review of Ecology and Systematics*, *21*, 423–447. https://doi.org/10.1146/annurev.ecolsys.21.1.423

Churakova-Sidorova, O. V., Lienert, S., Timofeeva, G., Siegwolf, R., Roden, J., Joos, F., & Saurer, M. (2020). Measured and modelled source water δ18O based on tree-ring cellulose of larch and pine trees from the permafrost zone. *iForest - Biogeosciences and Forestry*, *13*(3), 224. (world). https://doi.org/10.3832/ifor3212-013

Cicoira, A. (2020). *On the Dynamics of Rock Glaciers* [PhD]. University of Zurich.

Cleveland, W. S. (1978). Robust Locally Weighted Regression and Smoothing Scatterplots. *Journal of the American Statistical Association*, *74*(368), 829–836. https://doi.org/10.1080/01621459.1979.10481038

Coplen, T. B. (1995). Letter to the Editor: New IUPAC guidelines for the reporting of stable hydrogen, carbon, and oxygen isotope-ratio data. *Journal of Research of the National Institute of Standards and Technology*, *100*(3), 285. https://doi.org/10.6028/jres.100.021

Craig, H. (1961). Standard for Reporting Concentrations of Deuterium and Oxygen-18 in Natural Waters. *Science*, *133*(3467), 1833–1834. https://doi.org/10.1126/science.133.3467.183

Cui, M., Jiang, Y., Xue, F., Cao, P., & Kang, M. (2025). Soil temperature explains radial growth of coniferous trees more effectively than air temperature in mountainous cold temperate habitat. *Ecological Indicators*, *176*, 113667. https://doi.org/10.1016/j.ecolind.2025.113667

Dansgaard, W. (1964). Stable isotopes in precipitation. *Tellus*, *16*(4), 436–468. https://doi.org/10.3402/tellusa.v16i4.8993

Del Siro, C., Scapozza, C., Perga, M.-E., & Lambiel, C. (2023). Investigating the origin of solutes in rock glacier springs in the Swiss Alps: A conceptual model. *Frontiers in Earth Science*, *11*. https://doi.org/10.3389/feart.2023.1056305

Delaloye, R., Lambiel, C., & Gärtner-Roer, I. (2010). Overview of rock glacier kinematics research in the Swiss Alps. *Geographica Helvetica*, *65*(2), 135–145. https://doi.org/10.5194/gh-65-135-2010

Dietermann, N., & Weiler, M. (2013). Spatial distribution of stable water isotopes in alpine snow cover. *Hydrology and Earth System Sciences*, *17*(7), 2657–2668. https://doi.org/10.5194/hess-17-2657-2013

Dobbert, S., Pape, R., & Löffler, J. (2022). The application of dendrometers to alpine dwarf shrubs – a case study to investigate stem growth responses to environmental conditions. *Biogeosciences*, *19*(7), 1933–1958. https://doi.org/10.5194/bg-19-1933-2022

Esper, J., Cook, E. R., & Schweingruber, F. H. (2002). Low-Frequency Signals in Long Tree-Ring Chronologies for Reconstructing Past Temperature Variability. *Science*, *295*(5563), 2250–2253. https://doi.org/10.1126/science.1066208

Fan, R., Maximov, T. C., & Sugimoto, A. (2023). Cellulose δ18O as a hydrological proxy: A case study for willows growing in Indigirka river lowland, Northeastern Siberia. *Polar Science*, *37*, 100964. https://doi.org/10.1016/j.polar.2023.100964

Fan, R., Shimada, H., Tei, S., Maximov, T. C., & Sugimoto, A. (2021). Oxygen Isotope Compositions of Cellulose in Earlywood of *Larix cajanderi* Determined by Water Source Rather Than Leaf Water Enrichment in a Permafrost Ecosystem, Eastern Siberia. *Journal of Geophysical Research: Biogeosciences*, *126*(9), e2020JG006125. https://doi.org/10.1029/2020JG006125

Fantucci, R., & McCord, A. (1995). Reconstruction of landslide dynamic with dendrochronological methods. *Dendrochronologia*, *13*(4), 43–58.

Farquhar, G. D., Ehleringer, J. R., & Hubick, K. T. (1989). Carbon isotope discrimination and photosynthesis. *Annual Review of Plant Physiology and Plant Molecular Biology*, *40*.

Farquhar, G. D., O'Leary, M., & Berry, J. (1982). On the Relationship Between Carbon Isotope Discrimination and the Intercellular Carbon Dioxide Concentration in Leaves. *Australian Journal of Plant Physiology*, *9*(2), 121–137. https://doi.org/10.1071/PP9820121

Ferrio, J. P., Araus, J. L., Buxó, R., Voltas, J., & Bort, J. (2005). Water management practices and climate in ancient agriculture: Inferences from the stable isotope composition of archaeobotanical remains. *Vegetation History and Archaeobotany*, *14*(4), 510–517. https://doi.org/10.1007/s00334-005-0062-2

Fonti, P., von Arx, G., García-González, I., Eilmann, B., Sass-Klaassen, U., Gärtner, H., & Eckstein, D. (2010). Studying global change through investigation of the plastic responses of xylem anatomy in tree rings. *New Phytologist*, *185*(1), 42–53. https://doi.org/10.1111/j.1469-8137.2009.03030.x

Francon, L., Corona, C., Till-Bottraud, I., Choler, P., Roussel, E., Carlson, B. Z., Morin, S., Girard, B., & Stoffel, M. (2021). Shrub growth in the Alps diverges from air temperature since the 1990s. *Environmental Research Letters*, *16*(7), 074026. https://doi.org/10.1088/1748-9326/ac0b67

Fritts, H. (1976). *Tree Rings and Climate*. Academic Press.

Fry, B. (2006). *Stable Isotope Ecology*. Springer. https://doi.org/10.1007/0-387-33745-8

Gärtner, H. (2001). *Holzanatomische Analyse diagnostischer Merkmale einer Freilegungsreaktion in Jahrringen von Koniferenwurzeln zur Rekonstrution geomorphologischer Prozesse* [Dissertation, Universitäts- und Landesbibliothek Bonn]. https://bonndoc.ulb.uni-bonn.de/xmlui/handle/20.500.11811/1703

Gärtner, H., Lucchinetti, S., & Schweingruber, F. H. (2015). A new sledge microtome to combine wood anatomy and tree-ring ecology. *IAWA Journal*, *36*(4), 452–459. https://doi.org/10.1163/22941932-20150114

Gärtner-Roer, I., Heinrich, I., & Gärtner, H. (2013). Wood anatomical analysis of Swiss willow (Salix helvetica) shrubs growing on creeping mountain permafrost. *Dendrochronologia*, *31*(2), 97–104. https://doi.org/10.1016/j.dendro.2012.09.003

Gärtner-Roer, I., & Nyenhuis, M. (2010). Volume Estimation, Kinematics and Sediment Transfer Rates of Active Rockglaciers in the Turtmann Valley, Switzerland. In J.-C. Otto & R. Dikau (Eds), *Landform—Structure, Evolution, Process Control* (pp. 185–198). Springer. https://doi.org/10.1007/978-3-540-75761-0_12

Gray, J., & Thompson, P. (1977). Climatic information from 18O/16O analysis of cellulose, lignin and whole wood from tree rings. *Nature*, *270*(5639), 708–709. https://doi.org/10.1038/270708a0

Grießinger, J., Bräuning, A., Helle, G., Schleser, G. H., Hochreuther, P., Meier, W. J.-H., & Zhu, H. (2019). A Dual Stable Isotope Approach Unravels Common Climate Signals and Species-Specific Responses to Environmental Change Stored in Multi-Century Tree-Ring Series from the Tibetan Plateau. *Geosciences*, *9*(4), Article 4. https://doi.org/10.3390/geosciences9040151

Grießinger, J., Meier, W. J.-H., Bast, A., Debel, A., Gärtner-Roer, I., & Gärtner, H. (2021). Permafrost Biases Climate Signals in δ18O tree-ring Series from a Sub-Alpine Tree Stand in Val Bever/Switzerland. *Atmosphere*, *12*(7), 836. https://doi.org/10.3390/atmos12070836

Guo, D., & Wang, H. (2016). CMIP5 permafrost degradation projection: A comparison among different regions. *Journal of Geophysical Research: Atmospheres*, *121*(9), 4499–4517. https://doi.org/10.1002/2015JD024108

Hacke, U. G., & Sperry, J. S. (2001). Functional and ecological xylem anatomy. *Perspectives in Plant Ecology, Evolution and Systematics*, *4*(2), 97–115. https://doi.org/10.1078/1433-8319-00017

Haeberli, W. (1985). Creep of mountain permafrost: Internal structure and flow of alpine rock glaciers. *Mitteilungen Der Versuchsanstalt Für Wasserbau, Hydrologie Und Glaziologie an Der Eidgenossischen Technischen Hochschule Zürich*, *77*.

Haeberli, W., Hallet, B., Arenson, L., Elconin, R., Humlum, O., Kääb, A., Kaufmann, V., Ladanyi, B., Matsuoka, N., Springman, S., & Mühll, D. V. (2006). Permafrost creep and rock glacier dynamics. *Permafrost and Periglacial Processes*, *17*(3), 189–214. https://doi.org/10.1002/ppp.561

Hausmann, H., Krainer, K., Brückl, E., & Mostler, W. (2007). Internal structure and ice content of Reichenkar rock glacier (Stubai Alps, Austria) assessed by geophysical investigations. *Permafrost and Periglacial Processes*, *18*(4), 351–367. https://doi.org/10.1002/ppp.601

Heinrich, I., Gärtner, H., & Monbaron, M. (2007). Tension Wood Formed in Fagus Sylvatica and Alnus Glutinosa After Simulated Mass Movement Events. *IAWA Journal*, *28*(1), 39–48. https://doi.org/10.1163/22941932-90001617

Humlum, O. (2000). The geomorphic significance of rock glaciers: Estimates of rock glacier debris volumes and headwall recession rates in West Greenland. *Geomorphology*, *35*(1), 41–67. https://doi.org/10.1016/S0169-555X(00)00022-2

Ikeda, A., & Matsuoka, N. (2002). Degradation of talus-derived rock glaciers in the Upper Engadin, Swiss Alps. *Permafrost and Periglacial Processes*, *13*(2), 145–161. https://doi.org/10.1002/ppp.413

Ikeda, A., Matsuoka, N., & Kääb, A. (2008). Fast deformation of perennially frozen debris in a warm rock glacier in the Swiss Alps: An effect of liquid water. *Journal of Geophysical Research: Earth Surface*, *113*(F1). https://doi.org/10.1029/2007JF000859

Indermühle, A., Stocker, T. F., Joos, F., Fischer, H., Smith, H. J., Wahlen, M., Deck, B., Mastroianni, D., Tschumi, J., Blunier, T., Meyer, R., & Stauffer, B. (1999). Holocene carbon-cycle dynamics based on CO2 trapped in ice at Taylor Dome, Antarctica. *Nature*, *398*(6723), 121–126. https://doi.org/10.1038/18158

Iturrate-Garcia, M., Heijmans, M. M. P. D., Schweingruber, F. H., Maximov, T. C., Niklaus, P. A., & Schaepman-Strub, G. (2017). Shrub growth rate and bark responses to soil warming and nutrient addition – A dendroecological approach in a field experiment. *Dendrochronologia*, *45*, 12–22. https://doi.org/10.1016/j.dendro.2017.07.001

Jones, D. B., Harrison, S., Anderson, K., & Whalley, W. B. (2019). Rock glaciers and mountain hydrology: A review. *Earth-Science Reviews*, *193*, 66–90. https://doi.org/10.1016/j.earscirev.2019.04.001

Kääb, A., Frauenfelder, R., & Roer, I. (2007). On the response of rockglacier creep to surface temperature increase. *Global and Planetary Change, Climate Change Impacts on Mountain Glaciers and Permafrost*, *56*(1), 172–187. https://doi.org/10.1016/j.gloplacha.2006.07.005

Kagawa, A., Sano, M., Nakatsuka, T., Ikeda, T., & Kubo, S. (2015). An optimized method for stable isotope analysis of tree rings by extracting cellulose directly from crosssectional laths. *Chemical Geology*, *393–394*, 16–25. https://doi.org/10.1016/j.chemgeo.2014.11.019

Keeling, C. D. (1979). The Suess effect: 13Carbon-14Carbon interrelations. *Environment International*, *2*(4), 229–300. https://doi.org/10.1016/0160-4120(79)90005-9

Keeling, C. D., Piper, S. C., Bacastow, R. B., Wahlen, M., Whorf, T. P., Heimann, M., & Meijer, H. A. (2001). *Exchanges of Atmospheric CO2 and 13CO2 with the Terrestrial Biosphere and Oceans from 1978 to 2000. I. Global Aspects*. https://escholarship.org/uc/item/09v319r9

Kellerer-Pirklbauer, A., Bodin, X., Delaloye, R., Lambiel, C., Gärtner-Roer, I., Bonnefoy-Demongeot, M., Carturan, L., Damm, B., Eulenstein, J., Fischer, A., Hartl, L., Ikeda, A., Kaufmann, V., Krainer, K., Matsuoka, N., Morra Di Cella, U., Noetzli, J., Seppi, R., Scapozza, C., … Zumiani, M. (2024). Acceleration and interannual variability of creep rates in mountain permafrost landforms (rock glacier velocities) in the European Alps in 1995–2022. *Environmental Research Letters*, *19*(3), 034022. https://doi.org/10.1088/1748-9326/ad25a4

Körner, C. (2003). *Alpine Plant Life*. Springer. https://doi.org/10.1007/978-3-642-18970-8

Körner, C., & Hoch, G. (2006). A Test of Treeline Theory on a Montane Permafrost Island. *Arctic, Antarctic, and Alpine Research*, *38*(1), 113–119. https://doi.org/10.1657/1523-0430(2006)038%5B0113:ATOTTO%5D2.0.CO;2

Körner, C., & Paulsen, J. (2004). A world-wide study of high altitude treeline temperatures. *Journal of Biogeography*, *31*(5), 713–732. https://doi.org/10.1111/j.1365-2699.2003.01043.x

Krainer, K., & Mostler, W. (2002). Hydrology of Active Rock Glaciers: Examples from the Austrian Alps. *Arctic, Antarctic, and Alpine Research*, *34*(2), 142–149. https://doi.org/10.1080/15230430.2002.12003478

Krainer, K., Mostler, W., & Spötl, C. (2007). Discharge from active rock glaciers, Austrian Alps: A stable isotope approach. *Austrian Journal of Earth Sciences*, *100*. https://ajes.at/archive/ajes?view=article&id=32&catid=2

LaMarche, V. C. (1968). *Rates of Slope Degradation as Determined from Botanical Evidence, White Mountains, California*. U.S. Government Printing Office.

Lee, H., & Romero, J. (2023). *Climate Change 2023: Synthesis Report*. IPCC. https://www.ipcc.ch/report/sixth-assessment-report-cycle/

Lehejček, J., Buras, A., Svoboda, M., & Wilmking, M. (2017). Wood anatomy of Juniperus communis: A promising proxy for palaeoclimate reconstructions in the Arctic. *Polar Biology*, *40*(5), 977–988. https://doi.org/10.1007/s00300-016-2021-z

Leuenberger, M., Siegenthaler, U., & Langway, C. (1992). Carbon isotope composition of atmospheric CO2 during the last ice age from an Antarctic ice core. *Nature*, *357*(6378), 488–490. https://doi.org/10.1038/357488a0

Marcer, M., Cicoira, A., Cusicanqui, D., Bodin, X., Echelard, T., Obregon, R., & Schoeneich, P. (2021). Rock glaciers throughout the French Alps accelerated and destabilised since 1990 as air temperatures increased. *Communications Earth & Environment*, *2*(1), 81. https://doi.org/10.1038/s43247-021-00150-6

McCarroll, D., & Loader, N. J. (2004). Stable isotopes in tree rings. *Quaternary Science Reviews, Isotopes in Quaternary Paleoenvironmental Reconstruction*, *23*(7), 771–801. https://doi.org/10.1016/j.quascirev.2003.06.017

Myers-Smith, I., Elmendorf, S. C., Beck, P. S. A., Wilmking, M., Hallinger, M., Blok, D., Tape, K. D., Rayback, S. A., Macias-Fauria, M., Forbes, B. C., Speed, J. D. M., Boulanger-Lapointe, N., Rixen, C., Lévesque, E., Schmidt, N. M., Baittinger, C., Trant, A. J., Hermanutz, L., Collier, L. S., … Vellend, M. (2015). Climate sensitivity of shrub growth across the tundra biome. *Nature Climate Change*, *5*(9), 887–891. https://doi.org/10.1038/nclimate2697

Myers-Smith, I., Hallinger, M., Blok, D., Sass-Klaassen, U., Rayback, S. A., Weijers, S., J. Trant, A., Tape, K. D., Naito, A. T., Wipf, S., Rixen, C., Dawes, M. A., A. Wheeler, J., Buchwal, A., Baittinger, C., Macias-Fauria, M., Forbes, B. C., Lévesque, E., Boulanger-Lapointe, N., … Wilmking, M. (2015). Methods for measuring arctic and alpine shrub growth: A review. *Earth-Science Reviews*, *140*, 1–13. https://doi.org/10.1016/j.earscirev.2014.10.004

Nielsen, S., von Arx, G., Damgaard, C., Abermann, J., Buchwal, A., Büntgen, U., Treier, U., Barfod, A., & Signe, N. (2017). Xylem Anatomical Trait Variability Provides Insight on the Climate-Growth Relationship of Betula nana in Western Greenland. *Arctic, Antarctic, and Alpine Research*, *49*(3), 359–371.

Nikolaev, A. N., Fedorov, P. P., & Desyatkin, A. R. (2009). Influence of climate and soil hydrothermal regime on radial growth of Larix cajanderi and Pinus sylvestris in Central Yakutia, Russia. *Scandinavian Journal of Forest Research*, *24*(3), 217–226. https://doi.org/10.1080/02827580902971181

Nyenhuis, M. (2005). *Permafrost und Sedimenthaushalt in einem alpinen Geosystem*. Rheinischen Friedrich–Wilhelms–Universität Bonn.

Okabe, M., & Ito, K. (2008). *Color universal design (CUD): How to make figures and presentations that are friendly to colorblind people*. https://jfly.uni-koeln.de/color/#pallet

Olson, M. E., Anfodillo, T., Rosell, J. A., Petit, G., Crivellaro, A., Isnard, S., León-Gómez, C., Alvarado-Cárdenas, L. O., & Castorena, M. (2014). Universal hydraulics of the flowering plants: Vessel diameter scales with stem length across angiosperm lineages, habits and climates. *Ecology Letters*, *17*(8), 988–997. https://doi.org/10.1111/ele.12302

Owczarek, P., & Opała, M. (2016). Dendrochronology and extreme pointer years in the tree-ring record (AD 1951–2011) of polar willow from southwestern Spitsbergen (Svalbard, Norway). *Geochronometria*, *43*(1), 84–95. https://doi.org/10.1515/geochr-2015-0035

Paolini, L., Villalba, R., & Ricardo Grau, H. (2005). Precipitation variability and landslide occurrence in a subtropical mountain ecosystem of NW Argentina. *Dendrochronologia*, *22*(3), 175–180. https://doi.org/10.1016/j.dendro.2005.06.001

PERMOS. (2022). *Swiss permafrost bulletin 2021*. Swiss Permafrost Monitoring Network. https://www.permos.ch/fileadmin/Files/publications/swiss_permafrost_bulletin/PERMOS_bulletin_2023.pdf

Qi, X., Cherubini, P., Treydte, K., Li, M.-H., Wu, Z., He, H. S., Du, H., Fang, K., & Saurer, M. (2023). Growth responses to climate warming and their physiological mechanisms differ between mature and young larch trees in a boreal permafrost region. *Agricultural and Forest Meteorology*, *343*, 109765. https://doi.org/10.1016/j.agrformet.2023.109765

Reato, A., Borzi, G., Martínez, O. A., & Carol, E. (2022). Role of rock glaciers and other high-altitude depositional units in the hydrology of the mountain watersheds of the Northern Patagonian Andes. *Science of The Total Environment*, *824*, 153968. https://doi.org/10.1016/j.scitotenv.2022.153968

RGIK. (2023). Guidelines for inventorying rock glaciers: Baseline and practical concepts (version 1.0). *Rock Glacier Inventories and Kinematics*. https://doi.org/10.51363/unifr.srr.2023.002

Roden, J. S., & Ehleringer, J. R. (1999). Hydrogen and oxygen isotope ratios of tree-ring cellulose for riparian trees grown long-term under hydroponically controlled environments. *Oecologia*, *121*(4), 467–477. https://doi.org/10.1007/s004420050953

Roden, J. S., Lin, G., & Ehleringer, J. R. (2000). A mechanistic model for interpretation of hydrogen and oxygen isotope ratios in tree-ring cellulose. *Geochimica et Cosmochimica Acta*, *64*(1), 21–35. https://doi.org/10.1016/S0016-7037(99)00195-7

Roer, I. (2007). *Rockglacier kinematics in a high mountain geosystem*. Asgard-Verlag St. Augustin, Germany. https://www.parcs.ch/nwp/pdf_public/2014/28469_20140130_155608_roer_0551-1.pdf

Roer, I., & Nyenhuis, M. (2007). Rockglacier activity studies on a regional scale: Comparison of geomorphological mapping and photogrammetric monitoring. *Earth Surface Processes and Landforms*, *32*(12), 1747–1758. https://doi.org/10.1002/esp.1496

Rozanski, K., Araguás-Araguás, L., & Gonfiantini, R. (1993). Isotopic Patterns in Modern Global Precipitation. In *Climate Change in Continental Isotopic Records* (pp. 1–36). American Geophysical Union (AGU). https://doi.org/10.1029/GM078p0001

Saurer, M., Oettli, M., & Lehmann, M. M. (2025). A Simple Method for Triple Stable Isotope Analysis of Cellulose, Sugar, and Bulk Organic Matter—Advances and Limitations. *Rapid Communications in Mass Spectrometry*, *39*(4), e9957. https://doi.org/10.1002/rcm.9957

Saurer, M., Siegwolf, R., Borella, S., & Schweingruber, F. (1998). Environmental information from stable isotopes in tree rings of Fagus sylvatica. In M. Beniston & J. L. Innes (Eds), *The Impacts of Climate Variability on Forests* (pp. 241–253). Springer. https://doi.org/10.1007/BFb0009777

Saurer, M., Siegwolf, R. T. W., & Schweingruber, F. H. (2004). Carbon isotope discrimination indicates improving water-use efficiency of trees in northern Eurasia over the last 100 years. *Global Change Biology*, *10*(12), 2109–2120. https://doi.org/10.1111/j.1365-2486.2004.00869.x

Schaffer, N., MacDonell, S., Réveillet, M., Yáñez, E., & Valois, R. (2019). Rock glaciers as a water resource in a changing climate in the semiarid Chilean Andes. *Regional*

Environmental Change, *19*(5), 1263–1279. https://doi.org/10.1007/s10113-018-01459-3

Schweingruber, F. H., Hellmann, L., Tegel, W., Braun, S., Nievergelt, D., & Büntgen, U. (2013). Evaluating the wood anatomical and dendroecological potential of arctic dwarf shrub communities. *IAWA Journal*, *34*(4), 485–497. https://doi.org/10.1163/22941932-00000039

Šilhán, K. (2021). Dendrogeomorphology of Different Landslide Types: A Review. *Forests*, *12*(3), 261. https://doi.org/10.3390/f12030261

Steffen, C. (2025). *Assessing destabilization patterns of active rock glaciers in the Turtmann Valley incorporating a general typology for destabilized rock glaciers* [Master's Thesis]. Universität Zürich.

Steig, E. J., Fitzpatrick, J. J., Potter, N. J., & Clark, D. H. (1998). The geochemical record in rock glaciers. *Geografiska Annaler: Series A, Physical Geography*, *80*(3–4), 277–286. https://doi.org/https://doi.org/10.1111/j.0435-3676.1998.00043.x

Strunk, H. (1997). Dating of geomorphological processes using dendrogeomorphological methods. *CATENA*, *31*(1), 137–151. https://doi.org/10.1016/S0341-8162(97)00031-3

Sugimoto, A., Yanagisawa, N., Naito, D., Fujita, N., & Maximov, T. C. (2002). Importance of permafrost as a source of water for plants in east Siberian taiga. *Ecological Research*, *17*(4), 493–503. https://doi.org/10.1046/j.1440-1703.2002.00506.x

swisstopo. (1845). *Topographische Karte der Schweiz (Dufourkarte)* [Map]. Bundesamt für Landestopografie swisstopo. https://map.geo.admin.ch/#/map?lang=de&center=2622073.58,1117505.27&z=6.818&topic=ech&layers=ch.swisstopo.hiks-dufour&bgLayer=ch.swisstopo.pixelkarte-farbe&featureInfo=default

swisstopo. (2005). *Permafrosthinweiskarte* [Map]. Bundesamt für Landestopografie swisstopo. https://map.geo.admin.ch/#/map?lang=de&center=2621774.67,1116234.86&z=9.395&topic=ech&layers=ch.bafu.permafrost&bgLayer=ch.swisstopo.pixelkarte-farbe&featureInfo=default

swisstopo. (2026). *Landeskarte* [Map]. Bundesamt für Landestopografie swisstopo. https://map.geo.admin.ch/#/map?lang=de&center=2621774.67,1116234.86&z=9.395&topic=ech&layers=&bgLayer=ch.swisstopo.pixelkarte-farbe&featureInfo=default

Taylor, S., Feng, X., Kirchner, J. W., Osterhuber, R., Klaue, B., & Renshaw, C. E. (2001). Isotopic evolution of a seasonal snowpack and its melt. *Water Resources Research*, *37*(3), 759–769. https://doi.org/10.1029/2000WR900341

Treydte, K. S., Schleser, G. H., Helle, G., Frank, D. C., Winiger, M., Haug, G. H., & Esper, J. (2006). The twentieth century was the wettest period in northern Pakistan over the past millennium. *Nature*, *440*(7088), 1179–1182. https://doi.org/10.1038/nature04743

van der Sleen, P., Groenendijk, P., & Zuidema, P. A. (2015). Tree-ring δ18O in African mahogany (*Entandrophragma utile*) records regional precipitation and can be used for climate reconstructions. *Global and Planetary Change*, *127*, 58–66. https://doi.org/10.1016/j.gloplacha.2015.01.014

van Tatenhove, F., & Dikau, R. (1990). Past and Present Permafrost Distribution in the Turtmanntal, Wallis, Swiss Alps. *Arctic and Alpine Research*, *22*(3), 302–316. https://doi.org/10.1080/00040851.1990.12002794

Vystavna, Y., Matiatos, I., & Wassenaar, L. I. (2020). 60-year trends of *δ*18O in global precipitation reveal large scale hydroclimatic variations. *Global and Planetary Change*, *195*, 103335. https://doi.org/10.1016/j.gloplacha.2020.103335

Wershaw, R. L., Friedman, I., & Heller, S. J. (1966). Hydrogen isotope fractionation in water passing through trees. In *Advances in Organic Geochemistry* (pp. 55–67). Pergamon.

West, G. B., Brown, J. H., & Enquist, B. J. (1999). A general model for the structure and allometry of plant vascular systems. *Nature*, *400*(6745), 664–667. https://doi.org/10.1038/23251

White, J. W. C., Vaughn, B. H., & Michel, S. E. (2015). *Stable Isotopic Composition of Atmospheric Carbon Dioxide (13C and 18O) from the NOAA ESRL Carbon Cycle Cooperative Global Air Sampling Network* [Data set]. University of Colorado, Institute of Arctic and Alpine Research (INSTAAR). ftp://aftp.cmdl.noaa.gov/data/trace_gases/co2c13/flask/

Williams, M. W., Knauf, M., Caine, N., Liu, F., & Verplanck, P. L. (2006). Geochemistry and source waters of rock glacier outflow, Colorado Front Range. *Permafrost and Periglacial Processes*, *17*(1), 13–33. https://doi.org/10.1002/ppp.535

Zhu, L., Wang, M., Camarero, J. J., Cooper, D. J., Yuan, D., Chen, Z., Wang, X., & Cherubini, P. (2024). Permafrost melting enhances growth but leads to less intra-annual density fluctuations in boreal *Larix gmelinii* forests at its southernmost limit in northeast China. *Ecological Indicators*, *164*, 112158. https://doi.org/10.1016/j.ecolind.2024.112158

9. Appendix

9.1 Location and Isotope Values

ID	Coordinates (LV95)	Altitude (m a.s.l)	d18O - A	d18O - B	d18O - C	d13C - A	d13C - B	d13C - C
1	2622024/1116690	2579	26.40533			-24.8943		
2	2622025/1116687	2575	24.37947			-24.8555		
3	2622024/1116688	2572	25.41092	23.91656		-25.1155	-25.262	
4	2622019/1116695	2568	25.99735	24.77924		-25.0643	-25.3497	
5	2622012/1116756	2557	25.75989	24.92703	26.0519	-24.4682	-25.0447	-25.1552
6	2622018/1116766	2554	27.98185	25.36013		-24.0717	-24.6611	
7	2622009/1116761	2560	26.7121	24.22761	24.85074	-25.4638	-25.699	-26.0834
8	2622005/1116768	2533	27.40975	24.67056	25.36525	-24.8435	-25.0169	-25.3542
9	2621981/1116781	2548	27.27025	24.51612		-24.5493	-24.2529	
10	2621981/1116781	2548	28.50242	25.52435		-24.378	-24.8241	
11	2621981/1116781	2548	25.68635	24.67355		-24.5907	-24.4856	
12	2621981/1116781	2548	25.88022	24.92966	23.87387	-24.9256	-25.1358	-25.5287

Table 2: Coordinates, altitude and isotopic values (‰) of all sampled shrubs on the active site. A = 2016 – 2025, B = 2006 – 2015, C = <2006

ID	Coordinates (LV95)	Altitude (m a.s.l)	δ18O - A	δ18O - B	δ18O - C	δ13C - A	δ13C - B	δ13C - C
13	2621749/1117064	2389	23.92366	23.27609	23.52351	-22.503	-23.2667	-23.5859
14	2621744/1117061	2381	22.71067	24.28881	23.44012	-25.6241	-24.3718	-24.8006
16	2621753/1117074	2378	24.97376	25.81034	25.67752	-24.6626	-23.6009	-24.2869
17	2621723/1117073	2375	24.91729	23.83523	22.34968	-23.8006	-24.1172	-23.8491
18	2621726/1117079	2378	24.57557	24.50954	24.6023	-23.5646	-24.0943	-24.9062
19	2621724/1117073	2378	23.75202	23.26011	21.86801	-24.6568	-23.8201	-24.0936
20	2621738/1117078	2373	24.68835	25.07109	23.84293	-25.3346	-25.5099	-25.6904
21	2621702/1117117	2364	24.13321	23.48985		-24.1833	-24.7597	
22	2621711/1117123	2361	22.60009	22.31183	23.14492	-23.9704	-23.5555	-23.9506
23	2621716/1117127	2358	27.04132	25.58831	23.68322	-24.5615	-24.1842	-24.1733
24	2621719/1117132	2357	22.37928	24.38324	24.12911	-24.9552	-24.341	-24.0197

Table 3: Coordinates, altitude and isotopic values (‰) of all sampled shrubs on the inactive site. A = 2016 – 2025, B = 2006 – 2015, C = <2006

ID	Coordinates (LV95)	Altitude (m a.s.l)	δ18O - A	δ18O - B	δ18O - C	δ13C - A	δ13C - B	δ13C - C
25	2621844/1117070	2368	24.39343	24.30162	24.30264	-23.9054	-24.0252	-23.974
26	2621838/1117065	2366	27.06402	25.27888	23.94258	-24.7339	-25.2884	-24.7603
27	2621836/1117063	2368	26.02339	24.52513	25.45903	-23.6784	-23.7325	-24.1682
28	2621837/1117057	2371	24.12051	23.30072	23.56161	-23.3147	-23.2932	-23.8023
29	2621830/1117048	2378	25.91565	23.79639	25.14043	-22.8605	-22.3867	-22.3602
30	2621836/1117042	2379	25.99495	25.80358	24.54633	-23.8134	-23.7382	-24.2304
31	2621824/1117040	2383	25.17833	23.9509	23.57679	-24.5057	-24.5868	-23.3324
32	2621833/1117034	2384	25.62338	25.0452	24.14733	-23.8943	-24.055	-24.6201
33	2621857/1117048	2384	26.03523	25.55605	22.79089	-23.8612	-23.1646	-23.1744
34	2621858/1117041	2388	27.17362	24.82946		-23.7385	-23.4291	
35	2621864/1117040	2389	24.65858	23.34265	24.03942	-23.9204	-24.2007	-23.8293
36	2621868/1117034	2390	25.93906	24.62951		-22.0979	-22.261	

Table 4: Coordinates, altitude and isotopic values (‰) of all sampled shrubs on the middle site. A = 2016 – 2025, B = 2006 – 2015, C = <2006

ID	Coordinates (LV95)	Altitude (m a.s.l)	δ18O - A	δ18O - B	δ18O - C	δ13C - A	δ13C - B	δ13C - C
37	2621879/1117082	2377	23.96457	23.93247	23.60022	-23.008	-22.3142	-23.1233
38	2621874/1117085	2376	24.2329	23.59331	22.16584	-23.3078	-23.1207	-24.1351
39	2621872/1117070	2374	23.9063	23.67012	23.60205	-23.0391	-22.4433	-22.8337
40	2621873/1117085	2374	25.73208	25.61024	25.43592	-24.3623	-23.936	-23.5167
41	2621850/1117128	2355	25.08947	24.65495	23.77502	-24.9257	-24.1214	-24.8128
42	2621847/1117128	2351	24.62726	23.57438	23.50568	-24.5243	-24.6323	-24.4715
43	2621858/1117121	2354	25.33204	24.00544		-24.1476	-24.2229	
44	2621861/1117121	2359	24.32322	24.48871	23.40724	-22.9622	-22.9407	-23.3564
45	2621863/1117117	2356	25.65735	23.37714		-24.123	-23.3274	
46	2621868/1117115	2358	24.19331	23.63493	22.53098	-23.9179	-23.5163	-23.8718
47	2621868/1117114	2362	23.51041	23.84389	23.17964	-25.2137	-24.7958	-24.8519
48	2621870/1117115	2362	26.33713	25.0366	23.60561	-24.1335	-24.2208	-24.2245

Table 5: Coordinates, altitude and isotopic values (‰) of all sampled shrubs on the reference site. A = 2016 – 2025, B = 2006 – 2015, C = <2006

9.2 VLA Values

ID	Site	2016-2025	2006-2015	1996-2005	1986-1995	1976-1985	1966-1975	1956-1965	1946-1955
W1	active	479							
W2	active	493							
W3	active	560	437						
W4	active	659	413						
W5	active	1178	793	430					
W6	active	931	512						
W7	active	752	570	421	286				
W8	active	960	453	339					
W9	active	642	408						
W10	active	965	676						
W11	active	1043	665						
W12	active	1074	520	293					
W13	inactive	419	301	249					
W14	inactive	1769	1513	1300	982	660	396		
W16	inactive	771	800	685	356				
W17	inactive	970	1447	1371	1130	817	540	457	
W18	inactive	1064	895	899	866	891	542	434	396
W19	inactive	1013	746	657	444				
W20	inactive	702	913	660	530	449	399		
W21	inactive	763	511						
W22	inactive	766	783	695	489				
W23	inactive	988	676	428					
W24	inactive	534	625	553	435				
W25	middle	1468	1293	1184	1127	1064			
W26	middle	1703	1370	1008	920	632	455	337	
W27	middle	709	529	528	427				
W28	middle	919	681	423					
W29	middle	665	481	327					
W30	middle	948	818	495					
W31	middle	883	702	666	574				
W32	middle	1023	917	735	448	304			
W33	middle	953	654	405	409	284			
W34	middle	964	545						
W35	middle	752	666	633	528	391			
W36	middle	620	411						
W37	reference	836	580	433					
W38	reference	637	732	596	583	492	394		
W39	reference	659	641	483					
W40	reference	732	637	516	320				
W41	reference	760	805	481					
W42	reference	710	604	482					
W43	reference	602	396						
W44	reference	828	776	642	597	406			

W45	reference	1260	702						
W46	reference	1501	1259	1145	905	821	714		
W47	reference	772	755	566	441				
W48	reference	1257	1153	858	554				

Table 6: Average VLA (μm²) of all sampled shrubs for all decades

ID	Site	0-10	11-20	21-30	31-40	41-50	51-60	61-70	71-80
1	active	479.0879							
2	active	492.6993							
3	active	436.5492	560.3195						
4	active	412.7004	658.9301						
5	active	429.8327	792.7057	1178.348					
6	active	512.2342	930.7823						
7	active	286.2205	421.377	569.8733	751.6004				
8	active	339.1562	452.6485	960.2696					
9	active	408.1969	642.2528						
10	active	676.2537	965.1704						
11	active	665.41	1043.004						
12	active	292.6104	520.1708	1073.858					
13	inactive	249.4236	301.1565	418.9531					
14	inactive	396.1426	660.0099	981.829	1300.207	1512.589	1769.461		
16	inactive	356.1897	684.8531	799.8132	770.5962				
17	inactive	457.4772	540.4388	817.1365	1130.492	1371.279	1446.576	969.6979	
18	inactive	396.2438	433.7778	541.8504	891.4677	866.4039	898.5962	894.9353	1064.275
19	inactive	443.6932	656.699	746.4165	1012.742				
20	inactive	398.5492	448.8879	530.4985	660.1049	912.7665	702.2112		
21	inactive	510.733	762.9186						
22	inactive	489.2688	694.5134	783.0921	765.9942				
23	inactive	428.4334	676.4266	988.4089					
24	inactive	435.1391	552.7511	624.8172	533.66				
25	middle	1063.766	1126.968	1183.875	1293.149	1467.891			
26	middle	336.9901	455.4041	632.102	920.0544	1008.324	1370.288	1702.716	
27	middle	426.6974	528.3894	529.0723	708.6947				
28	middle	423.1005	680.6926	918.9682					
29	middle	326.6587	481.4475	665.2612					
30	middle	494.8264	818.2722	947.6786					
31	middle	573.7842	665.8955	701.5755	882.7585				
32	middle	304.3063	448.3396	734.509	917.2675	1022.902			
33	middle	283.5401	409.0672	404.7487	653.5858	953.4223			
34	middle	545.2417	963.663						
35	middle	391.2162	527.8566	633.4265	666.1451	752.1011			
36	middle	410.7984	620.0576						
37	reference	433.0532	579.8266	836.0452					
38	reference	393.6146	492.4153	583.2157	596.1609	732.2201	636.831		
39	reference	483.1721	641.1435	659.0764					
40	reference	319.9631	516.1017	637.0065	732.4973				
41	reference	480.88	804.74	759.9182					

42	reference	482.1682	603.7871	710.2654					
43	reference	396.0649	602.0367						
44	reference	406.3797	596.8963	642.162	776.3728	828.3969			
45	reference	701.9515	1259.668						
46	reference	713.9281	820.6592	905.0269	1145.121	1259.281	1500.627		
47	reference	441.4188	566.4439	754.8068	771.6769				
48	reference	553.9181	857.5435	1153.375	1256.848				

Table 7: Average VLA (µm²) of all sampled shrubs for all age periods

9.3 Ring-Width Values

ID	2016-2025	2006-2015	1996-2005	1986-1995	1976-1985	1966-1975	1956-1965	1946-1955	1936-1945
1	0.444								
2	0.215	0.2							
3	0.221	0.092	0.05						
4	0.245	0.203	0.03						
5	0.419	0.305	0.11	0.185					
6	0.7	0.23	0.13						
7	0.577	0.292	0.171	0.117778					
8	0.742	0.24	0.2						
9	0.39	0.261667							
10	0.483	0.134	0.11						
11	0.454	0.453							
12	0.601	0.383	0.14						
13	0.22	0.223	0.124286						
14	0.099	0.152	0.279	0.179	0.096	0.158	0.24		
16	0.256	0.191	0.329	0.215	0.2				
17	0.444	0.321	0.231	0.116	0.08	0.124	0.396667		
18	0.264	0.097	0.13	0.107	0.121	0.043	0.068	0.14	0.473333
19	0.158	0.097	0.176	0.241667					
20	0.176	0.231	0.149	0.174	0.118	0.135	0.1675		
21	0.362	0.38625							
22	0.275	0.295	0.296	0.408					
23	0.201	0.25	0.174						
24	0.099	0.126	0.217	0.271	0.184				
25	0.136	0.136	0.212	0.221	0.307				
26	0.461	0.229	0.28	0.294	0.326	0.214	0.131111		
27	0.192	0.166	0.246	0.179					
28	0.368	0.269	0.164	0.195					
29	0.276	0.169	0.3575						
30	0.209	0.186	0.1875						
31	0.131	0.124	0.091	0.201	0.426667				
32	0.235	0.256	0.41	0.111	0.23125				
33	0.281	0.28	0.071	0.087	0.1775				
34	0.288	0.215556							
35	0.164	0.096	0.17	0.219	0.293333				

36	0.364	0.405							
37	0.288	0.385	0.441667						
38	0.313	0.266	0.22	0.26	0.218	0.315			
39	0.191	0.238	0.287143						
40	0.176	0.149	0.242	0.091	0.19				
41	0.429	0.544	0.361667						
42	0.248	0.144	0.48						
43	0.351	0.382							
44	0.092	0.192	0.099	0.132	0.4				
45	0.195	0.42625							
46	0.23	0.196	0.155	0.087	0.076	0.254	0.115		
47	0.074	0.115	0.157	0.253	0.285				
48	0.319	0.266	0.176	0.25					

Table 8: Average ring width (mm) of all sampled shrubs for all decades

ID	01. Okt	Nov 20	21-30	31-40	41-50	51-60	61-70	71-80	81-90
1	0.444								
2	0.207	0.28							
3	0.071	0.155	0.485						
4	0.116	0.218	0.41						
5	0.104	0.246	0.443	0.39					
6	0.171	0.532	0.886667						
7	0.111	0.208	0.269	0.62					
8	0.179	0.357	0.837143						
9	0.319	0.38							
10	0.102	0.446	0.455						
11	0.453	0.454							
12	0.232	0.526	0.592						
13	0.139	0.25	0.201429						
14	0.179	0.09	0.18	0.266	0.158	0.101	0.13		
16	0.183	0.33	0.199	0.317	0.073333				
17	0.303	0.083	0.106	0.136	0.251	0.423	0.42		
18	0.248	0.072	0.054	0.098	0.111	0.138	0.097	0.22	0.246667
19	0.226	0.152	0.12	0.13					
20	0.155	0.139	0.116	0.209	0.126	0.286	0.1075		
21	0.383	0.36							
22	0.344	0.288	0.332	0.212					
23	0.174	0.25	0.201						
24	0.253	0.243	0.157	0.097	0.11				
25	0.307	0.221	0.212	0.136	0.136				
26	0.122	0.252	0.32	0.298	0.262	0.259	0.454444		
27	0.179	0.246	0.166	0.192					
28	0.177	0.218	0.386	0.295					
29	0.233	0.239	0.29						
30	0.19	0.203	0.19						
31	0.295	0.094	0.112	0.144	0.1				
32	0.204	0.145	0.432	0.247	0.21125				

33	0.129	0.07	0.169	0.333	0.2225				
34	0.22	0.291111							
35	0.228	0.207	0.101	0.146	0.183333				
36	0.434	0.288333							
37	0.416	0.364	0.263333						
38	0.317	0.188	0.277	0.202	0.278	0.33375			
39	0.301	0.206	0.175714						
40	0.095	0.225	0.173	0.178	0.06				
41	0.46	0.516	0.356667						
42	0.48	0.144	0.248						
43	0.421	0.242							
44	0.365	0.11	0.114	0.199	0.05875				
45	0.42	0.145							
46	0.213	0.133	0.06	0.165	0.196	0.206	0.1775		
47	0.302	0.238	0.13	0.103	0.0675				
48	0.193	0.265	0.329	0.185					

Table 9: Average ring width (mm) of all sampled shrubs for all age periods

Personal Declaration

I hereby declare that the submitted thesis is the result of my own, independent work. All external sources are explicitly acknowledged in the thesis.

In the creation of this thesis, I used generative AI for specific tasks. I used ChatGPT (Version 5) for grammatical and stylistic checks of my text and to check RStudio coding scripts. All tasks performed by AI have been checked by me, the author of this text. I take full responsibility for the text.

Location, Date: Winterthur, 22.5.26

Signature: U. Frey